

Long-term Implications of Ethanol-based Fuel on an Aviation Aircraft Fuel System

By

Daren Davoux

A thesis submitted

in partial fulfillment of the requirements for the

Master of Science

Major in Engineering

South Dakota State University

2007

Acknowledgements

With this page I am afforded the opportunity to give thanks to those with whom I am indebted, both in this work and in life.

First I would like to thank superiors, who have been both advisors and teachers. Dr. Helder, to you I owe this very degree. You pulled me into graduate school by simply saying I was wanted. You have guided, encouraged, and trusted me every step along the long path. For this, and so much words cannot express, I thank you.

Dr. Hietpas, you showed me example, in the technical nature of this project, in teaching, and in character. You have continually gone before me without even realizing. Thank you.

I must thank the entire faculty of this grand department, who have poured themselves into me. Without exception, every one has valued student beyond all else. Research, journals, memos will perish, but that which is in the students will last.

To my parents, who raised me from the beginning, who have loved me through everything. How can I express appreciation to those who I owe everything to? You have been patient and consistent, to a child shaky and insecure. Never picture perfect, just a plain man and his wife, who clawed in faith with hands and feet, and somehow made faith to fly.

And to you, Jesus who is called Christ, my Savior and God. In whom I have hoped and dreamed, and not been ashamed. You alone are everything. In you alone do I live and move and have my being. I do not know what tomorrow holds, but I

know you have never failed, and you hold me. And I can only hope in the power of your Spirit and the grace of your providence. For some reason you have chosen me, though it cost you everything. Thank you, that someday I'll be a good son. Someday I will make you proud. Thank you, for delivering me from the power of darkness and conveying me into your kingdom. Thank you, for supping with me, just like you said you would, even daily bearing my burden. Thank you, Jesus, for you, just for you.

Abstract

Long Term Effects of Aviation Grade Ethanol on a TCM Fuel System

Daren Davoux

The objective of this project is to determine the effects of long-term subjection of an aircraft fuel system to ethanol based fuel. The fuel system investigated was manufactured by Teledyne Continental Motors, and included the fuel pump, flow controller, and auxiliary components such as a flow divider, hoses and fittings.

The project entailed the design and implementation of both an enclosed fuel system incorporating a TCM 646212-23A1 fuel pump and 639715A16 fuel flow controller, as well as supporting electronic devices capable of varying the fuel flow settings according to a simulated flight schedule, while monitoring the performance of the tested parts. Once the system was designed and constructed, the system was subjected to an automated test lasting over nine months, during which the system was monitored to observe performance as subjected to ethanol based fuel.

Finally, after nine months of operation, the test was concluded, the data was gathered and analyzed, and the performance of the fuel system was evaluated. The fuel system had logged over 3700 hours of simulated flight time, and another 1800 hours of fuel system soaking. Since the manufacturer recommended time before

overhaul for this specific system was 1800 hours, under normal conditions, this fuel system would have undergone two overhauls during this period. The test was concluded because of a failure of the DC motor used to power the fuel pump. This motor was not part of the fuel system; its failure was a result of worn and corroded brushes.

With regard to the performance of the pump, the data revealed little change in fuel pressure throughout the test (5.8 % decline, worst-case); though the torque required to circulate the fuel had fallen 6% after an initial break-in period. When the data were considered together, these changes likely revealed the deteriorating condition of the motor, not deterioration within the fuel pump.

Regarding the fuel servo, the data indicated the fuel pressure exiting the servo for the fuel flow divider had fallen approximately 12%. However, since the inlet pressure (pump pressure) had fallen 5.8% over the same period, the majority of this change most likely reflected the condition of the fuel pump and motor drive, not deterioration within the servo. Also, data indicated the torque required to adjust the mixture and throttle settings had increased approximately 7 and 27% respectively. Though these results may indicate some deterioration of the seals within the fuel servo, the results were not alarming, since neither leakage was observed nor did external testing indicate similar changes.

When all factors are considered together – the deterioration of the motor, the length of the test exceeding beyond two recommended overhauls - the data indicates ethanol-based fuel caused no abnormal wear to the fuel system.

Table of Contents

Title Page	i
Acceptance Page	ii
Acknowledgments	iii
Abstract	v
Table of Contents	viii
List of Tables	xii
List of Figures	xiii
 Chapter	
1. Introduction	1
1.1. Purpose	1
1.2. Background	1
1.3. Rig testing	3
1.4. Objectives	8
2. Project Requirements	9
2.1. Operational Requirements	9
2.2. Mechanical Requirements	10
2.2.1. Mechanical Requirements Overview	11
2.2.2. Module 1: Fuel Pump	13
2.2.3. Module 2: Fuel Servo	15
2.2.4. Module 3: Auxiliary Parts	17
2.3. Electronic Requirements	19

2.3.1. Electronic Requirements Overview	19
2.3.2. Module 1: Fuel Pump	20
2.3.3. Module 2: Fuel Servo	20
2.3.4. Module 3: Auxiliary Electronic Devices	21
3. Project Design	22
3.1. Design Overview	22
3.2. User Interface	26
3.3. Data Acquisition and Control	29
3.4. Interface Board	30
3.5. Module 1: Fuel Pump Drive	32
3.5.1. Fuel Pump Mechanical Design	32
3.5.2. Fuel Pump Speed Control	32
3.5.3. Fuel Pump Measurements	37
3.6. Module 2: Fuel Servo Electronics	43
3.6.1. Lever Arm Position Control	44
3.6.2. Servo Measurements	49
3.7. Module 3: Auxiliary Electronic Devices	58
4. Data Collection and Analysis	68
4.1. Test overview	68
4.2. Description of Data	70
4.2.1. Continuous Data	70
4.2.2. Event Summarized Data	74

4.3 Module 1: Fuel Pump	79
4.3.1. Fuel Pressure	79
4.3.2. Motor Current	86
4.3.3. Visual Inspection	95
4.3.4. Summary and Conclusions	95
4.4. Module 2: Fuel Servo	98
4.4.1. Throttle Actuation Peak Current	98
4.4.2. Mixture actuation Peak Current	107
4.4.3. Throttle Fuel Pressure	113
4.4.4. Visual Inspection	120
4.4.5. Fuel Servo Overall Conclusions	120
4.5. Auxiliary System Parts	122
4.5.1. Fuel Filter	122
4.5.2. Fuel Lines	123
4.5.3. Fuel Tank	123
4.5.4. Flow Divider	123
4.5.5. Summary and Conclusions	123
4.6. Data Analysis Summary and Conclusions	124
5. Project Conclusions	125
5.1. System Design	125
5.2. Ethanol Fuel Performance	128
References	132

Appendix A: Servo Actuator Manufacturer Specification Data.....	134
Appendix B: Position Transducer Manufacturer Specification Data	136
Appendix C: Humidity Sensor Manufacturer Specification Data	138
Appendix D: Air Temperature Sensor Manufacturer Specification Data	145
Appendix E: Fuel Temperature Sensor Manufacturer Specification Data	147

List of Tables

Table 2.1. Rig Test Timing Cycle	10
Table 3.1. DAQ Specification	30
Table 4.1. Example Data from April 1st, 2005	71
Table 4.2. Fuel Pump Pressure, Summarized Data	75
Table 4.3. Summary Statistics for Pump Pressure	82
Table 4.4. Motor Current Statistics	90
Table 4.5. Summary Statistics for Throttle Actuation Current	105
Table 4.6. Summary Statistics for Mixture Actuation Current	109
Table 4.7. Summary Statistics for Throttle Fuel Pressure	116

List of Figures

Figure 1.1. Cessna Rig Test Setup	4
Figure 1.2. TCM Fuel System Rig Test	7
Figure 2.1. Basic Fuel Flow Diagram	12
Figure 2.2. Module Definition	13
Figure 2.3. TCM Fuel Pump	15
Figure. 2.4. Simplified TCM Fuel Servo Diagram	16
Fig. 2.5. TCM six-cylinder Fuel Flow Divider	18
Fig. 2.6. Fuel Filter	18
Figure 3.1. System Overview	23
Figure 3.2. System Interface Flowchart	24
Figure 3.3. Fuel Pump Motor, Motor Drive and Coupling	25
Figure 3.4. Fuel Servo Setup	26
Figure 3.5. User Interface	28
Figure 3.6. DAQ/Electronic Interface	31
Figure 3.7. Motor Control Command Signal Block Diagram	35
Figure 3.8. Motor Control Signal Detailed Design	36
Figure 3.9. Module 1 Detailed Schematic	37
Figure 3.10. Pressure Sensor Flowchart	38
Figure 3.11. Pump Pressure Sensor Schematic	39
Figure 3.12. Motor Current Measurement Flowchart	41
Figure 3.13. Motor Current Measurement Circuit Design	42

Figure 3.14. Position Control Scheme Flowchart	45
Figure 3.15. Servo Mechanical Setup	46
Figure 3.16. Summation Node Detailed Design	46
Figure 3.17. Power Amplifier Circuit Board	48
Figure 3.18. Power Amplifier	48
Figure 3.19. Detailed Diagram of Module 2 Measurements	50
Figure 3.20. Example Actuation Current During An Event Transition	52
Figure 3.21. Actuator Peak Current Measurement Scheme	53
Figure 3.22. Current to Voltage and Absolute Value Circuit	54
Figure 3.23. Peak Detection Circuit	56
Figure 3.24. Humidity Sensor Flow Chart	60
Figure 3.25. Humidity Sensor Design	61
Figure 3.26. Fuel Temperature Sensor R/T curve	62
Figure 3.27. Temperature Sensor Flow Chart	63
Figure 3.28. Fuel Temperature Sense Circuit	64
Figure 3.29. Temperature versus Voltage at J1-18	65
Figure 3.30. Air Temperature Thermister R/T Curve	66
Figure 3.31. Air Temperature versus Voltage Curve	67
Figure 4.1. Fuel Pump Pressure and RPM, January 29, 2005	72
Figure 4.2. Fuel Pump Pressure and RPM, April 20, 2005	73
Figure 4.3. Fuel Pump Pressure and RPM, September 14, 2005	73
Figure 4.4. Average Fuel Pump Pressure and Standard Deviation	76

Figure 4.5. Explanation of Sample to Sample Data and Cumulative Data	78
Figure 4.6. Fuel Pressure Data	80
Figure 4.7. Summarized Fuel Pressure Data	85
Figure 4.8. Example Motor Current Data on March 18th 2005	87
Figure 4.9. Average Motor Current and Standard Deviation	88
Figure 4.10. Example I_{thr} During an Event Transition	99
Figure 4.11. Example I_{thr} Data Over a Single Cycle	100
Figure 4.12. I_{thr} Throughout the Test, with Regression Analysis	102
Figure 4.13. Mixture Current Measurements on Jan 30th 2005	108
Figure 4.14. Summarized Mixture Actuation Current	111
Figure 4.15. Fuel Pressure from the Fuel Servo to the Flow Divider	115
Figure 4.16. Fuel Pressure from the Servo to the Flow Divider	116

1. Introduction

1.1. Purpose

Indications from the industry and from government suggest that the future of 100LL as an aviation fuel may be short. To the extent possible, an alternative fuel needs to be developed that can replace 100LL with minimal industry invasiveness. To be acceptable, this new fuel must retain the advantageous properties of 100LL while avoiding the introduction of any undesirable properties. Prior to acceptance, a new fuel must undergo a series of tests, beginning with basic soak testing, to screen for material incompatibility. Once materials have been screened, more elaborate tests are required to further verify the safety and efficacy of the fuel within a fuel system. These tests include rig testing and flight testing. To fulfill the need for rig testing, the following work was performed to explore the viability of an ethanol-based fuel for general aviation piston engines.

1.2. Background

Within the realm of spark ignition, internal combustion aircraft engines, there are two major manufacturers representing the bulk of the engines found in use, namely Teledyne Continental Motors (TCM) and Textron Lycoming Engines (TLE). Either manufacturer produces an extensive line of engine systems with various models, sizes and amenities. Engines can be turbocharged or standard, carbureted or injected, pistons can be opposed or inline, and the engine size can vary from less than 200 to over 700

cubic inches. Before an alternative fuel can be approved for use within any of these engines, a series of tests must be conducted to identify any engine failure modes and potential safety issues.

Testing began with an exploration of airframe material compatibility to ethanol and ethanol/100LL blends through a large suite of soak tests at the University of North Dakota Energy and Environmental Research Center (UND-EERC). Materials included metals such as steel and aluminum, and polymers such as rubber and plastics [1]. This type of test is a broad material screening process from which non-compatible materials can be identified and eliminated before more rigorous test methods are employed.

Significant flight testing has been conducted with a Cessna C-180 aircraft equipped with a TCM O-470U/TS engine. This engine is carbureted, opposed, displaces 470 in³, and employs several miscellaneous features indicated by the U/TS suffix. Testing included cool climb, hot fuel climb, detonation resistance, engine restart, engine endurance, and aircraft operational testing. The result of this testing culminated in the issuance of a Supplemental Type Certificate (STC) for both the engine and airframe.

Similar testing is currently underway at South Dakota State University on several other types of aircraft, including fuel economy testing on a single engine Mooney 201 equipped with a Lycoming IO-360-D1A engine. Also, combustion analysis/detonation testing is being performed on a dual engine Piper Seneca equipped with one Lycoming

IO-360-C1E6 engine and one LIO-360-C1E6, as well as a Grumman AgCat G164B aircraft equipped with a Pratt and Whitney R-1340 radial engine.

1.3. Rig Testing

Soak testing provided a basic indication of material compatibility to a certain fuel which led to more rigorous flight testing, such as that described in the previous section. However, on multiple occasions soak testing failed to properly reveal a material's response when the material was subjected to typical stresses encountered both in manufacture and operation, such as stretching, compression, rubbing, submersion and evaporation, operating temperatures and pressure, etc [2]. An example was in the original development of 100LL aviation fuel in the 1970's. As the fuel began to be implemented among the general public, an extensive list of problems began to develop, relating to seal swelling and shrinkage, as well as other issues related to the viscosity of the fuel. Significant actions were required to correct these issues [2].

To assist in preventing such issues in the future, small scale testing referred to as a rig test was mandated by the Federal Aviation Administration. Rig testing consists of cycling a fuel through a fuel system's components as the components are actuated in a fashion emulating typical aircraft operation. Figure 1.1 shows an example rig test setup developed by Cessna Aircraft [2]. The various pressure and flow rate gauges can be clearly seen in the figure. Fuel is cycled continuously through an aircraft's fuel pump

and flow controller, as an operator adjusts the pump speed and settings of the fuel servo, and records the corresponding data, revealing the status of the components.

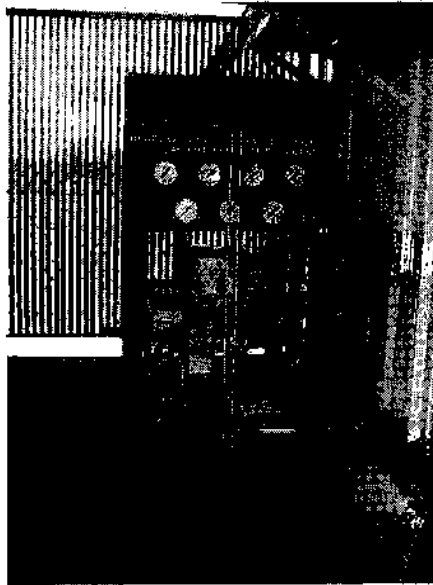


Figure 1.1. Cessna Rig Test Set-Up. (photo courtesy Cessna Aircraft).

To date, rig testing has been performed and documented only twice, with little corresponding formal regulations regarding test setup and procedures. Both tests were performed by Cessna Aircraft, the first test began in August of 1996, ended April of 1997, and was detailed in [2]. This test was conducted using 82UL fuel, as a potential aviation fuel. A second set of tests were performed between January and August of 2001. These tests evaluated both Aviation Grade Ethanol 85% (AGE85) and Ethyl tertiary butyl ether (ETBE) as candidate aviation fuels, in comparison with 100LL [3].

The test described in [2], performed on 82UL, showed several instances of fuel seepage, though none were considered substantial, nor led to test shutdown. The test described in [3] using AGE85 and ETBE concurrent with 100LL likewise found several leakage issues, though they were considered more severe than with 100LL, and led to component failures.

The project described in this paper tested the dynamic effect of AGE fuel using components manufactured by Teledyne TCM Motors. The components themselves were a model 646212-23A1 fuel pump and model 639715A16 fuel flow controller, commonly referred to as a fuel servo. These particular parts are often found incorporated into an IO-520 engine and were chosen as typical representatives of fuel injection systems manufactured by TCM Engines. Initial calibrations set the components to operate at 120% of required fuel flow, with excess flow shunted back to the fuel tank.

The test reported here was loosely modeled after Cessna's rig test design. As stated in the preceding discussion, rig testing is an uncommon test with little background and loosely defined testing methods. Cessna testing created an enclosed fuel system with continual fuel flow, but relied on component disassembly and inspection, performed at the test conclusion, with little data regarding system status throughout the course of the test. The rig test described in this paper attempted to provide more information regarding system status during the test, without disassembly and minimal external contact.

Ethanol-based fuel was stored in a fuel tank and circulated through the pump and fuel servo. A DC motor rotated the pump at speeds consistent with aircraft flight. As the fuel was circulated, actuators (small DC motors) adjusted the mixture and throttle settings, emulating the settings that occur during stages of engine priming, idle, taxi, takeoff, cruising, descent, taxi and shutdown, when the system simply sat idle and soaked in the fuel. During operation, data were recorded to measure the status of the system throughout the test. These data included humidity, air and fuel temperature, pump and throttle pressure, and the electrical current through the pump motor, as well as the peak current of the actuators during a transition. These final three metrics are indicators of the torque required to pump the fuel as well as adjust the fuel servo settings. A personal computer controlled the timing and operation of the test and recorded the data throughout each test cycle. The TCM rig test setup is shown in Figure 1.2.

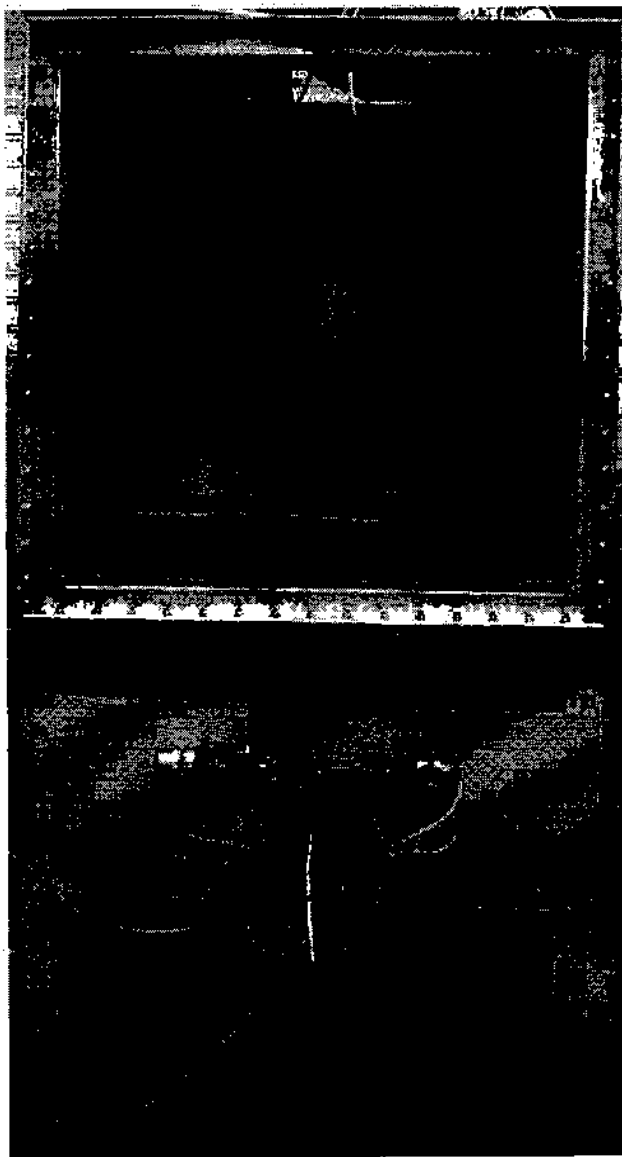


Figure 1.2. TCM Fuel System Rig Test.

1.4. Objectives

The purpose of this project was to determine the effects of ethanol-based fuel on TCM manufactured fuel system components over the course of a typical lifetime, excluding the influence of internal combustion. Factors considered included the condition of slip rings, valves and internal surfaces after 4000 hours of cycling fuel at various speeds, mixture and throttle settings. The test was intended to continuously subject the fuel system to emulated flight fuel flow conditions, as well as continuously log data capable of indicating changes in the status and performance of the fuel system. As with the rig tests conducted by Cessna, the fuel temperature was not heated, but regulated by ambient conditions.

The data provided an indication of the amount of torque required to circulate the fuel as a determinant of the status of the pump seals, bearings and internal walls. Also, the torque required to adjust the mixture and throttle settings was to be evaluated as an indicator of the condition of the slip rings around the fuel servo adjustment levers. As an indication of pump and servo performance, the fuel pressure leaving the pump and the fuel pressure returning to the tank through the flow divider also needed recording.

2. Project Requirements

This chapter presents the requirements related to the test described in this paper. Beginning with a discussion of the operational requirements, this chapter then presents the mechanical requirements, and concludes with the electronic requirements.

2.1. Operational Requirements

The test required a TCM fuel pump and fuel servo to circulate AGE fuel through a closed system for a total of 4000 hours, plus an additional 1500 hours of soak time, during which the fuel was not circulating.

The objective was to simulate an aircraft's lifetime operation. Therefore, the time requirement was divided into a repetitive seven event cycle, during which the pump speed and throttle/mixture settings were adjusted in a manner consistent with aircraft operation. Table 2.1 displays the event timing scheme. The timing scheme was created through the advice of several licensed pilots, with significant experience flying aircraft relevant to the tested components.

Since the system was to run continuously, the design was required to be completely automated; once the event parameters were set, the pump speed and servo settings were to adjust automatically according to the timing scheme.

Table 2.1. Rig Test Timing Cycle

Event	Duration	Pump Speed (RPM)	Throttle Position (%)	Mixture Position (%)
Prime Engine	1 minute	0	100	100
Start Engine	1 minute	700	0	100
Taxi	5 minutes	1000	10	100
Takeoff	10 minutes	2700	100	100
Cruise	3 hours	2400	70	70
Descent	5 minutes	1800	50	100
Taxi	5 minutes	1000	10	100
Shutdown	2 hours	0	0	0

Since changes in the status and performance of the fuel system were to be monitored, data pertinent to the system needed to be continuously logged throughout the test. The data included air and fuel temperature, humidity, fuel pressure leaving the pump, and fuel pressure to the flow divider. Finally, data regarding the torque applied to circulate the fuel and adjust the mixture/throttle settings was needed to indicate performance degradation of the fuel pump and servo throughout the test.

The system was required to sample and log the data into an Excel spreadsheet every three seconds during the initial 30 seconds of each event transition, and every 30 seconds thereafter.

2.2. Mechanical Requirements

This section describes the physical system exposed to ethanol fuel including the fuel tank, lines, pump, etc. Beginning with an overview of the physical system as it

interacts between components, the following sections describe individual components and test requirements related to the components.

2.2.1. Mechanical Requirements Overview

This project was intended to simulate the performance of a TCM manufactured fuel pump and servo. The simulation required isolation of the fuel pump and servo from the rest of an aircraft and subjection of these parts to an emulated aircraft lifetime of pumping fuel and adjusting the mixture and throttle settings. A closed system was required in which AGE fuel was circulated from a stationary tank through a fuel filter by the fuel pump. The fuel then flowed into the fuel servo where it was returned to the fuel tank either through a flow divider (emulating fuel flow to the engine), or straight back to the tank via a return hose. Figure 2.1 gives a pictorial explanation of the circulation paths.

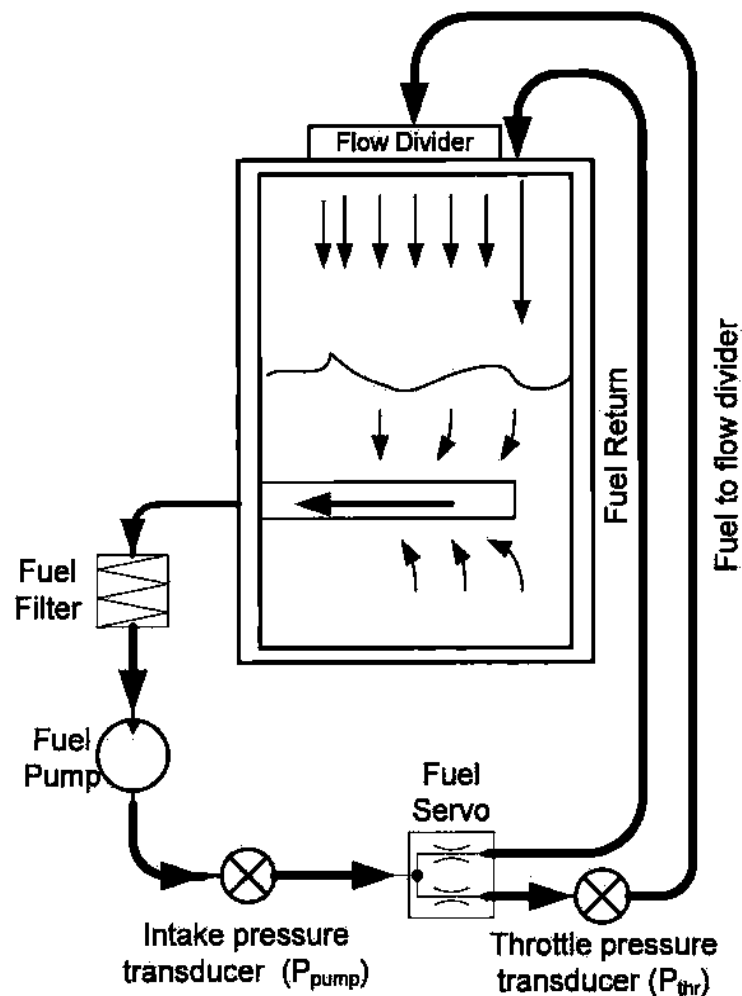


Figure 2.1 Basic Fuel Flow Diagram.

The mechanical system can be divided into three modules each having specific functions and external requirements. The module definitions are shown in Fig. 2.2. The first module included the fuel pump, the second included the fuel servo, and the final consisted of the auxiliary parts and flow divider. Two pressure transducers were introduced into the system at significant points within the circulation path.

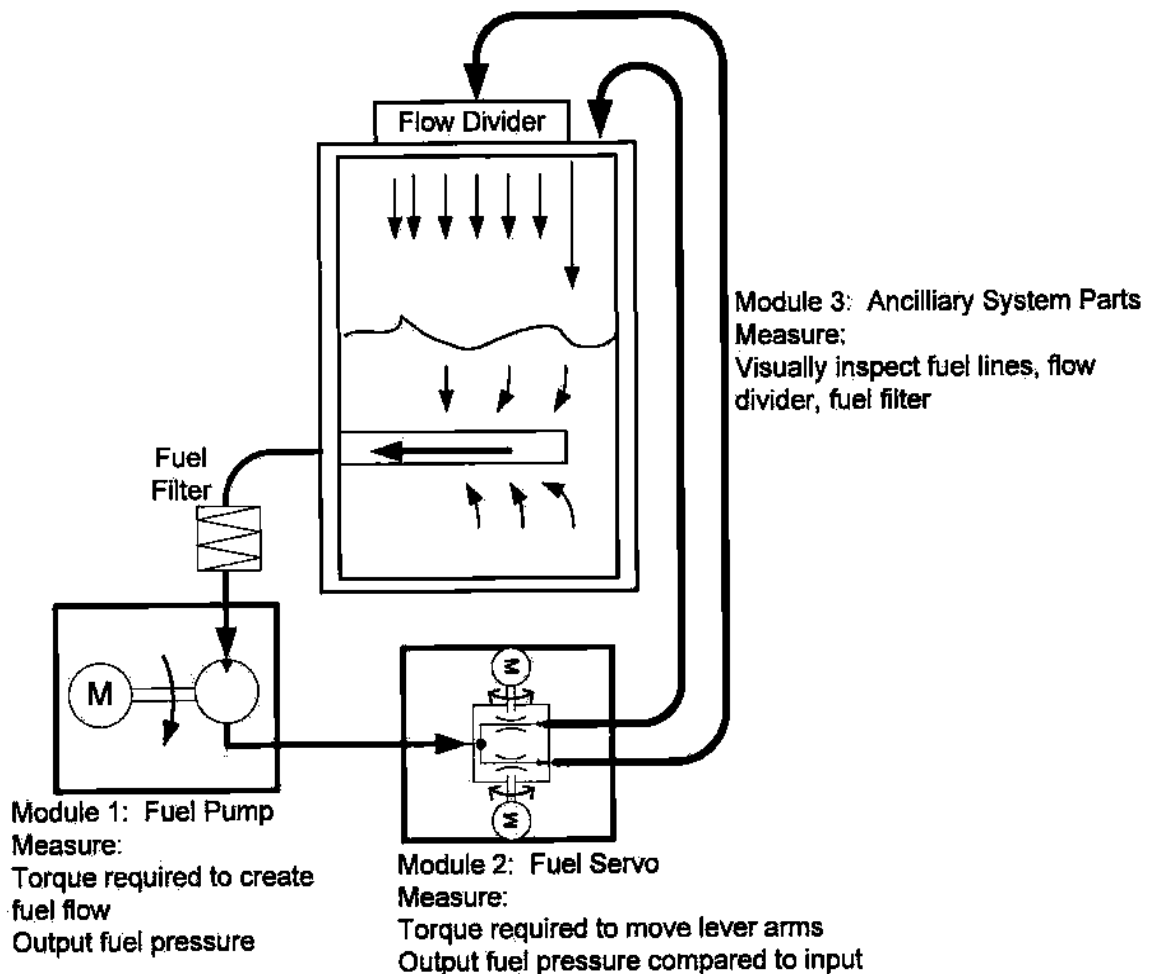


Figure 2.2. Module Definitions.

2.2.2 Module 1: Fuel Pump

The pump evaluated in the test was a TCM fuel pump model 646212-23A1 (serial number B03BA170R), normally found integrated into an IO520-B aircraft engine. This style of pump is of a rotary vane design, and under takeoff conditions is expected to

operate at 2700 RPM. By rotating the internal shaft, turbine blades within the pump circulates the fuel. Figure 2.3 shows an image of the particular pump used. The system design was required to rotate the pump at various speeds according to the timing scheme of Table 2.1.

Possible degradations within the fuel pump include corrosion/buildup of the seals resulting in a change in the torque required to pump an equal amount of fuel, or corrosion/buildup along the walls of the pump, resulting in a change in the output fuel pressure. The test was required to record these metrics as an indirect indicator of pump degradation.

The described fuel pump is calibrated with a 20% overflow. A new or overhauled fuel pump is designed to circulate 120% of the needed fuel; any fuel not required by the engine is shunted back to the aircraft fuel tank. This establishes the threshold level considered alarming within the test. Provided the fuel pump continues to operate within 20% of original levels, the unit is delivering all the fuel required by the engine. The torque requirements do not share in a specified tolerance. So long as the motor is capable of circulating the fuel, it is considered working. Therefore, increasing torque requirements could lead to a failure mode, as the pump may become locked. Decreasing torque requirements imply the pump is working more efficiently.



Figure 2.3. TCM Fuel Pump.

2.2.3. Module 2: Fuel Servo

The fuel servo required for the test was a TCM model 639715A16 fuel flow controller, normally integrated into an IO520-B aircraft engine. This particular servo relies on a pair of levers to vary the fuel throttle and mixture. A simplified diagram is shown in Fig. 2.4. The throttle lever adjusts the amount of fuel allowed to enter the servo, and the mixture lever adjusts the ratio of fuel flowing to the flow divider (emulating fuel for combustion) and the return hose. Both lever arms had a 90° range of motion, and their position adjusted the mixture and throttle, respectively. The mixture's arc was centered when the lever arm is extended perpendicular to the fuel outlet, and the throttle lever's arc was centered when the arm is parallel to the fuel outlet. The system design needed to be able to consistently adjust the position of the lever arms throughout.

the test to emulate the settings of the timing scheme of Table 2.1. Initial testing of the required torque to position the lever arms revealed that at most three kg-cm was required to induce rotation of the lever arms at the desired rotational speed, chosen to be approximately 20 RPM. The test was intended to provide only a rough estimate for motor sizing.

When installed in an aircraft, the pilot rotates a pair of control levers which are linked through several meters of a stiff cable/housing line to the servo installed near the engine. A motion of the pilot's entire arm is required within the cockpit to position the control levers, and far exceeds the torque required to position the lever arm at the servo. Doubling or even tripling the torque required to position the lever arms at the servo would likely be imperceptible to the pilot. The lever arms must remain mobile, however, changes of 100% are not considered alarming over unit's lifetime.

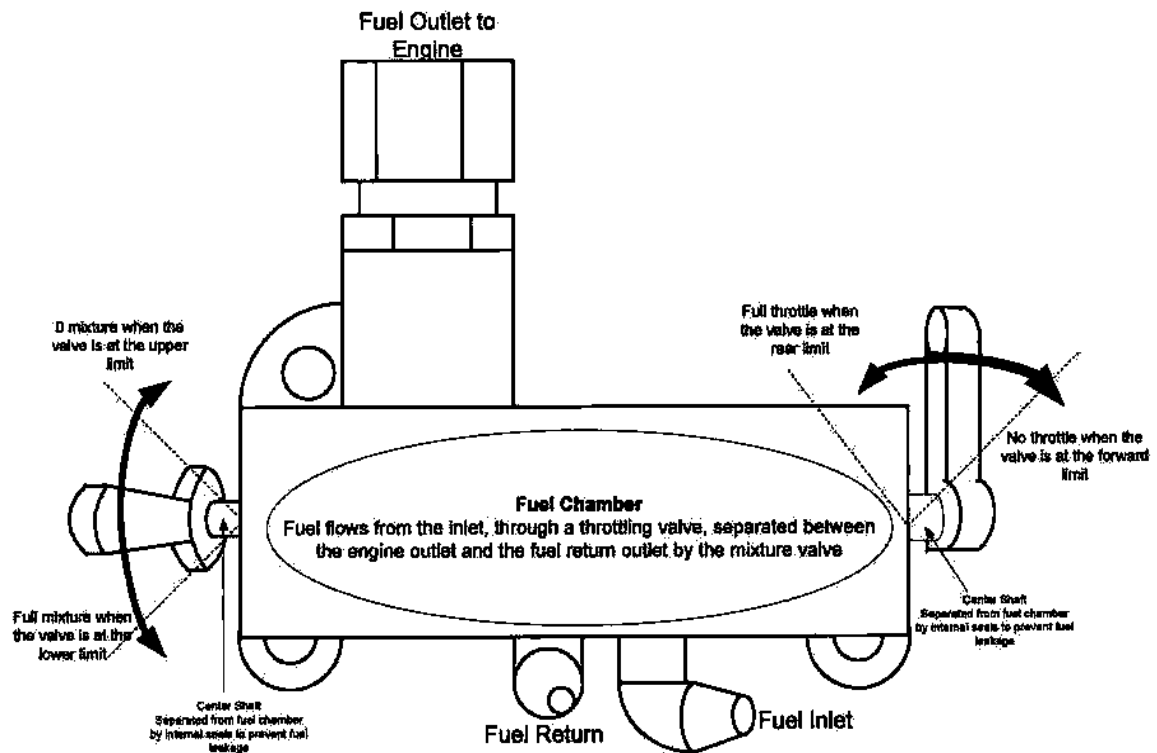


Fig. 2.4. Simplified TCM Fuel Servo Diagram.

Possible degradations within the fuel servo resulting from ethanol fuel include corrosion or buildup on the seals around the lever arm's center shaft, resulting in a change in the torque required to adjust the lever arms, or corrosion/buildup within the fuel chamber and flow separation paths themselves, resulting in a change in the output fuel pressure. The test was required to measure these parameters.

2.2.4. Module 3: Auxiliary Parts

The final mechanical parts required for evaluation throughout the test included a flow divider, shown in Fig. 2.5, fuel filter (see Fig. 2.6), fuel tank and fuel lines, (see Fig. 1.2, Fig. 3.4). The flow divider was responsible for ensuring an equal amount of fuel flow to the six cylinders, as well as preventing leakage by stopping all fuel flow if the input fuel pressure fell below a certain threshold. The fuel tank was required to store the fuel used throughout the test and the filter was required to prevent damaging particulates from circulating through the system. A visual inspection at the conclusion of the test was also required to reveal degradations to any of these parts.



Fig. 2.5. TCM six-cylinder Fuel Flow Divider.

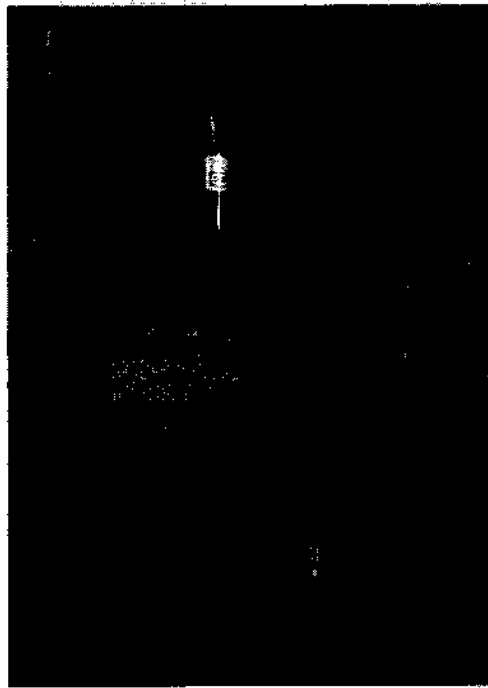


Figure 2.6. Fuel Filter.

The fuel tank itself was constructed out of 1/8th inch sheet aluminum, bolted along the seams using a mixture of 10-32 brass and galvanized nuts and bolts. A clear sheet of 1/4 inch tempered glass was placed at the front of the tank, to allow visual observation of the fuel throughout the test. The glass was sealed using standard silicon caulk, and the metal joints were sealed using polysulfide epoxy.

2.3 Electronic Requirements

This section describes the electronic requirements of the test, such that the mechanical system could be evaluated for its response to AGE. It begins with an

overview of the electronic requirements. Then requirements specific to the fuel pump, servo and auxiliary electronics will be discussed.

2.3.1. Electronic Requirements Overview

The operational and mechanical requirements stated that the test would necessitate two functions: control and measurement. The electronic system was required to automate the system settings, namely pump speed and servo lever arm positions at predetermined intervals. The electronic system was also required to continuously log the data regarding the status of the system. The data was required to be stored at a maximum of 30 second intervals. The data was to be stored into spreadsheet files that would be evaluated at during the test.

2.3.2. Module 1: Fuel Pump

The timing scheme presented in Table 2.1 indicates the speed of the pump must be adjusted to various levels for specific intervals of time. The range of speed settings for this particular pump was zero to 2700 RPM, simulating a fuel pump in an aircraft from shutdown to takeoff. The electronic system was required to provide a means of rotating the fuel pump, and automatically adjust the speed of the fuel pump according to the timing scheme. Also, the electronic system was required to indicate the torque applied to the fuel pump as a determinant of the status of the seals and bearings, as well as measure the pressure of the fuel flowing out of the pump, as an indication of the condition of the walls along the fuel path.

2.3.3. Module 2: Fuel Servo

The timing scheme presented in Table 2.1 indicates the position to which each of the servo's lever arms must be adjusted throughout the test. The adjustments required a 90° range of motion, and must move at a speed consistent with a pilot adjusting a control in the cockpit, approximately 20 RPM. The electronic system was required to automatically position these lever arms in a controlled fashion, as well as indicate the torque required for the adjustment as an indication of the condition of the seals surrounding the lever arm axial shafts. Also, the fuel pressure leaving the servo needed to be measured, as an indication of the condition of the walls and valves within the servo.

2.3.4. Module 3: Auxiliary Electronic Devices

Finally, the operational requirements stated that the air/fuel temperatures and the ambient humidity throughout the test were to be measured. The electronic system was required to record this data as well.

3. Project Design

The previous chapter detailed several assumptions, requirements and goals related to the test. This chapter details design of the test system implemented to evaluate the mechanical fuel system discussed in Section 2.2. First, an overview of the system is presented, listing interdependencies between modules, controllers and sensors. Then, the detailed design of particular modules, controllers and sensors is offered.

3.1. Design Overview

The project design methodology is summarized in Fig. 3.1. A computer was interfaced to the mechanical modules such that the settings of the fuel pump and servo were controlled according to the timing scheme presented in Section 2.2. Also, the data pertinent to the status of the rig test were continuously logged by the computer.

Figure 3.2 gives a pictorial explanation of the system. First, the computer yielded the highest level control of the system by providing a user interface, as well as automating the event timing according to the lifetime requirements, while logging data collected throughout

A commercial-off-the-shelf (COTS) data acquisition card (DAQ) provided a means of input/output communication between the computer and the external electronics shown in the interface board. The DAQ card transformed the PC's binary numbers to

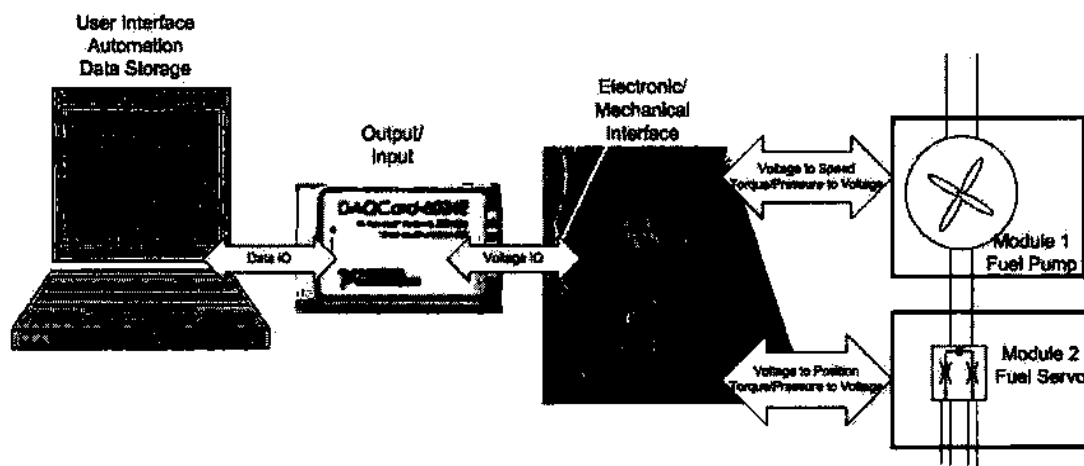


Figure 3.2. System Interface Flowchart.

The external electronic system was designed to provide the electronic/mechanical interface to the physical system. Here, control voltages from the DAQ card were implemented to cause the fuel pump to run at desired speeds, and the actuators to move to desired positions. The electronic system was also responsible for converting metrics such as pressure and temperature into discernable voltages for the DAQ to measure.

Module 1 revolved around the TCM fuel pump described in Section 2.2.2. A 48 V, 8.1 A permanent magnet DC (PMDC) motor and motor drive was chosen to provide power needed to circulate the fuel. Figure 3.3 shows the motor used, coupled to the rear of the pump. For a complete description of the motor refer to Section 3.5. The coupling itself was custom designed and built by SD Tool and Die, operating in Brookings, SD.



Figure 3.3. Fuel Pump Motor, Motor Drive and Coupling.

The fuel servo tested was described in Section 2.3.3, and an image of the actual setup is shown in Figure 3.4. The lever arms were positioned with the small DC motors marked by A and B; these will be referred to as the actuators throughout this text.

The fuel pressures were also measured at the servo. The inlet pressure (corresponding to the pump pressure) was measured by the lower pressure transducer, marked with a C in the diagram, and the fuel pressure to the flow divider was measured with the transducer marked as D.

During the test, ephemeris data were also recorded, including fuel and air temperature and ambient humidity.

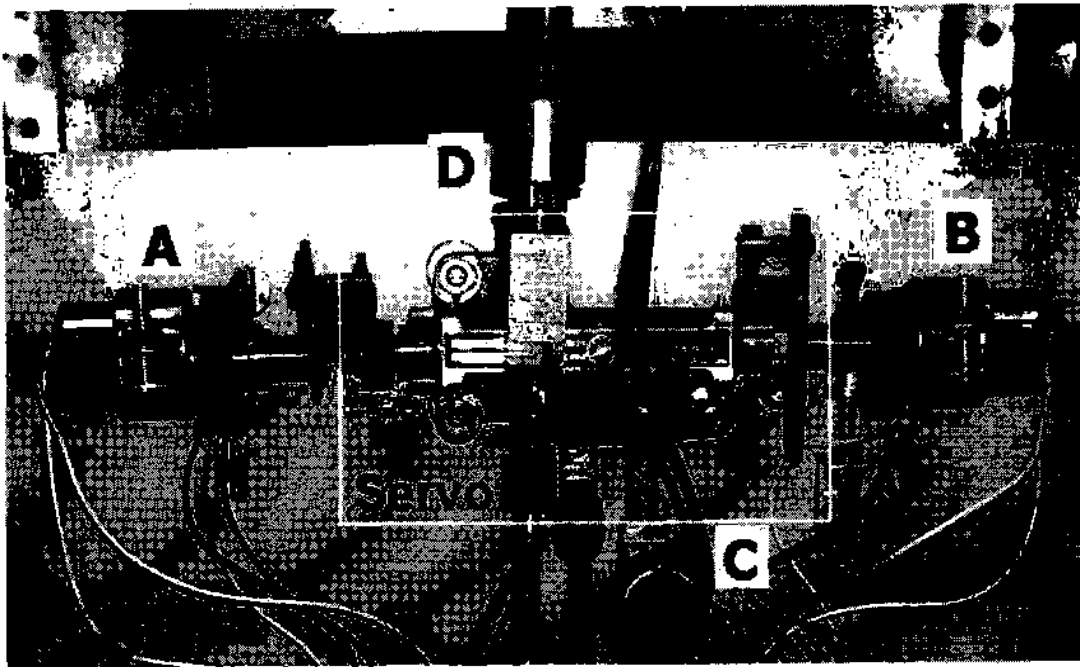


Figure 3.4. Fuel Servo Setup.

3.2. User Interface

National Instruments Labview software was used to create a user interface between the test setup and the observer. Information regarding the software can be obtained through National Instruments at www.NI.com. The selection of this software was determined by two factors. First and foremost, this software was packaged together with the DAQ card chosen. The DAQ card itself will be discussed in the next section;

and since the software and hardware were packaged together, they were designed to be fully compatible with one another. Also, this software was chosen because it provides a simple framework for creating application-specific graphical user interfaces. An image of the interface built for this project is shown in Fig. 3.5.

Running graphs of the measured data were displayed in the top portion of the interface. In reading order, the upper left graph displayed the pump and throttle pressure, the adjacent graph displayed the motor current, then the right graph showed the servo actuation currents. Below, the air and fuel temperatures were displayed, and finally, the ambient humidity.

The settings for the eight events were controlled by the portion in the lower half of the interface. Here the user set the duration of each event, followed by the speed of the fuel pump during the event, and the sliders were used to set the position of the mixture and throttle lever arms.

As the test ran, the data were stored into Excel spreadsheet files for evaluation. Data were saved every three seconds during the first 30 seconds of an event, and stored every 30 s until the onset of the next event. Each file contained six cycles (approximately 32 hours) worth of data, with each sample time stamped in the first column, with following columns listing air temperature, humidity, fuel temperature, throttle pressure, pump pressure, motor current, peak throttle current, peak mixture current, mixture setting, throttle setting, and motor speed.



Figure 3.5. User Interface.

3.3. Data Acquisition (DAQ) and Control

Overall, the project required a portable computer to be able to both control certain system parameters (pump speed, position of the mixture and throttle lever arms) and measure other parameters (fuel pressures, torques, etc.). The fulcrum of the electronic system therefore revolved around a computer interface card, capable of both input (analog to digital conversion) and output (digital to voltage) interface. A National Instruments 6024E PCMCIA Data Acquisition Card (DAQ) was chosen as the interface. Reference [4] includes a full manufacturer specification datasheet. Because this card is capable of sampling 16 analog channels, has two ± 10 V analog output channels, eight TTL capable digital output ports, as well as two general purpose counters, capable of recognizing an external trigger, or generating a controlled trigger, all the input/output requirements of the project were met. Table 3.1 presents the relevant specifications of the DAQ, as well as a description of the use of the ports. As a secondary criterion for the selection of this particular device, and as mentioned in the preceding section, the DAQ card was packaged with Labview software. Since both were National Instrument products designed to complement each other, software compatibility issues were prevented.

Table 3.1 DAQ specifications

Specification	Number	Range	Use
Analog Input Channels	16	+/- 10V	Measure: Fuel/Air Temperature Fuel Pressure (pump and throttle) Humidity Motor Current (Pump, Mixture, Throttle)
Digital Counters	2	TTL	Peak Detector Reset
Digital Output Channels	8	TTL	Pump motor speed control signal
Analog Output Channels	2	+/- 10V	Mixture/Throttle actuator control signal

3.4. Interface Board

The DAQ card was interfaced to the other modules via an electronic interface mounted on an interface board, designed and assembled primarily by myself, with assistance and advice provided by Dr. Stephen Hietpas. The board component layout is shown in Fig. 3.6. Connector J1, located at the left of the figure, interfaced the DAQ card to the board through a series of 24 AWG wires. The board was powered using an AC to DC power supply, having supply voltages of +24, +15, +5 and -15 V. The 24 V supply was separated from the other voltages and was used to power the humidity sensor. Electrical grounding and the remaining supply voltages were connected through J2. External connections between the electronics and mechanical system were grouped in connectors J3 through J5. Individual electronic components within the board are discussed in Sections 3.5 and 3.6, as they relate to their respective modules.

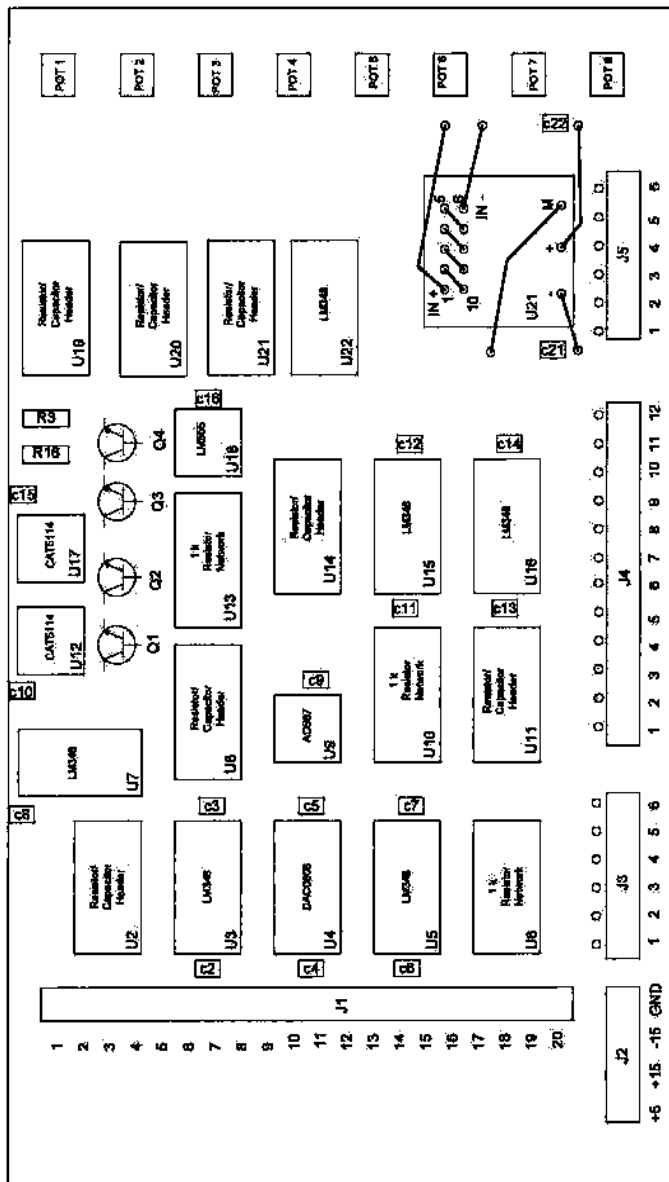


Figure 3.6. DAQ/Electronic Interface.

3.5. Module 1: Fuel Pump Drive

Section 2.3.2 described the requirements of Module 1. These included providing a means of controlling the speed of the fuel pump, as well as measuring the torque required to pump the fuel, and the pressure of the fuel exiting the fuel pump. The following sections describe the design of the interface between the computer and the fuel pump. First, the pump speed control system is described, followed by the measurement scheme used to monitor the status of the fuel pump throughout the test.

3.5.1. Fuel Pump Mechanical Design

The fuel pump requirements were described in Section 2.2.2. The pump had to be coupled to the motor. As mentioned, this coupling was custom designed by SD Tool and Die. The coupling was a simple aluminum block housing which linearly affixed the motor shaft to the rotary shaft of the fuel pump, as well as maintaining a stable base for both the pump and motor. The coupling was direct; no gearing was incorporated, resulting in a one-to-one motor-speed to pump-speed relationship.

3.5.2. Fuel Pump Speed Control

The fuel pump was powered by a COTS system, consisting of a PMDC motor and motor drive. Selection of a PMDC drive was convenient, in that motor speed is dependent on applied voltage and, at reasonable loads, the speed is independent of load

[5]. Based on the loading anticipated throughout this test, an open-loop speed control system was considered sufficient to satisfy test requirements.

Sizing the motor was particularly subjective. All that was certain was that the speed of the motor had to be variable between zero and 2700 RPM continuous. The load itself was difficult to characterize, in that it had to be considered not only at the onset of the test, but also inferred at the end, after many thousands of hours of operation. During this period the load may have varied drastically, or perhaps not at all (hence the purpose of performing a test). Based on industrial recommendations and prior experience of Dr. Steven Hietpas, a model 3130-48/0 PMDC Servo motor, having a nominal rating of 3300 RPM at 48 Vdc and 8.1 A was chosen. At rated speed, this motor was capable of producing approximately 80 oz-in of torque, which was, at the onset of the test, oversized. However, an oversized motor seemed appropriate, as the load at the end of the test was indefinite, and could increase significantly.

Similarly, selecting the motor drive was subjective. All that was certain was that it needed a means of varying the applied voltage to the motor to vary the speed, determined by a simple 0 to 10 V command signal, as well as supply all the needed power at full load. Again, based on industrial recommendations and prior experience, a Dynetic Systems model D-700 servo amplifier was chosen, because it was designed to be fully compatible with the selected motor, and was capable of varying the voltage applied to the motor. This motor drive had a maximum continuous output of 6 A at 48 Vdc, and

regulated the motor speed through pulse-width-modulation (PWM) of the power applied to the motor. The voltage applied to the motor was pulsed between 0 and +48 V at a high frequency (33 kHz). By varying the percentage of time the voltage was applied to the time when no voltage was applied, the average voltage to the motor was likewise varied, and with it, the average speed of the motor.

Control of the duty cycle was accomplished by supplying the motor drive with a 0 to 10 V command signal. At 10 V command, the armature was continuously supplied with 48 V, and with a 5 V command, the armature was supplied with +48 V for 15 μ s, and 0 V for 15 μ s, with other command-signal/pulse-width ratios determined accordingly.

The command signal was created using the digital I/O lines of the DAQ card. Figure 3.7 presents a schematic diagram of the conversion of the user specified pump speed to a corresponding command voltage. First, the software converts the desired speed set by the user (in RPM) to a corresponding 8-bit digital number. The digital output port of the DAQ was set to this number, and a digital-to-analog converter (D/A) on the interface board created a 0 to 10 V command signal.

The equation shown within the triangle of Fig. 3.7, relating the desired RPM to a digital number was determined through empirical testing. The speed of the motor was measured as the command voltage was increased from 0 to 10 V. The speed/voltage measurements were then transformed back to a digital number with a range of 0 to 255.

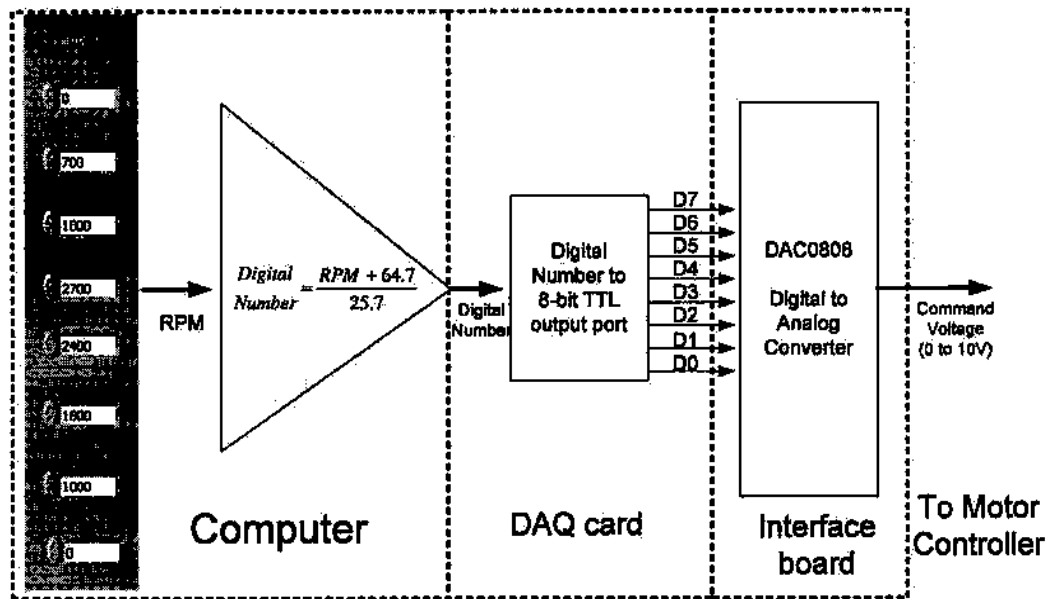


Figure 3.7. Motor control command signal block diagram.

The corresponding circuit design is shown in Fig. 3.8. An AD587 precision voltage regulator provided a 10 V reference voltage. This voltage was the upper rail for the DAC0808 D/A converter. The DAQ card set the digital output lines D0 through D7. When designed as shown in Fig. 3.8, the voltage at pin 8 of the LM348 corresponded to the analog voltage represented by the binary code in pins D0 through D7. The circuit comprised of the LM348, R59, R60 and R61 operates as an amplifier with unity gain. The control signal, referenced to ground, was wired to the motor drive through interface board interconnects J3-5 and 6.

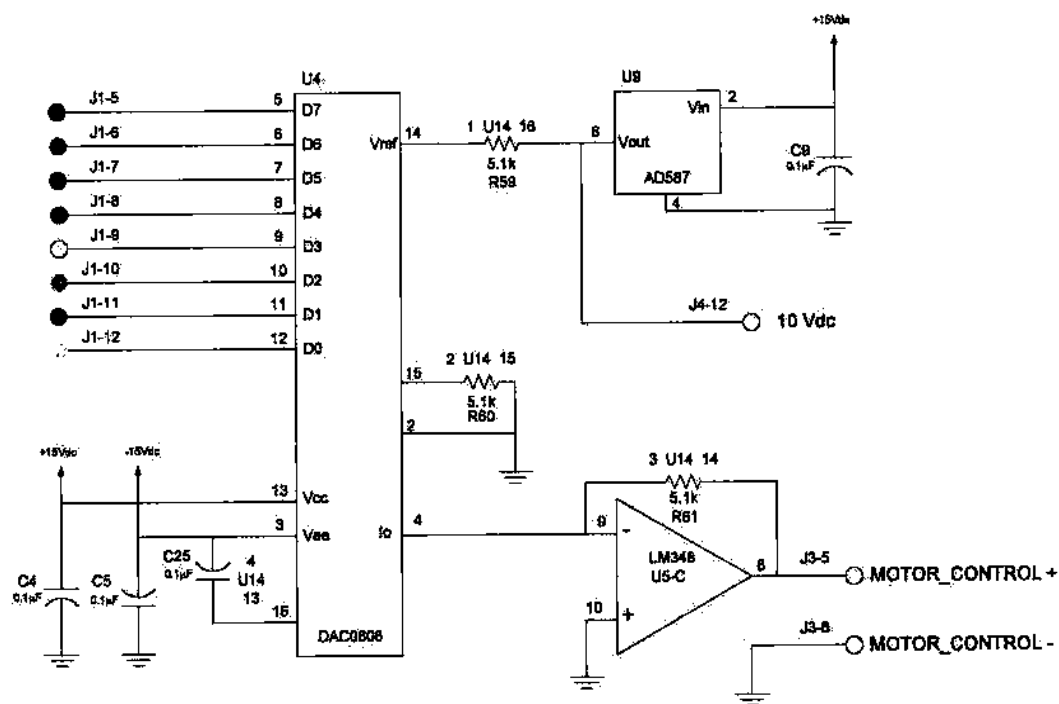


Figure 3.8. Motor Control Signal Detailed Design.

The speed control system described is open loop, i.e. no speed feedback is incorporated. Because the design incorporated a PMDC motor, as mentioned previously, so long as the average armature voltage remained consistent throughout the test, the speed of the motor likewise remained consistent, assuming reasonable loading. Since the applied voltages were determined solely by solid state electronics within the motor drive, the applied armature voltage could be assumed to remain consistent throughout the test.

3.5.3. Fuel Pump Measurement

The electronic design revolving around the fuel pump provided the measurement of two parameters: the current required by the pump motor (I_{mot}) and the output fuel pressure (P_{pump}). Figure 3.9 provides a detailed schematic of the measurements regarding Module 1.

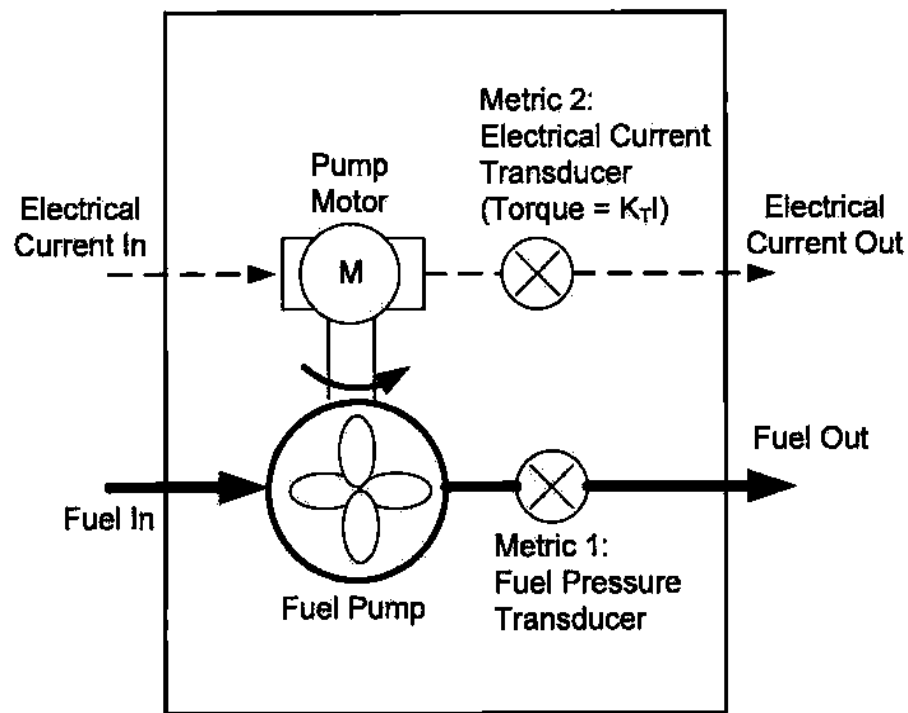


Figure 3.9. Module 1 Detailed Diagram.

Metric 1: Fuel Pressure leaving the pump (P_{pump})

The first indicator to be discussed regarding pump performance was the fuel pressure from the pump to the fuel servo. This metric indicates fuel flow rate; changes

indicates performance change of the pump. Figure 3.10 presents the flowchart regarding the design approach for this metric. The fuel flows through a pressure transducer, which produces a voltage having a range of 0 to 5, corresponding to the fuel pressure according to (3.1). The voltage is amplified on the interface board to have a range of 0 to 10 V, which is measured by the DAQ card. The PC converts the measured voltage back to the corresponding pressure by inverting (3.1).

$$V_{pump} = \frac{P_{pump}}{12.5} + 0.5 \text{ (V)} \quad (3.1)$$

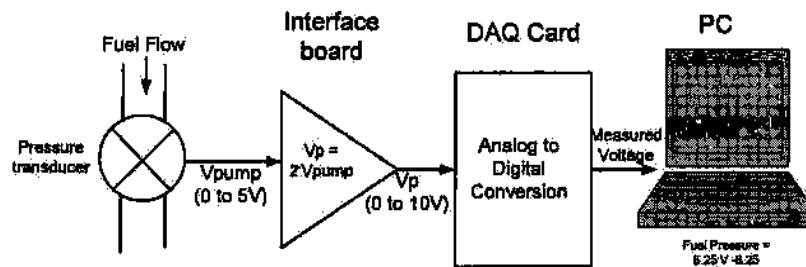


Figure 3.10. Pressure Sensor Flow Chart.

A fuel pressure transducer was placed at the inlet port of the fuel servo. The circuit schematic is shown in Fig. 3.11. A Kavlico P155 fuel pressure transducer was chosen to monitor the fuel pressure. This particular sensor was chosen, as it had an appropriate range of fuel pressure (0 to 50 PSD), and was donated. Full specifications are found at [6]. By supplying the sensor with a 5 V potential, the sensor was designed by the manufacturer to produce an output voltage with a range of 0.5 to 4.5 V. The

specifications for this particular sensor, supplied by the manufacturer, state that the output voltage is linear, and given by (3.1). The design shown in Fig. 3.11 supplies the sensor through J4-7, and grounds through J4-5. The output voltage, V_{pump} , is applied to a non-inverting amplifier with a gain of 2, stepping V_{pump} up to 9 V at full scale. The DAQ recorded this voltage at pin 16 of J1.

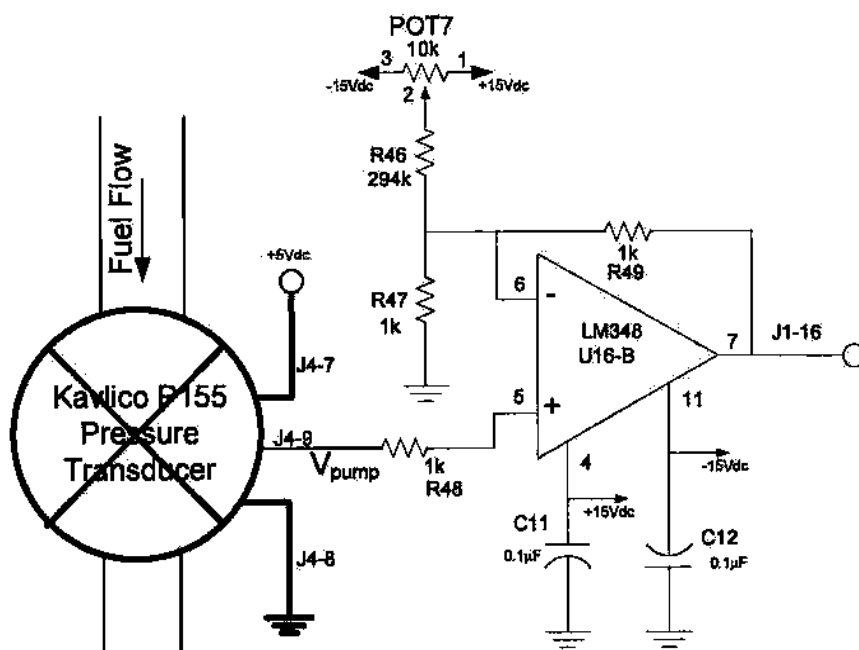


Figure 3.11. Pump pressure sensor schematic.

Throughout the subsequent circuit designs, LM348 operational amplifiers are typically incorporated into an amplifier stage. Appendix A includes a full datasheet, provided by National Semiconductor. This simple integrated circuit (IC) incorporates four individual op-amps into a single chip, reducing the total number of chips needed on

the interface board, as well as allowing four amplifiers to be supplied with a single ± 15 V source. The 15 V bipolar supplies were applied on pins 4 and 12 of each IC, with the capacitors included to reduce noise from the power supply, and neither will be shown in further schematics.

All integrated circuits have inherent non-idealities resulting from fabrication, manufacture, and material variation [7, 8]. Often these non-idealities are negligible. However, to account for these non-idealities, standard circuit design practice includes means to minimize or negate these effects. The potentiometer/resistor network shown in Fig. 3.11, composed of POT7 and R46, serve this purpose. By incorporating these components, small (less than ± 0.05 V) offset voltages resulting from IC non-idealities can be nulled, if needed. The potentiometer was set by grounding J4-9, and adjusting until zero voltage was observed at J1-16. Once set, the potentiometer was untouched throughout the duration of the test.

Metric 2: Motor Current (I_{mot})

For any given DC motor, the torque applied by the motor is given by (3.2) [9]. This equation indicates a direct linear relationship between motor current (I_{mot}) and applied torque (T). The torque constant, labeled K_T , is unique for any individual motor, but constant for that motor. Therefore, monitoring I_{mot} throughout the test gave an indirect indication of the torque applied by the motor to circulate the fuel, and changes in I_{mot} indicated changes in the load of the motor.

$$T = K_T I_{mot} \quad (3.2)$$

Figure 3.12 presents a pictorial diagram outlining the process used to monitor the motor current throughout the test. A current transducer/sense resistor converted the motor current into a measurable voltage, which went through an amplifier to scale the voltage to a level more accurately sampled by the DAQ card.

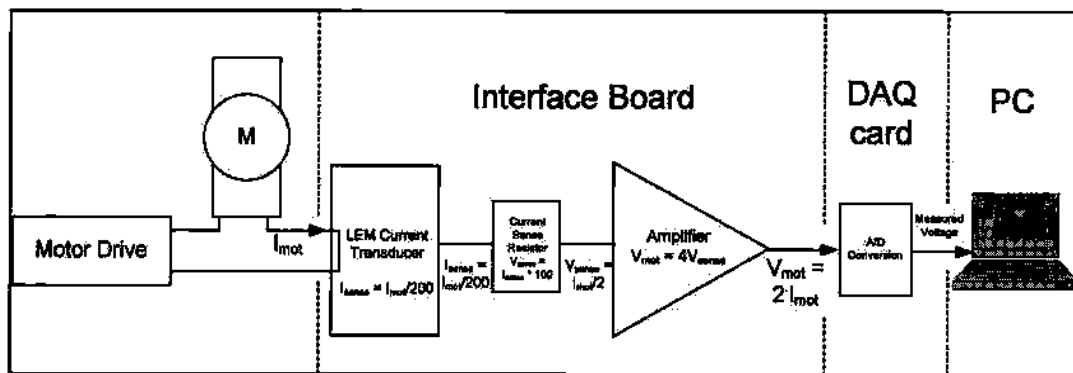


Figure 3.12. Motor Current Measurement Flowchart.

The detailed circuit design is shown in Fig. 3.13. The motor current entered the interface board via interconnect J5 pin 1, which is tied to an LEM LA25-NP current transducer. The motor current then exits the current transducer and returned to the motor drive via J5-2.

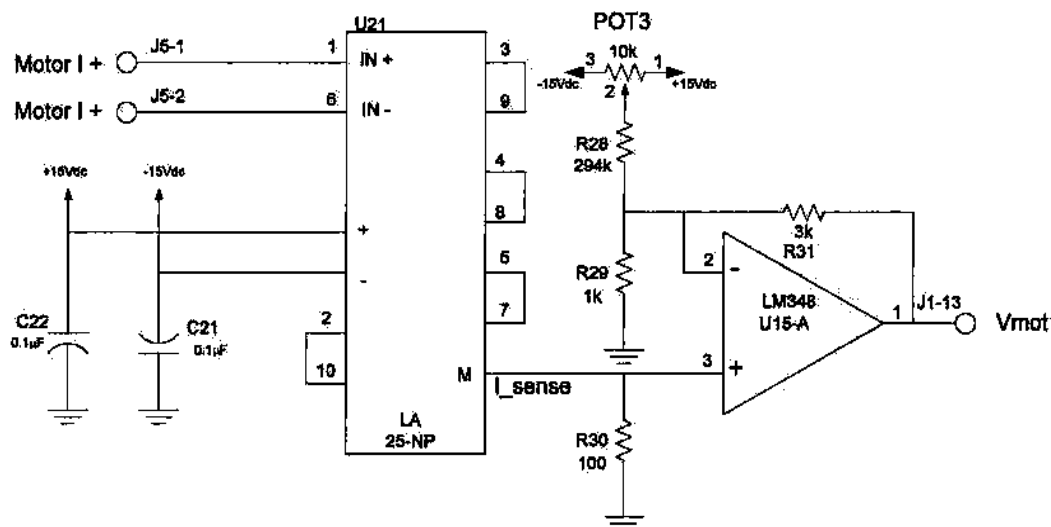


Figure 3.13. Motor Current Measurement Circuit.

Because the voltages at J5-1 and 2 are floating, and the current through the motor could be considerable, the LEM current transducer is incorporated into the circuit. Manufacturer specifications are given in [10]. These transducers are designed to galvanically isolate a large input current from the sensitive electronics required for accurate measurement. They create a copy of the input current, at low power, scaled by a factor determined by the wiring of pins 2 through 10, excluding pin 6, the high-current return pin. The transducer's reduction factor has a range of 0.001 to 0.005. With the pins wired as shown in Fig. 3.14, the current transducer reduces the motor current by a factor of 200, resulting in I_{sense} , which is shunted through a $100\ \Omega$ current sense resistor to ground. Therefore, the voltage at pin 3 of the LM348 op-amp is half the motor current. Preliminary testing indicated the motor current would not exceed 5 A, therefore the voltage at pin 3 of the op-amp ranges between 0 and 2.5. The op-amp is designed as an

amplifier with a gain of 4, yielding a range of 0 to 10 V, to allow the DAQ card full range of measurement. So, after all the scaling, sensing and amplification, the voltage measured by the DAQ at J1-13 has a magnitude twice that of I_{mot} .

The system was calibrated by monitoring the motor current and the voltage at J1-13 with a Tektronix TDS-420 oscilloscope and current probe. This allows the computer to calculate the measured voltage to a corresponding motor current.

3.6. Module 2: Fuel Servo Electronics

Section 2.3.3 described the design requirements for Module 2, the fuel servo. These included a means of controlling the position of the lever arms, both the mixture and the throttle, while measuring the torque required to adjust the mixture/throttle settings between events, and also the fuel pressure between the servo and the flow divider.

The following sections describe the design of the interface between the DAQ and the fuel servo. First, a discussion of the position control system for the mixture and throttle lever arms. Then, the design of the fuel servo monitoring electronics is discussed, including the torque monitoring system and the pressure sensor.

3.6.1. Lever Arm Position Control

The fuel servo tested in this work was described in Section 2.2.3, and the design requirements were presented in Section 2.3.3. Among these requirements was a means of controlling the position of the lever arms over a range of 90° . This section presents the design approach utilized to fulfill this requirement.

A procedural diagram describing the position control scheme is shown in Fig. 3.14. The user set the desired mixture/throttle setting at the computer. The setting is converted to an analog voltage, V_C , by the DAQ card. At the summation node, the position feedback voltage, V_f , is subtracted from V_C , resulting in an error voltage, V_e . An amplifier supplied a DC motor with power, causing rotation of the lever arm. As the feedback voltage, V_f approaches V_C , V_e decreased, reducing the voltage applied to the motor, V_A . When the feedback voltage equals the command voltage, the error signal is zero, the power amplifier no longer has a signal to amplify, therefore, no power is supplied to the motor, and the lever arm remains in place.

At an angular velocity consistent with an aircraft pilot adjusting between mixture/throttle settings (15-30 RPM), initial testing indicated the torque required to rotate the lever arms was approximately three kg-cm. To actuate this motion, two simple 12 V DC motors, manufactured by Jameco Reliapro, model number GH12-1641T-L-R, were chosen. These motors were rated for 20 RPM with a load of three kg-cm (full specs are included in Appendix A). The position transducers were manufactured by

Honeywell/Clarostat, a pair of hollow-shaft rotary potentiometers, TH100 series with a 90° range of motion, and total impedance of $10\text{ k}\Omega$ (see Appendix B for manufacturer specifications). These allowed the appropriate range of motion, as well as related the angle of the lever to a corresponding voltage, as explained next.

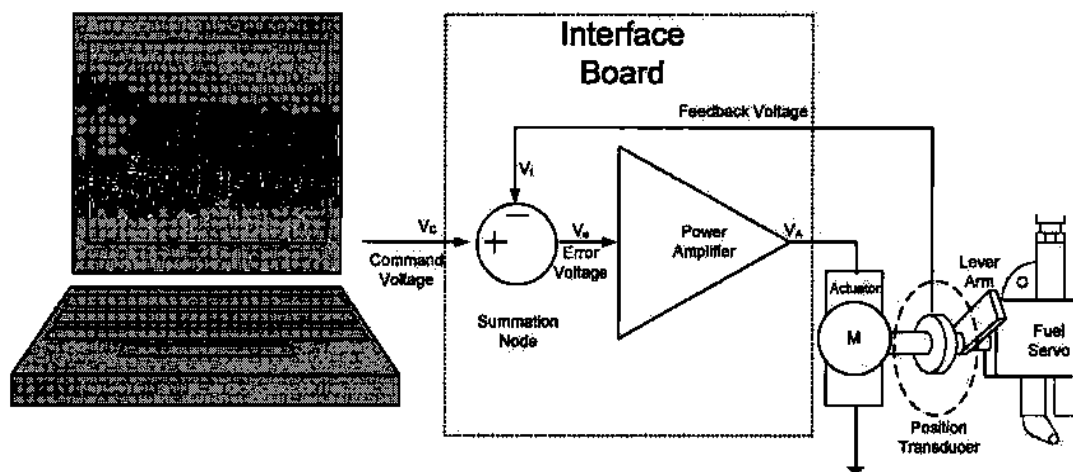


Figure 3.14. Position Control Scheme Flowchart.

Figure 3.15 shows the actual system setup. The actuators are at the far left and right of the image, mechanically coupled to the servo lever arms through the position transducers.

The circuit design of the summation node is shown in Fig. 3.16. The electronic circuit for only the mixture's lever arm is shown; the electronics governing the throttle arm are identical. The position potentiometer was supplied with 10 V via J4-12. As the position of the lever arm rotates, the voltage at the wiper, corresponding to V_f of Fig. 3.14, varies between 0 and 10 V . U15-D, an LM348 op-amp is designed as an inverter,

with a gain of -1. The control signal, V_C , enters the circuit from the DAQ via J1-14. U15-B is designed as a buffer; the voltage at pin 7 is equal to V_C . By joining the voltages of pin 7 and pin 14 through resistors R57 and R58 as shown, the voltage at J4-10 corresponds to half the summation of V_C and $-V_f$, effectively subtracting V_f from V_C to produce V_e as shown in Fig. 3.14.

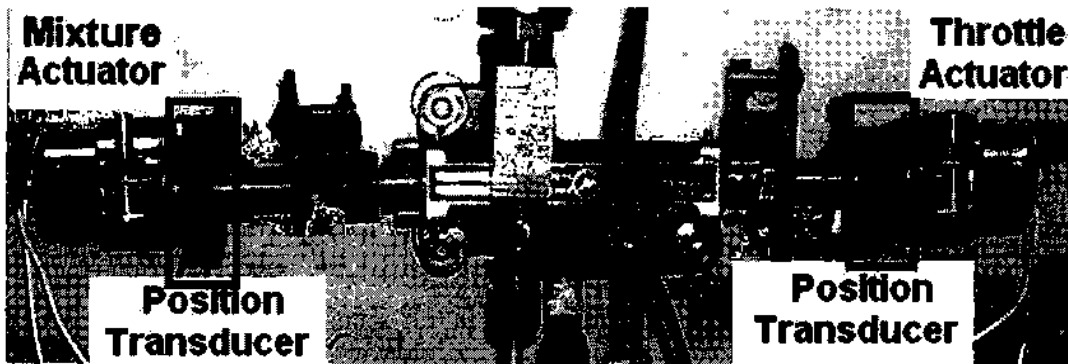


Figure 3.15. Servo Mechanical Setup.

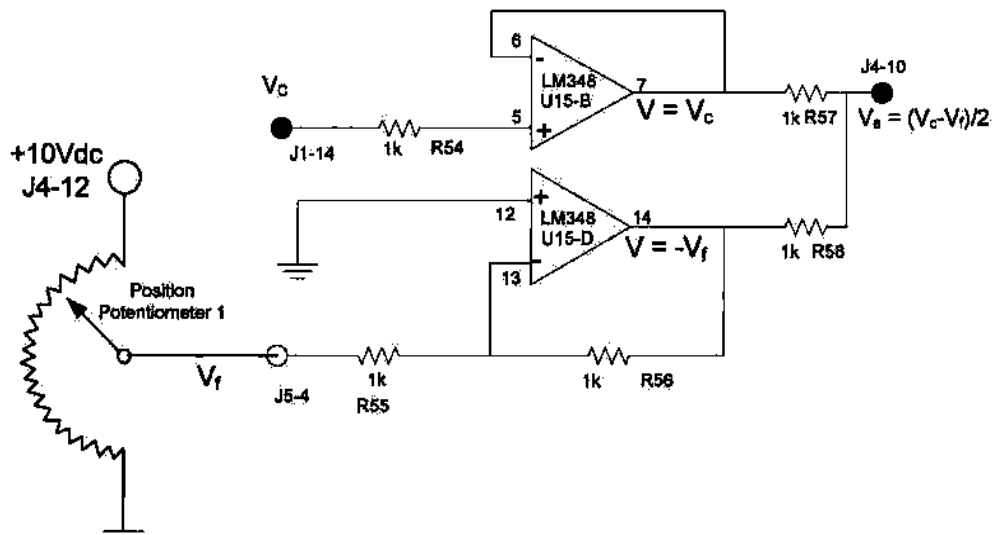


Figure 3.16. Summation Node Detailed Design.

The error voltage was applied to the power amplifier. The power amplifier was placed on a separate board to allow independent power supplies. Figure 3.17 shows the layout of the second board, and Fig. 3.18 shows the detailed design of the power amplifier. The actuation of the lever arms required more current than LM348 op-amps are capable of sourcing/sinking. Therefore, a pair of amplifiers designed to operate with higher output currents were needed. Such a design may allow a potentially damaging scenario. If the lever arm reached a physical limit, yet the error voltage had not reached 0, a motor stall would result. Under this condition, the motor may draw excessive current, overheat and burn out. Therefore, it was expedient to provide some means of limiting the amount of current the motors can draw. The amplifiers chosen were a pair of MS Kennedy 0041 medium power op-amps, having a maximum output current of 0.5 A. This limit was sufficient to prevent damaging current being supplied to the motors. See [11] for manufacturer specifications. To provide some isolation between the actuators (having higher power requirements) and the other electronics (designed for small signals), the amplifiers were given individual power supplies. A pair of 5 V bi-polar DC to DC converters, manufactured by Astrodyne Technologies, part number ASD06-24D5 were used. These stepped the 24 V power source down to dual output voltages of +/- 5 V.

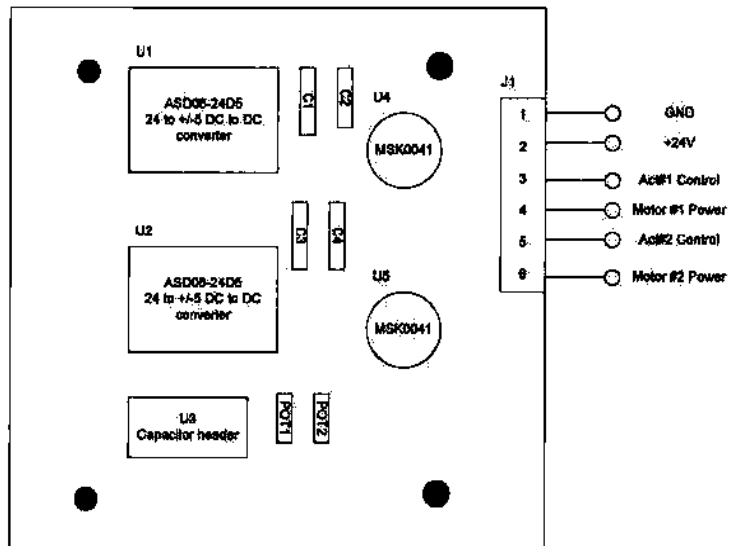


Figure 3.17. Power Amplifier Circuit Board.

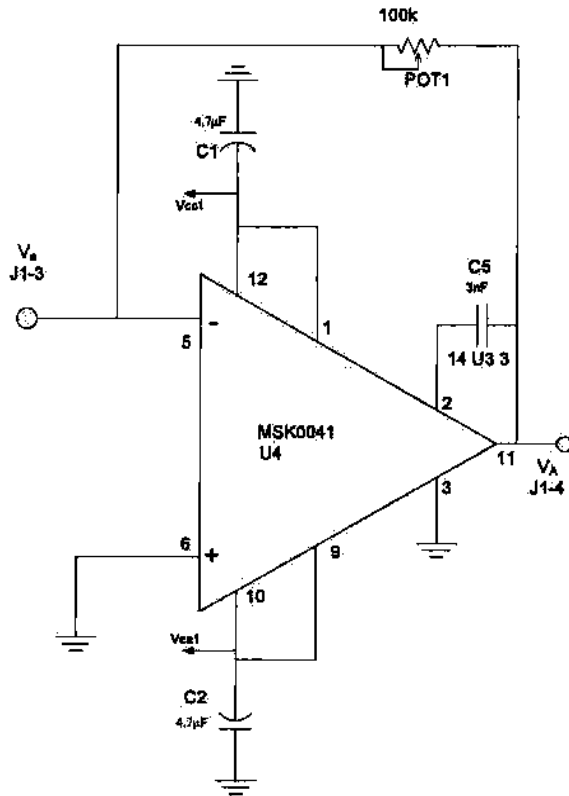


Figure 3.18. Power Amplifier.

Again, only the power amplifier of the mixture lever arm is presented, as the throttle amplifier was an identical design. The error voltage of Fig. 3.16 enters the second board via J1-3. The MSK0041 is designed in an inverting fashion, with a selectable gain determined by the resistance of the potentiometer POT1. The applied voltage, V_A , supplies the actuators with the Electro-Motive-Force (EMF) required to excite the armature and force rotation via J1-4, completing the loop of Fig. 3.15.

3.6.2. Servo Measurements

Section 2.3.3 presented several measurements that needed to be recorded regarding the fuel servo. These include the torque required to position both the throttle and mixture lever arms from one setting to another. Also, the fuel pressure leaving the servo for the flow divider was also required. This section presents the design implemented to measure these three parameters. The first was the fuel pressure leaving the servo for the flow divider. The second and third were the torque required to position the mixture and throttle lever arms. An approach similar to that used to measure the torque applied by the pump motor was used to measure the torque applied to the mixture and throttle lever arms.

As discussed in Section 3.5.2, the torque applied by a DC motor is linearly proportional to the armature current, by (3.2). Therefore, by monitoring the electrical

current of the actuators, an indirect indication of the torque required to position the lever arms was attained.

Figure 3.19 gives a pictorial summary of the instrumentation method used to monitor the fuel servo.

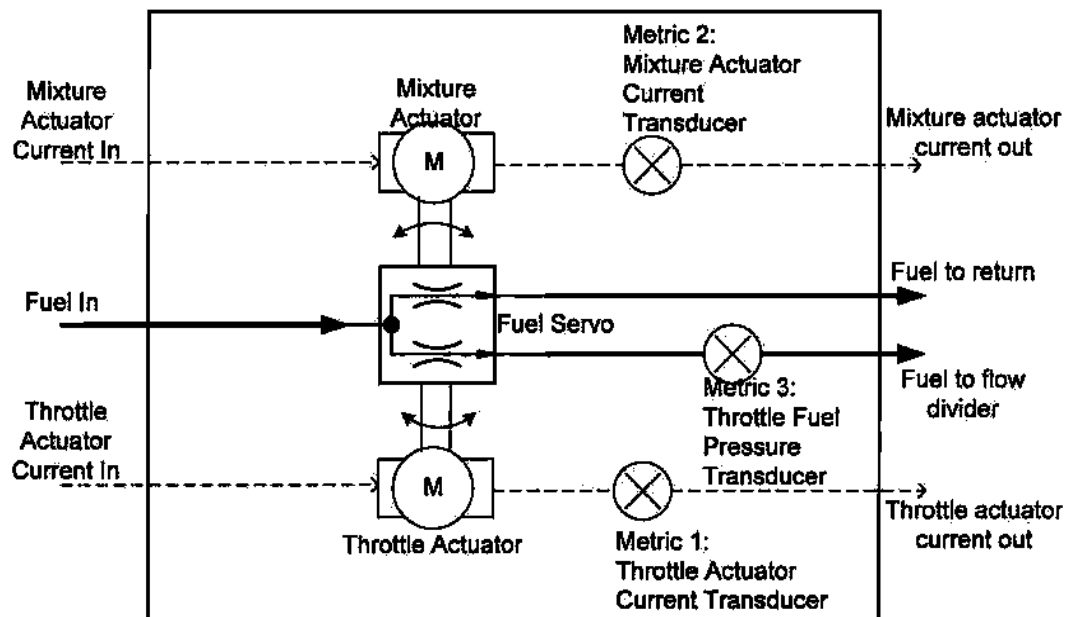


Figure 3.19. Detailed Diagram of Module 2 Measurements.

Only the peak current of the actuators during event transitions was measured by the current transducers for two reasons. The first was the nature of the actuator's electrical current waveform. During a transition, the torque applied to a lever arm was expected to begin at 0, when the arm was not being moved, increase to a maximum in order to overcome stiction, then gradually descend back to zero as the arm reached the

desired position. Therefore, the *peak* current (corresponding to the peak torque) became the critical piece of data. The peak was also measured because the system was designed to require less than two seconds to adjust the lever arm; however, the system was sampled approximately every 30 seconds.

Figure 3.20 gives an example waveform of the current required to position the throttle lever arm during a transition as the throttle lever arm was adjusted from cutoff to full throttle. The actuator's electrical current is shown in blue. The system electronics implemented a peak detection scheme, shown in black. This data was recorded using a Tektronix TDS-420 oscilloscope.

At the onset, before the motor began to move the lever, the motor current was near 0, and no torque was being applied to the lever arm. When the transition began at 0.02 seconds, the applied torque increased to a maximum, as the motor overcame stiction and rotated the lever arm. Then, as the lever arm inertia reduced the needed torque, and finally as the lever neared its desired position and the speed of rotation slowed, the applied torque reduced, and the electrical current returned to 0.

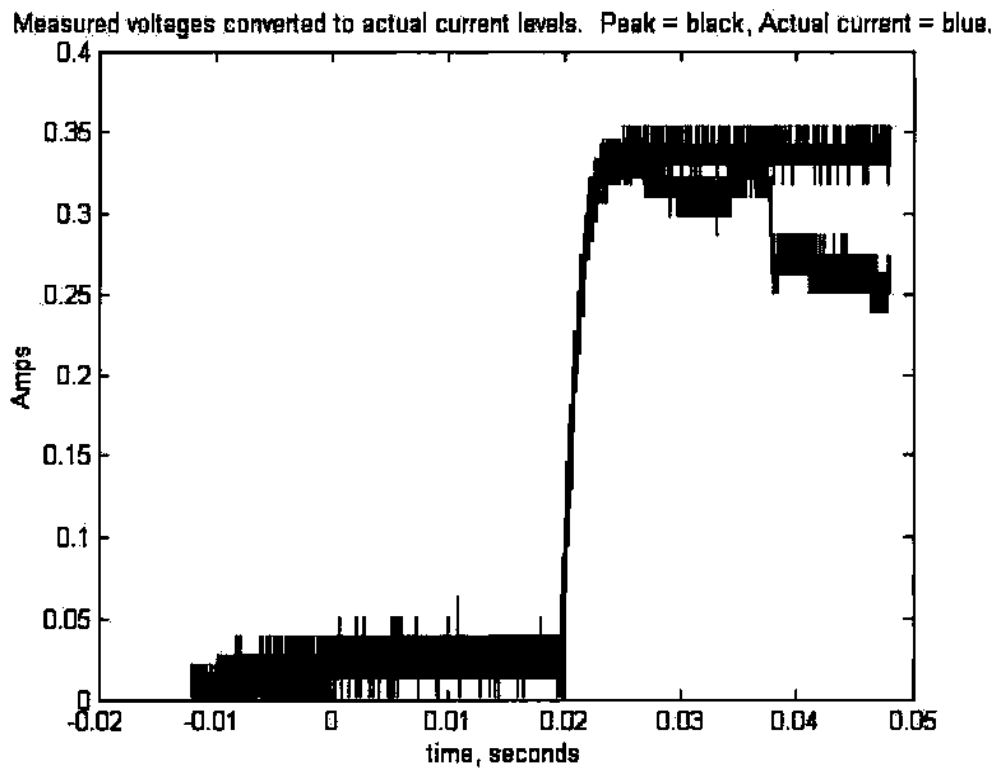


Figure 3.20. Example Actuation Current during an Event Transition.

The electronic system was designed to latch the peak value of the current and hold it the entire length of the event, as shown by the black curve of Fig. 3.20. Prior to the onset of a subsequent event, the computer forced a reset of the peak detection electronics, to allow observation of the peak during the next transition.

Metrics 1 and 2: Actuator Peak Current

This section presents the design of the peak detection scheme for the mixture lever arm. The throttle lever arm is not discussed, since it is identical in design to that of

the mixture. Figure 3.21 gives a pictorial explanation of the design approach. The electrical current of the actuator is first converted to a measurable voltage, V_i . Then, considering that the rotation may be either forward or reverse, V_i is passed through an absolute value circuit, such that V_{abs} is positive, regardless of the rotation of the actuator. Finally, the peak of V_{abs} is latched, and this voltage (V_{peak}) is sampled and stored in the computer by the DAQ.

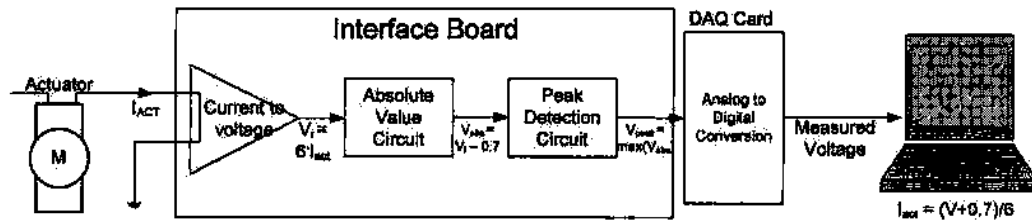


Figure 3.21. Actuator Peak Current Measurement Scheme.

A detailed design of the current-to-voltage stage (blue) and the absolute value stage (red) is shown in Fig. 3.22. Beginning at the actuator, the current enters the interface board via J5-3, where it is shunted to ground through a 1Ω current-sense resistor, resulting in a voltage at pin 3 of the LM348 op-amp of equal magnitude to the actuator current. The LM348 op-amp is designed as a non-inverting amplifier with a gain of 6, producing V_i at pin 1 of the amplifier. With a gain of 6, and assuming the maximum actuation current possible was 0.5 A, V_i was limited to 3 V. This was chosen for circuit stability. The peak detection circuit was found to give erroneous results when the input voltage exceeded approximately 3.2 V.

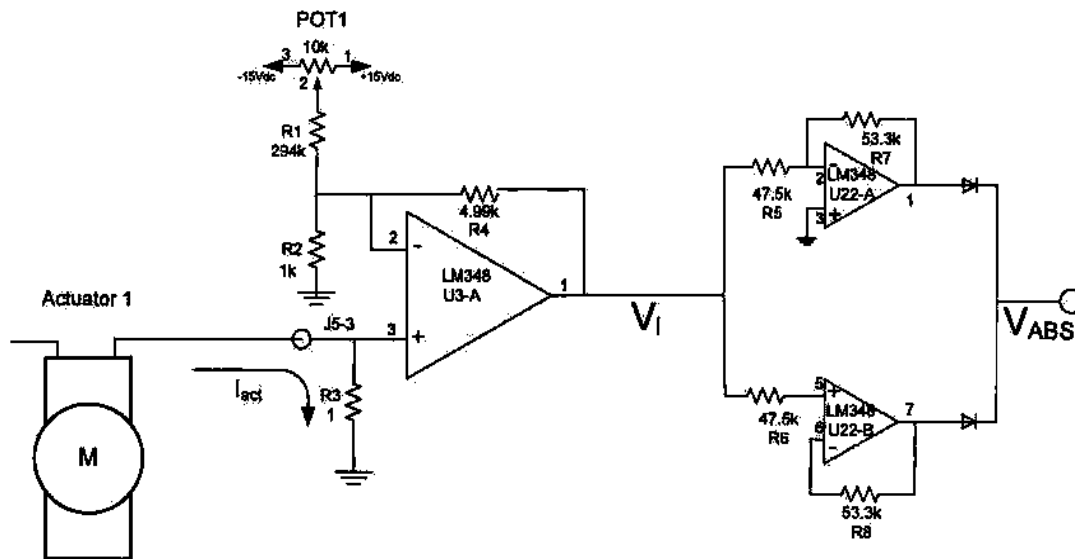


Figure 3.22. Current to Voltage and Absolute Value Circuit.

The absolute value stage (red in Fig. 3.22) operates by applying V_i through two parallel circuits. The top circuit, revolving around the LM348 labeled U22-A inverts V_i ; the lower circuit, designed around U22-B, simply buffers V_i . Therefore, pin 1 of U22-A is $(-V_i)$, and pin 7 of U22-B is V_i itself. If V_i is originally positive, then the lower diode is forward biased, and the upper diode is reversed, allowing the positive voltage to pass, less the voltage drop across the diode. If V_i is originally negative, then the upper diode is forward biased, and the lower reversed, again allowing the positive voltage to pass, less the diode voltage. The resistance of R5 was chosen such that the impedance seen by the amplifier stage was relatively large (a factor of 10 greater than R4), preventing overloading the op-amp. R7 introduced a small gain into the system, to compensate for

any loading effects. By nature, op-amp buffers (the lower path of the absolute value circuit) have high input impedance, regardless of the values of R6 and R8, and therefore are often shorted. However, shorting these resistors can leave a buffer sensitive to sudden voltage spikes [12]. By including R6 and R8, this susceptibility is minimized. The specific values were chosen simply to mirror the upper path.

The peak detection circuit is shown in Fig. 3.23. The design revolves around an AD5220 digital potentiometer. This particular chip, manufactured by Analog Devices, was chosen as it is a standard IC, therefore easily obtainable, and other manufacturers produce similar chips, but packaged inappropriately. The full specifications can be downloaded by [13]. This device has a 10 k Ω internal resistor with 128 taps between pin 6 and pin 3. The resistance at the wiper (pin 5) increments when the following three conditions are met: i) the direction is set to “up” by applying a TTL-high voltage (+5 V) to pin 2; ii) the chip is enabled (TTL-low voltage (0 V) at pin 7); and iii) the voltage at INC (pin 1) transitions from TTL-high to TTL-low. The resistance at the wiper decrements under the same conditions, except the direction must be set to “down” by applying a TTL-low voltage to pin 2.

The LM555 timer was designed to produce a 100 kHz square wave as the clock signal for the AD5220. By applying this repetitive pulse to the INC pin, the chip incremented or decremented (dependent on the status of the CS and U/D pins) at a rate of

100 000 taps per second. At a clock frequency of 100 kHz, the potentiometer required 1.28 ms for the wiper to travel from 0 to 10 k Ω , and vice versa.

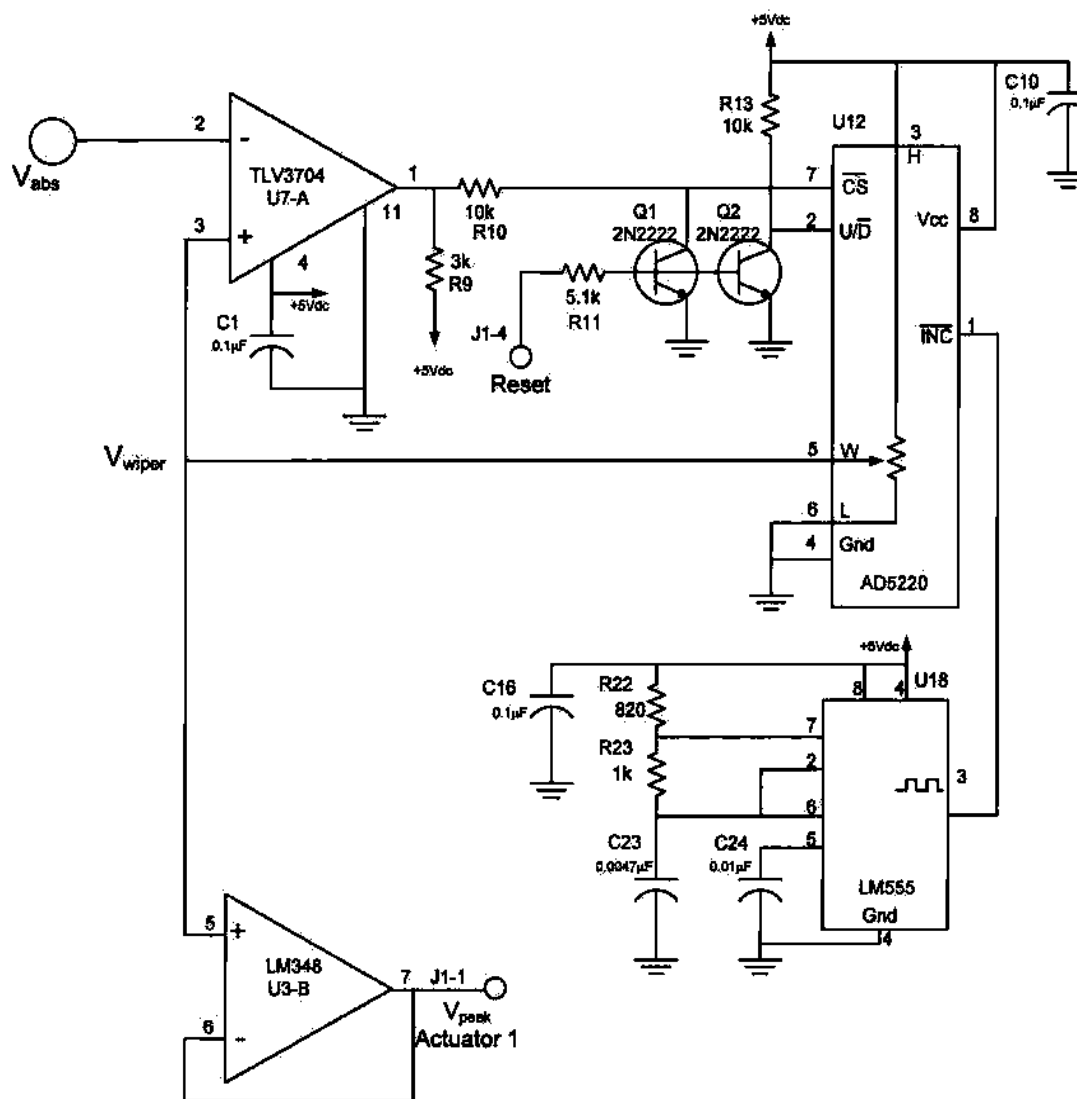


Figure 3.23. Peak Detection Circuit.

The design required a TTL capable comparator, and for circuit reliability from issues relating to the internal impedance of the AD5220, the comparator also had to be of a push-pull variety. A Texas Instruments TLV3704 was used to meet these needs. Consult [13] for full specifications. This IC enables/disables the AD5220 based on the comparison of V_{abs} to V_{wiper} . If V_{abs} exceeds V_{wiper} , the comparator grounded pin 7 of the AD5220, thus enabling the chip and allowing the wiper to increment/decrement. By continuously pulling the direction pin (pin 2 of the AD5220) to +5 V, the wiper is forced to increment at each clock pulse. As the wiper increments, V_{wiper} increases, until finally exceeding V_{abs} . At that point the comparator produces a TTL-high voltage, disabling the chip, and preventing the wiper from incrementing or decrementing. Thus, V_{wiper} latches the peak of V_{abs} . The op-amp of U3-B then buffers V_{wiper} , and the voltage was measured by the DAQ at J1-1.

The computer resets the peak by applying a +5 V pulse to J1-4 for two (2) ms, using the digital counter of the DAQ card. The pulse activates transistors Q1 and Q2. By activating Q1, the CS pin is shorted to ground, and by activating Q2, the U/D pin is shorted to ground, and therefore, during the reset pulse, at each clock cycle the wiper decrements. The AD5220 requires 1.28 ms to traverse the full scale, by holding the reset pulse for two (2) ms, a full reset of the AD5220 is ensured.

This particular design offers significant advantage over other designs, generally requiring capacitors to store charge, which will dissipate with time. By design, this

circuit will latch the peak value and theoretically remain fixed for any period of time until the circuit is reset. However, this circuit does have a drawback, random intermittent spikes in the input, in the Enable or Up/Down pins of the digital potentiometer, etc, will result in latching an exaggerated value or sudden steps downward. Overall, This system will yield more accurate readings over long periods of time, but is more sensitive to circuit noise.

Metric 3: Throttle Fuel Pressure (P_{thr})

The third indicator of servo performance, the fuel pressure from the servo to the flow divider, was required for measurement. To this end, a fuel pressure transducer was placed at the throttle outlet port of the fuel servo. The electronic design is identical to that of the pressure transducer for the fuel pump, discussed in Section 3.5.2. The voltage was measured by the DAQ at J1-17.

3.7. Auxiliary Electronic Devices

Finally, the requirements stated that the system must monitor certain external data, namely the fuel and air temperatures, as well as the ambient humidity. This section describes the design and implementation of these sensors, beginning with the humidity sensor and progressing to the fuel temperature sensor, and finally the air temperature sensor.

Metric 1: Humidity

A COTS humidity sensor was placed in open air behind the interface board. This particular unit was an Omega EWS-TC-K humidity sensor, chosen because it was readily available and needed little manipulation to incorporate into our system. The manufacturer specifications are given in Appendix C. The sensor requires a supply voltage between 8 and 24 V DC, and is specified by the manufacturer to produce a 1 to 5 V output linearly related to the ambient humidity by (3.3).

$$V_{humid} = \frac{\%Humidity}{25} + 1 \quad (3.3)$$

Figure 3.24 presents a pictorial diagram illustrating the implementation of the humidity sensor scheme. The humidity sensor produces a humidity dependent voltage, V_{humid} , amplified by a set of components on the interface board, creating V_H . Then the DAQ card samples V_H and the computer converts the sampled voltage back to the corresponding humidity.

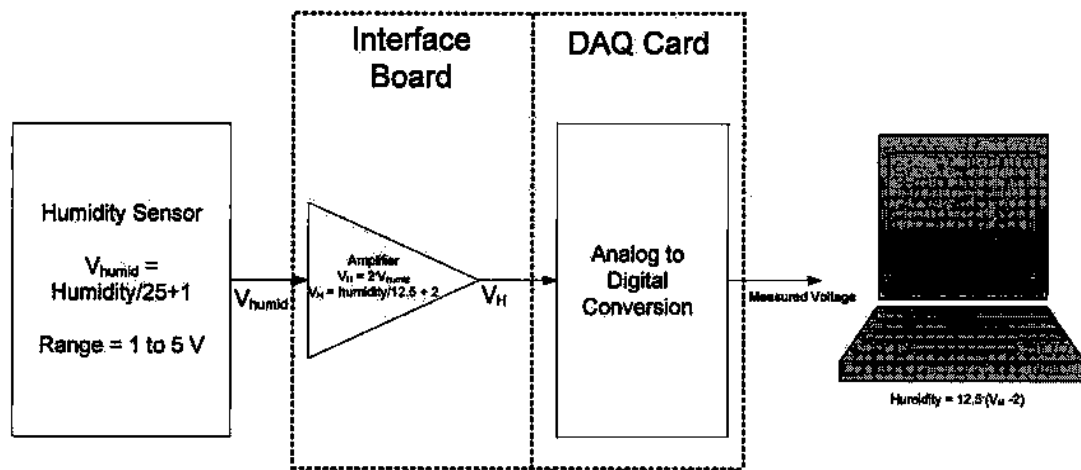


Figure 3.24. Humidity Sensor Flow Chart.

The circuit design is shown in Fig. 3.25. The humidity sensor applies V_{humid} to the input of a non-inverting amplifier with a gain of 2, designed similar to the pressure sensor discussed in section 3.5.3, producing V_H with a magnitude twice that of V_{humid} , boosting V_H to range from two to 10 V, allowing the DAQ to use its full voltage range for measurement. The DAQ then measures this voltage at J1-19, and the computer translates this voltage measurement back to the corresponding humidity.

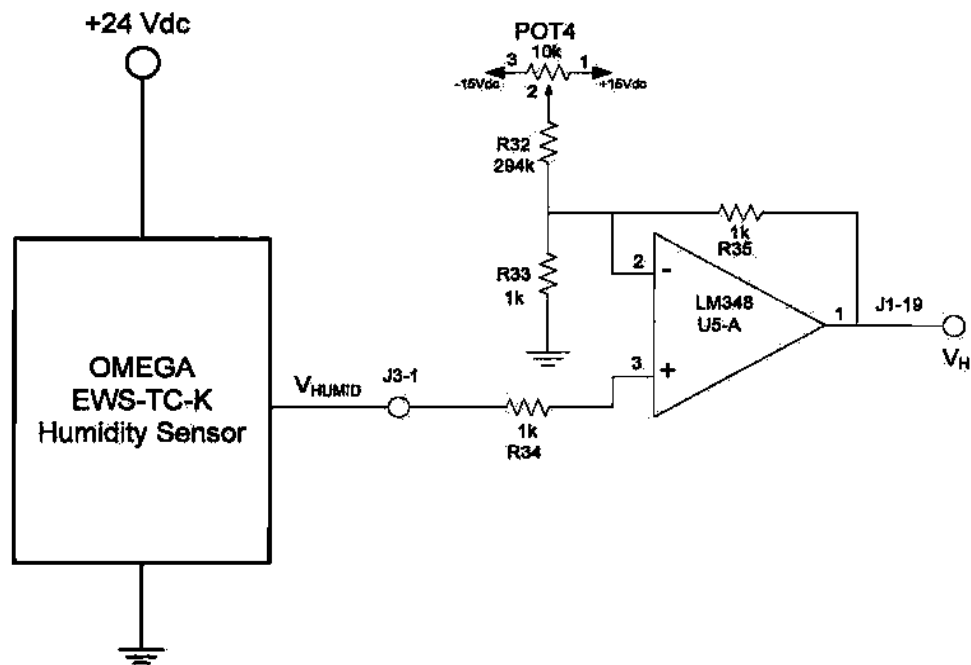


Figure 3.25. Humidity Sensor Design.

Metric 2: Fuel Temperature

A COTS liquid temperature sensor was submerged in the fuel throughout the test. This particular sensor was a Delphi coolant temperature sensor, part number 15461715. Appendix E lists the manufacturer specs. This sensor has sufficient temperature range for this test, operating between -40 and 150 °C. Further, the construction of the sensor was convenient - a thermister with two electrical contacts; as the temperature varied, the resistance between the contacts also varied, between 333 k Ω at -40 °C and 387 Ω at 120 °C. The full resistance-temperature curve was obtained from the manufacturer specification data, and is shown in Fig. 3.26. Finally, in the temperature range expected throughout this test (approximately 10 to 30 °C) the resistance varied between

approximately 5 and 20 k Ω , convenient values within the framework of the electronics discussed next.

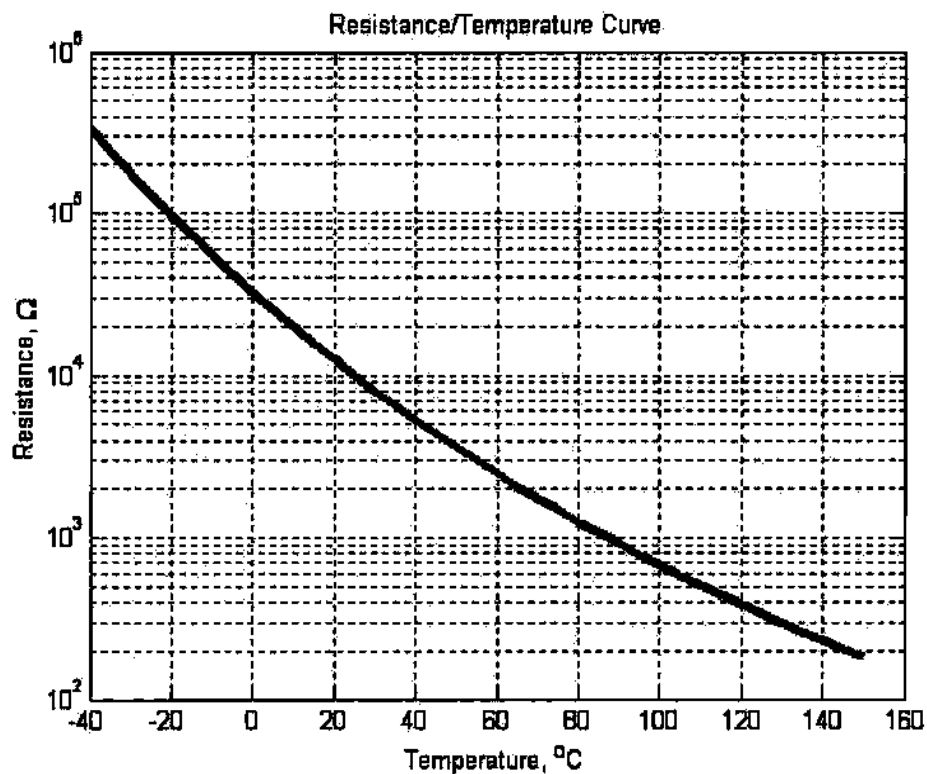


Figure 3.26. Fuel Temperature Sensor R/T curve (Source: Delphi Specifications).

Figure 3.27 presents a pictorial diagram describing the temperature measurement scheme. The voltage from the temperature sensor, V_{temp} , is a complex function dependent on the temperature. This voltage is applied to the interface board and is amplified by a factor of two to allow the DAQ to use its full 0 to 10 V measurement

range, resulting in V_T , which the DAQ samples. Finally, the PC calculates the corresponding temperature based on the measured voltage.

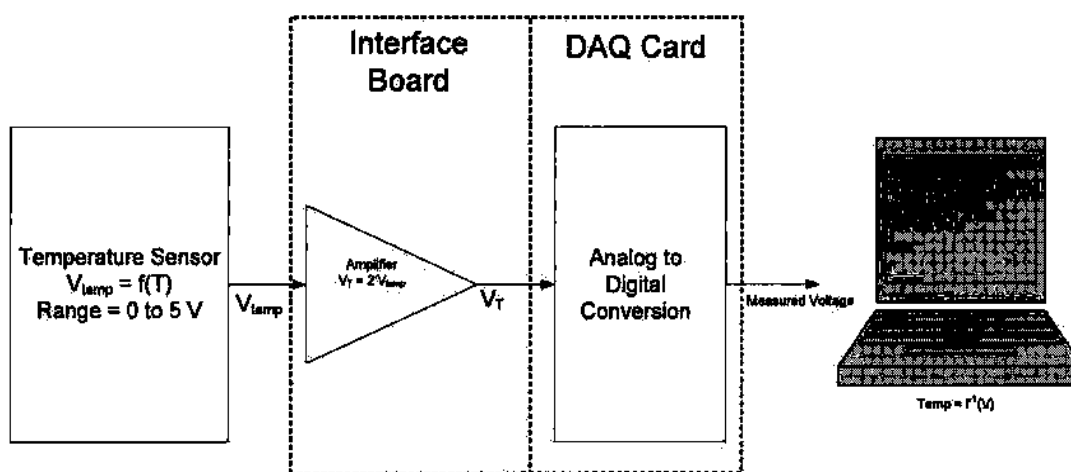


Figure 3.27. Temperature Sensor Flow Chart.

Figure 3.28 shows the temperature transducer circuit design. A $10\text{ k}\Omega$ resistor is placed in series with the thermister and pulled to $+5\text{ V}$. As the temperature of the fuel sensor varies, the voltage at J4-1 also varies, by simple voltage division. The non-inverting amplifier, U16-A, doubles the voltage at J4-1, resulting in a 0 to 10 V signal measured by the DAQ at pin J1-18. The PC then translated the measured voltage back to a corresponding temperature by applying (3.4).

$$T_{Fuel} = -0.0030 \times V_{Fuel}^7 + 0.1088 \times V_{Fuel}^6 - 1.6228 \times V_{Fuel}^5 + 12.6107 \times V_{Fuel}^4 - \dots \\ 54.6947 \times V_{Fuel}^3 + 132.5796 \times V_{Fuel}^2 - 181.4574 \times V_{Fuel} + 174.931 \quad (3.4)$$

Figure 3.29 graphs the voltage at J1-18 versus temperature, with a 7th order polynomial fit superimposed. First, the red asterisks correspond to the voltage measured by the DAQ, based on the manufacturer data and nominal component values within the circuit shown in Fig. 3.28. The continuous blue line corresponds to the voltage/temperature curve derived from (3.4).

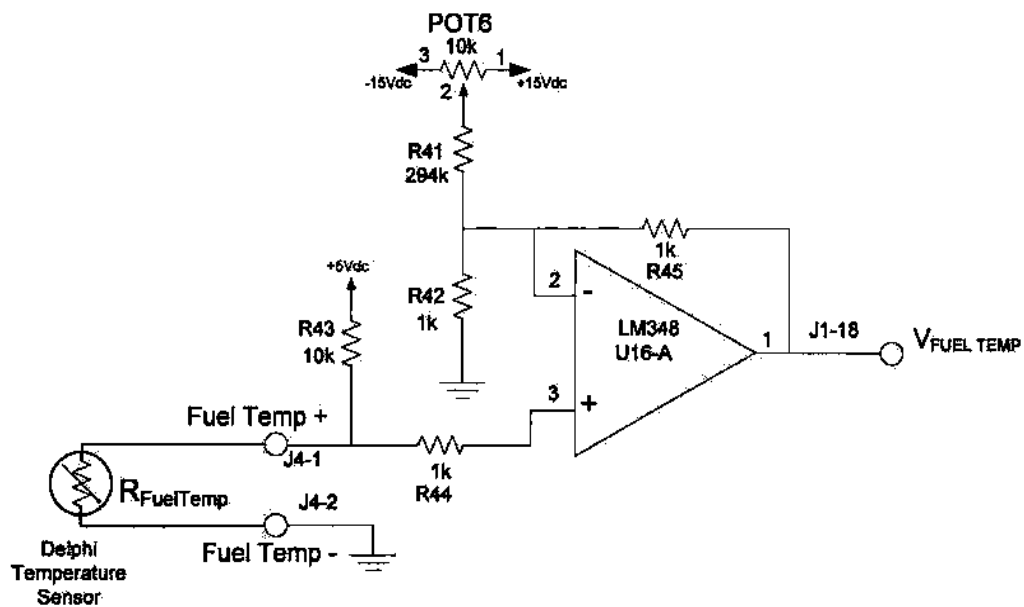


Figure 3.28. Fuel Temperature Sense Circuit.

At first glance, a 7th order fit appears excessively complex. This is deceptive, as a region of great error between a 7th order fit and a 4th order fit is very near our operating temperature region (about 20 °C). In this area, the difference between the 7th order fit and the 4th order fit is approximately 1 °C versus 4 °C. Thus, it was justified to implement a 7th order fit.

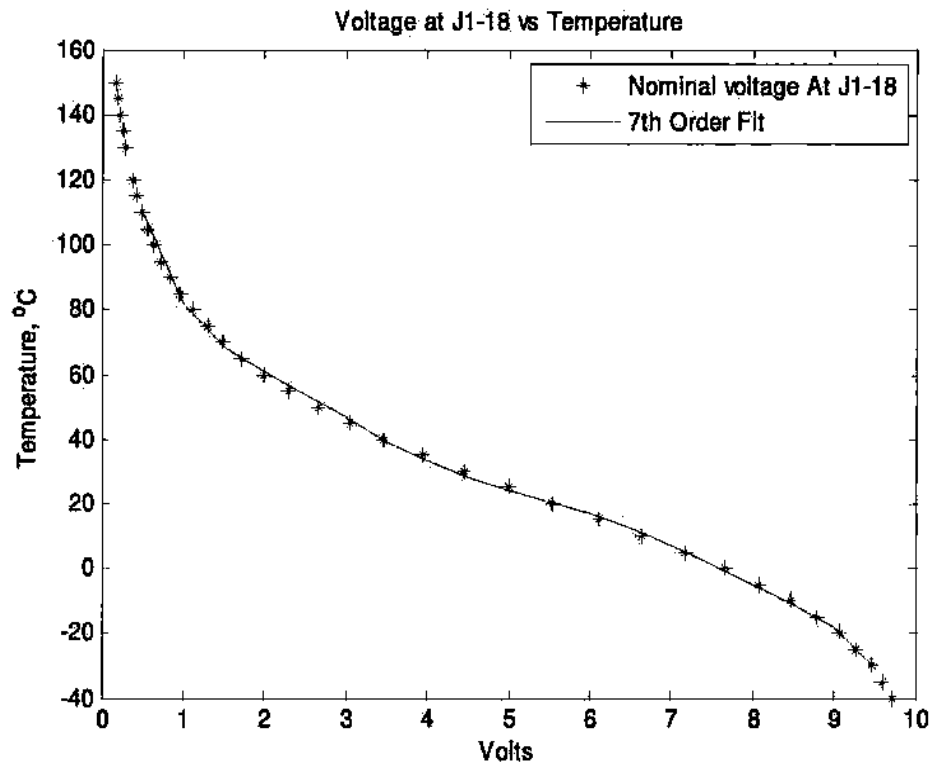


Figure 3.29. Temperature versus Voltage at J1-18, with a 7th order fit superimposed.

Metric 3: Air Temperature

As with the fuel temperature sensor, a COTS air temperature sensor was used to measure the ambient air temperature. This particular sensor was also manufactured by Delphi, part number 15416387, with specifications included in Appendix D. For the same reasons as the fuel temperature sensor, this particular sensor was also chosen, though it's operating temperature range was more limited, -40 to 90 °C. The

resistance/temperature curve is shown in Fig. 3.30, based on the manufacturer supplied specifications.

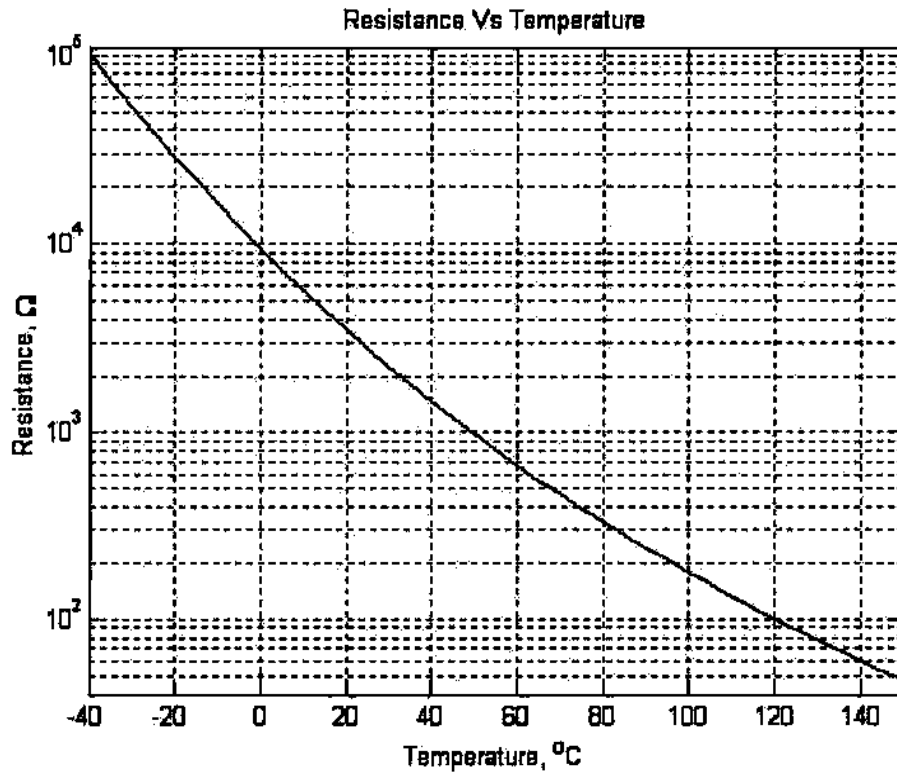


Figure 3.30. Air Temperature Thermistor R/T Curve (Source: Delphi Specifications).

The circuit design for the air temperature sensor is identical to that of the fuel temperature sensor. The corresponding transformation equation is given in (3.5). In this case a 5th order fit was sufficient to properly approximate the temperature/voltage curve shown in Fig. 3.31, having a worst-case error of +/- 0.5°C.

$$\begin{aligned} \text{Air Temp} = & -0.0107 \times V_{Air}^5 + 0.2850 \times V_{Air}^4 - 3.0297 \times V_{Air}^3 + \dots \\ & 16.1305 \times V_{Air}^2 - 51.0124 \times V_{Air} + 84.7935 \end{aligned}$$

(3.5)

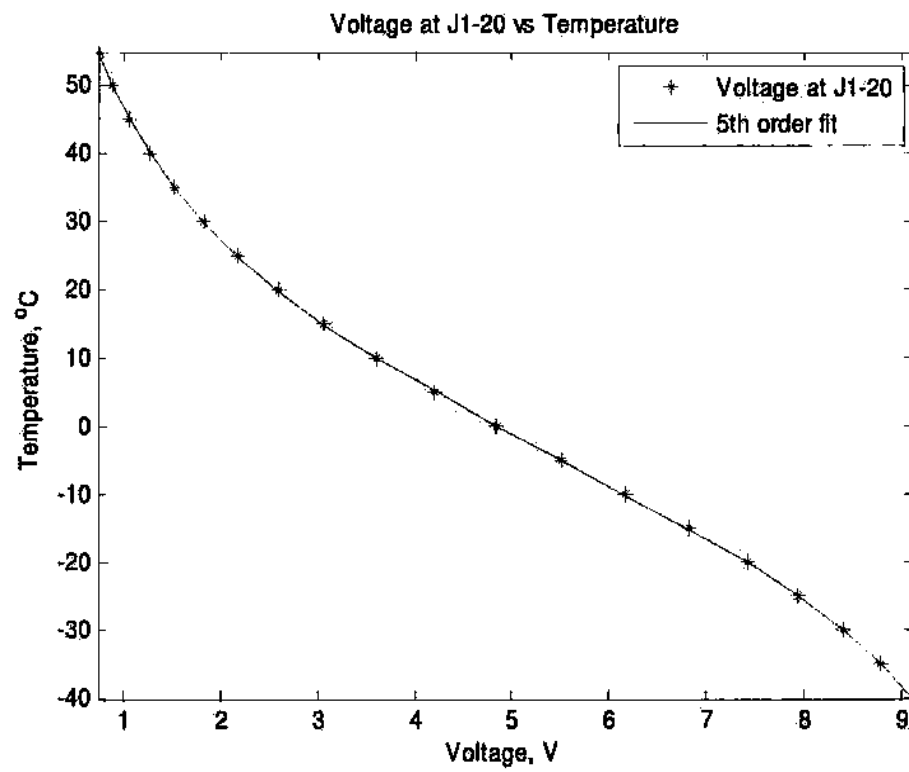


Figure 3.31. Air Temperature versus Voltage Curve.

4. Data Collection and Analysis

This section presents the data collection, results, and analysis of the rig test. It begins with an overview of the test itself; and progresses to a description of the collected data. Finally, an evaluation of the data is presented, relating the data to the status of the various components tested throughout.

4.1 Test Overview

The test described in this paper began January, 2005, and continued until September of 2005, when the pump drive motor failed from wear of the internal brushes of the motor. During this period of time, the ambient temperatures had varied between +2 and +48°C, while the ambient relative humidity had varied between 5 and 97%.

At the completion of the test, over 1070 simulated flight cycles had been repeated, corresponding to 5530 hours of total time logged, divided into 3712 hours with circulating fuel, and 1817 hours with the system soaking.

After six months of operation, 720 cycles - approximately 2450 hours of emulated flight time - system maintenance was performed for a variety of reasons, both electronic and mechanical. Throughout the test the system electronics and mechanics had drifted. Maintenance attempted to minimize the influence of these external factors on test data.

Electronic drift resulted in some variation of data measurements as well as of actuator position control. The second implication of electronic drift was especially hazardous: the mixture actuator was found to be oscillating randomly; and the throttle lever arm was reaching its mechanical limit - both possibly causing unusual servo and actuator wear.

The oscillation of the mixture lever arm was limited to periods when the mixture was at full rich, and was inconsistent, often the arm was able to lock in position, but other times a period of oscillation occurred, until the actuator finally settled. During maintenance the gain of the mixture actuator's power amplifier was reduced by reducing the resistance of POT1 shown in Fig. 3.21. This removed the oscillation, but decreased the accuracy of the position control.

The throttle lever arm was found to be reaching the mechanical limit, producing a high DC current through the actuator as the actuator tried to move the lever arm beyond the limit. The mechanical limit was only reached during the events "Engine Prime" and "Shutdown", when the throttle setting was near 0. Since a high current with no motion may damage the actuator, through overheating, this issue was addressed by adjusting the position of the lever arm at this extreme. Fortunately, since no fuel circulated during these events, this adjustment did not skew data collected regarding fuel pressure.

As the test progressed, the mechanical side of the system also drifted, as the parts, and especially couplings, expanded and contracted with temperature, and loosened through use. Mechanical maintenance included an external cleaning of the system, and tightening the mechanical couplings between the actuators and the servo lever arms.

4.2. Data Description

This section describes the format of the data collected throughout the test. It begins by discussing the raw data gathered from the PC. Then, the method and format for analysis is described to lay a foundation for the data analysis regarding specific metrics in following sections.

4.2.1 Continuous Data

Throughout the test, data regarding the fuel pressures, current drawn by the pump motor, peak current required to position the lever arms, air and fuel temperature, and humidity was recorded every 30 seconds and stored into Excel spreadsheets. Table 4.1 presents an example portion of such a file, from April 1st, 2005. This particular file recorded nearly 24 hours of data, ending at 8:32 AM on April 2nd, with 6000 samples of each parameter. All told, at the end of the test over 1.2 million samples were recorded.

Table 4.1. Example Data from April 1st, 2005

Time	Air T.	Hum.	Fuel T.	Throt. P.	Pump P.	Mot. I	Throt .I	Mix. I	Mix. Setting	Throttle Setting	Motor Setting
8:44:51 AM	12.97	37.195	11.462	1.66	1.111	0.535	0.222	0.283	10	10	0
8:44:53 AM	13.058	35.181	11.462	1.66	1.172	0.486	0.224	0.283	10	10	0
8:44:56 AM	12.97	36.523	11.396	1.66	1.233	0.485	0.224	0.284	10	10	0
8:44:59 AM	13.058	35.486	16.077	1.66	1.111	0.467	0.224	0.283	10	10	0
8:45:27 AM	13.014	35.913	11.527	15.698	1.172	0.234	0.01	0.06	10	0	700
8:45:29 AM	13.058	35.73	11.656	10.388	22.839	0.218	0.359	0.06	10	0	700
8:45:34 AM	13.058	36.279	11.656	10.022	22.595	0.804	0.36	0.06	10	0	700
8:45:36 AM	13.014	34.57	11.527	9.839	23.267	0.904	0.361	0.06	10	0	700
8:45:39 AM	13.101	37.439	11.527	9.839	22.595	1	0.353	0.06	10	0	700
8:45:42 AM	13.014	36.707	11.785	9.839	23.389	1.088	0.36	0.06	10	0	700
8:45:45 AM	13.058	35.608	11.721	10.144	23.206	1.013	0.36	0.06	10	0	700
8:45:49 AM	13.058	36.646	11.527	9.656	23.083	0.775	0.361	0.06	10	0	700
8:45:51 AM	13.058	36.279	11.527	9.839	28.21	0.828	0.36	0.058	10	0	700
8:45:54 AM	13.058	36.34	11.527	9.595	21.863	0.657	0.361	0.06	10	0	700
8:45:57 AM	13.014	35.73	11.527	9.961	23.755	0.745	0.361	0.059	10	0	700
8:46:00 AM	13.014	36.218	11.396	9.961	22.473	0.816	0.361	0.06	10	0	700
8:46:28 AM	13.058	34.998	11.527	9.412	23.145	0.848	0.109	0.076	10	1	1000
8:46:30 AM	13.058	36.523	11.396	10.022	28.943	0.979	0.304	0.076	10	1	1000
8:46:35 AM	13.014	36.218	11.527	10.449	26.624	0.766	0.303	0.076	10	1	1000

4/1/2005

Figures 4.1 through 4.3 present example data graphically; in these instances the plots show the pump pressure for three separate cycles, the first on January 29th, the second on April 20th, and the final on September 14th. The red curve shows the motor setting, in RPM, and the blue curve shows the pump pressure in PSI. By following the motor setting curve, the corresponding event can be deduced, from idle (motor setting = 700 RPM) to taxi (motor setting = 1000 RPM), to takeoff (motor setting = 2700 RPM), as determined by the timing scheme of Table 2.1.

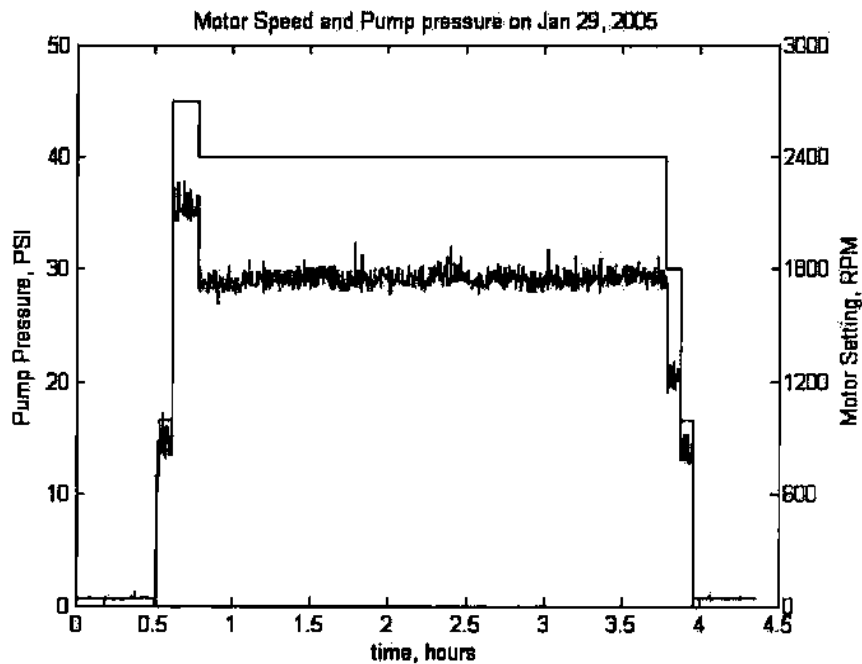


Figure 4.1. Fuel Pump Pressure and RPM, January 29, 2005.

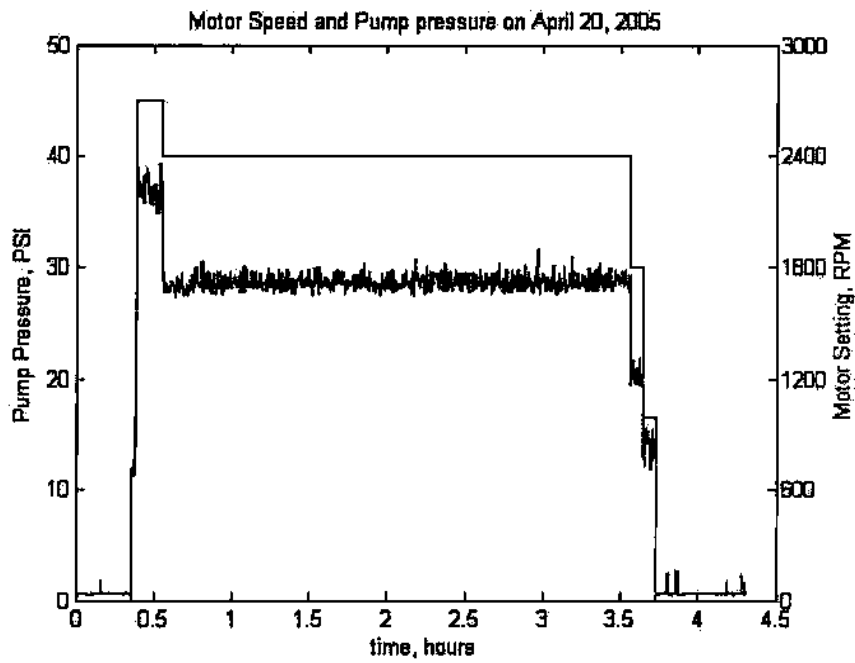


Figure 4.2. Fuel Pump Pressure and RPM, April 20, 2005.

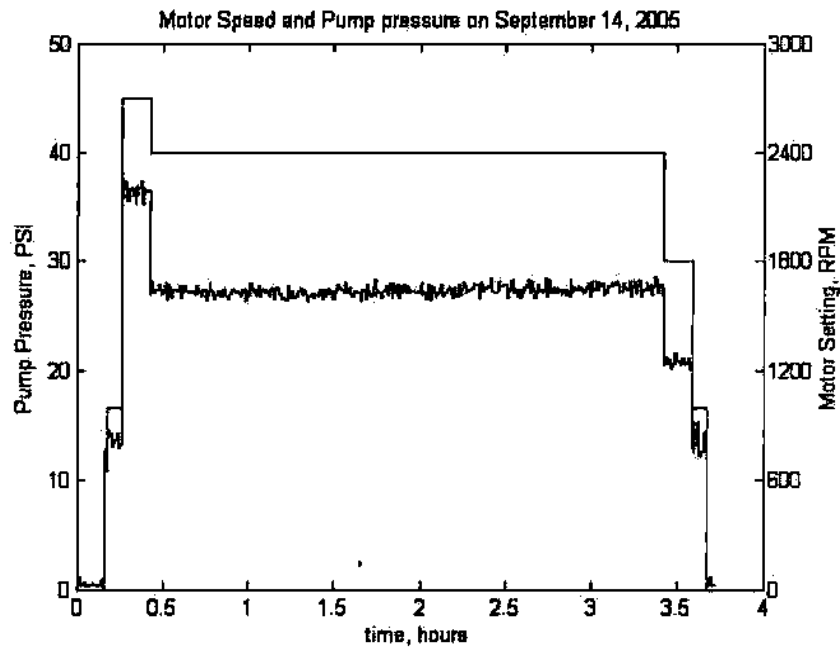


Figure 4.3. Fuel Pump Pressure and RPM, September 14, 2005.

4.2.2 Event Summarized Data

Several observations can be made from the graphs of Figs. 4.1 through 4.3. First, during each event, the fuel pressure reached a stable value, and then fluctuated about that level. For example, in Fig. 4.1, the pressure during the "Takeoff" event (from 0.6 hours to 0.8 hours, when the motor setting was at 2700 RPM) was approximately 37 PSI, +/- 1.5 PSI. During the subsequent event, "Cruise," (from 0.8 hours to 3.4 hours) the fuel pressure was about 27 PSI, +/- 1.5 PSI. Consistent behavior was exhibited throughout the test - the metric, whether motor current, fuel pressure, actuator current, etc, reached a stable level, fluctuating a bit due to noise, quantization error, etc. Therefore, each event within a simulated flight cycle was summarized with two values: the average of a particular metric during the event, and the standard deviation of all the measurements, within the event, referred to as the sample standard deviation.

Table 4.2 gives an example, using the data shown in Figs 4.1 through 4.3. For each event, the measurements of the fuel pressure were analyzed by the mean and standard deviation. From these three specific cycles, only slight evidence of system change was observed throughout the test. For example, the average pressure during the "Cruise" event was 28.54 PSI on Jan. 29th, was 28.65 PSI on April 20th, and concluded at 28.16 PSI on September 14th. During the same time, the standard deviation had declined from 0.75 PSI on January 29th, 0.60 PSI on April 20th, to 0.49 PSI on September 14th.

Observing the graphs validates these observations, as the fuel pressure shows less

fluctuation in Fig. 4.3 than Fig. 4.1.

Table 4.2. Fuel Pump Pressure Summarized Data

Date	Event	Mean Pressure (PSI)	Standard Deviation (PSI)
1/29/2005	Prime	0.84	0.10
4/20/2005	Prime	0.85	0.07
9/14/05	Prime	0.40	0.04
1/29/2005	Idle	12.01	0.56
4/20/2005	Idle	11.48	0.67
9/14/05	Idle	11.42	0.61
1/29/2005	Taxi	14.04	0.58
4/20/2005	Taxi	13.57	0.77
9/14/05	Taxi	13.97	0.46
1/29/2005	Takeoff	36.28	1.09
4/20/2005	Takeoff	36.04	0.93
9/14/05	Takeoff	36.85	0.85
1/29/2005	Cruise	28.54	0.75
4/20/2005	Cruise	28.65	0.60
9/14/05	Cruise	28.16	0.49
1/29/2005	Descent	20.42	1.15
4/20/2005	Descent	20.67	0.73
9/14/05	Descent	20.96	0.38
1/29/2005	Taxi	13.91	1.17
4/20/2005	Taxi	13.29	0.98
9/14/05	Taxi	13.72	0.77
1/29/2005	Shutdown	0.63	0.16
4/20/2005	Shutdown	0.58	0.19
9/14/05	Shutdown	0.44	0.14

By expanding the process described here to every event throughout the entire nine month test, trends were more observable. Figure 4.4 presents an example. Here the summarized data regarding the fuel pump pressure during the "Cruise" event is shown.

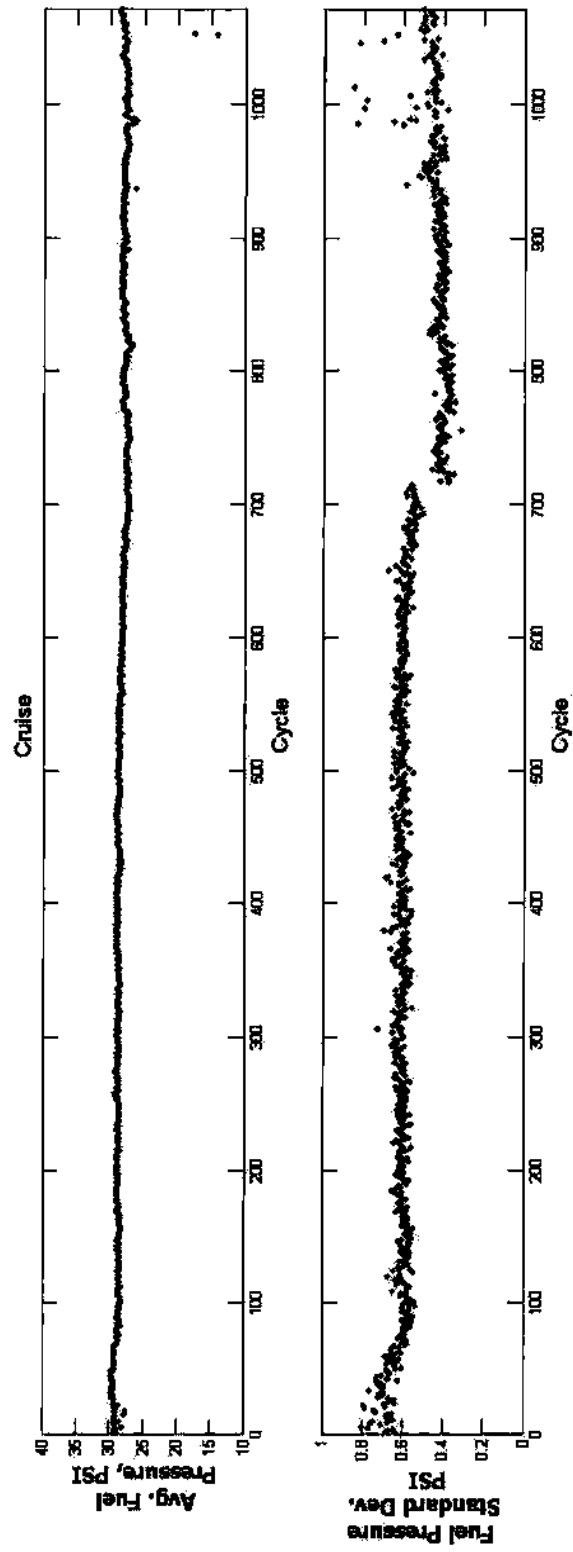


Figure 4.4. Average Fuel Pump Pressure and Standard Deviation.

The fuel pump pressure during the “Cruise” event was averaged for each cycle from the first on Jan. 27th, 2005 to the final on Sept. 26th, 2005, and placed chronologically in the graph, resulting in the plot of Fig.4.4. Each data point represents the average fuel pressure during a particular event and cycle. The x-axis tells the cycle number, and, in the upper graph, the y-axis shows the average fuel pressure, and the standard deviation is shown in the lower. Over the course of the test, the cycle was repeated over 1050 times. The “Cruise” event of Fig. 4.1 happened to be the 9th cycle in the test, and correspond to the 9th data point in Fig.4.4. The “Cruise” event of April 19th, shown in Fig. 4.2, corresponds to the 356th data point; and the “Cruise” event of Fig. 4.3 corresponds to the data point at cycle 1038 of Fig. 4.4.

Figure 4.5 clarifies these variables. In the upper graph, the mean within each cycle is shown as X_c , where X is the metric of interest (in this case the fuel pressure). The standard deviation within each cycle is shown as σ_c . The subscript ‘c’ refers to cycle-based statistic. By following the arrows, the corresponding summarized data is shown in the lower graph.

By summarizing the data as shown in Fig. 4.4 and 4.5, the experimental findings can best be evaluated for long term trends. Assuming a simple linear model for degradation, a regression line can be determined, and the magnitude of the slope indicates the amount of change in system performance throughout the test, as compared to a line of zero slope, indicating no change in readings.

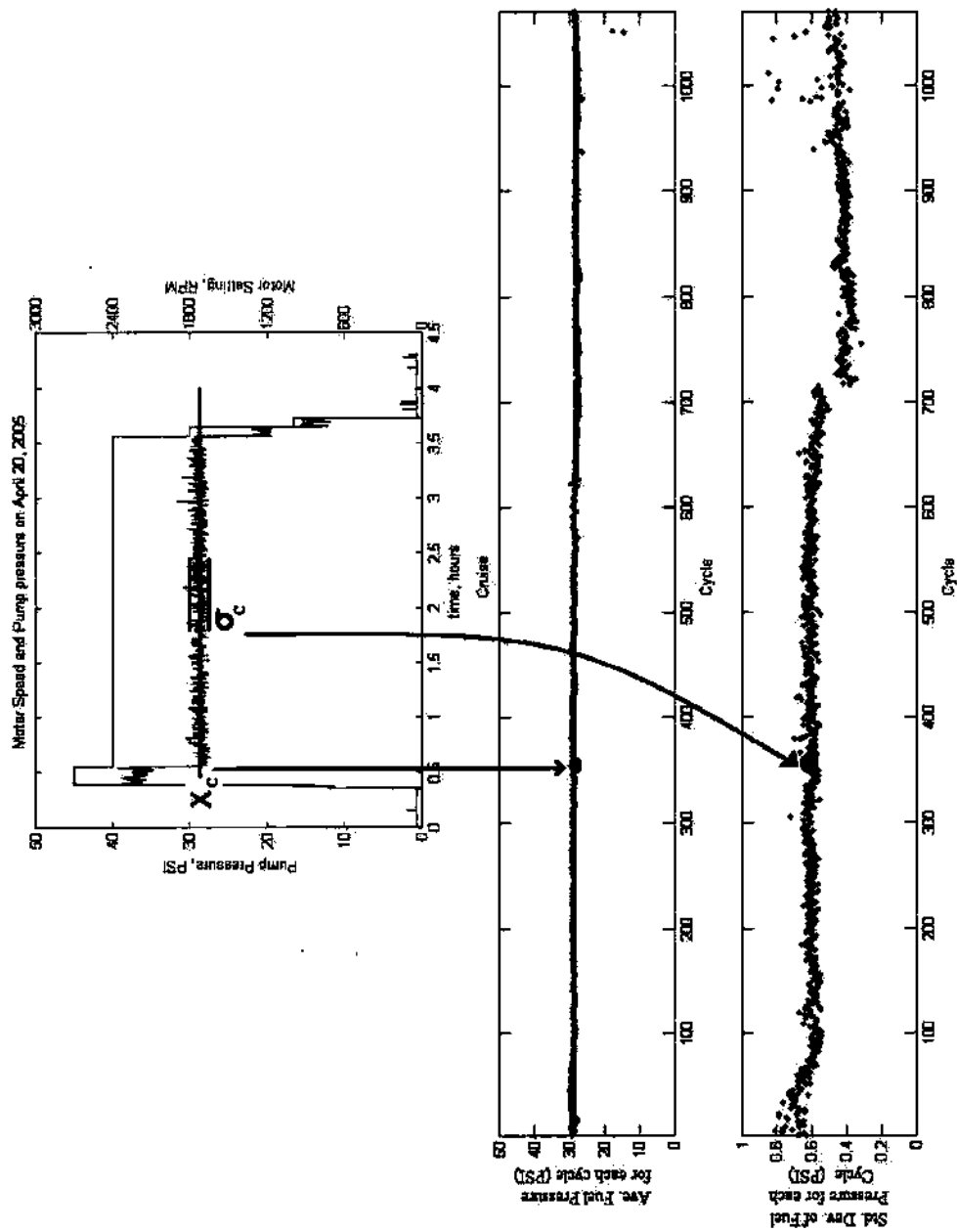


Figure 4.5. Explanation of Sample Data within a Cycle, and Cumulative Data.

4.3. Module 1: Fuel Pump

This section evaluates the data collected relevant to the fuel pump. These data include the line pressure of the fuel leaving the fuel pump for the servo, motor current measured throughout the test, indicating the torque applied to the pump, as well as a summary statement of the visual inspection performed on the pump at the conclusion of the test.

4.3.1. Fuel Pressure

The first indicator of the performance of the fuel pump was the outlet fuel pressure. Variations and trends in this metric corresponded to a changing flow rate of the fuel pump, or buildup/corrosion within the fuel lines

With the motor speed setting superimposed, several example cycles of fuel pressure data were presented in Figures 4.1 through 4.3. Here the pump pressure (P_{pump} , the pressure in the fuel line *from* the pump *to* the fuel servo) was shown in blue, and the motor speed setting shown in red, included for event reference.

As is observed in each figure, the faster the pump was turning (as indicated by the motor speed), the greater the fuel pressure in the line. Also, as described in Section 4.2.2, during each event the fuel pressure reached a steady-state level and fluctuated within a small margin (shown pictorially as X_C and σ_C in Fig. 4.5). The events are summarized and graphed in Fig. 4.6.

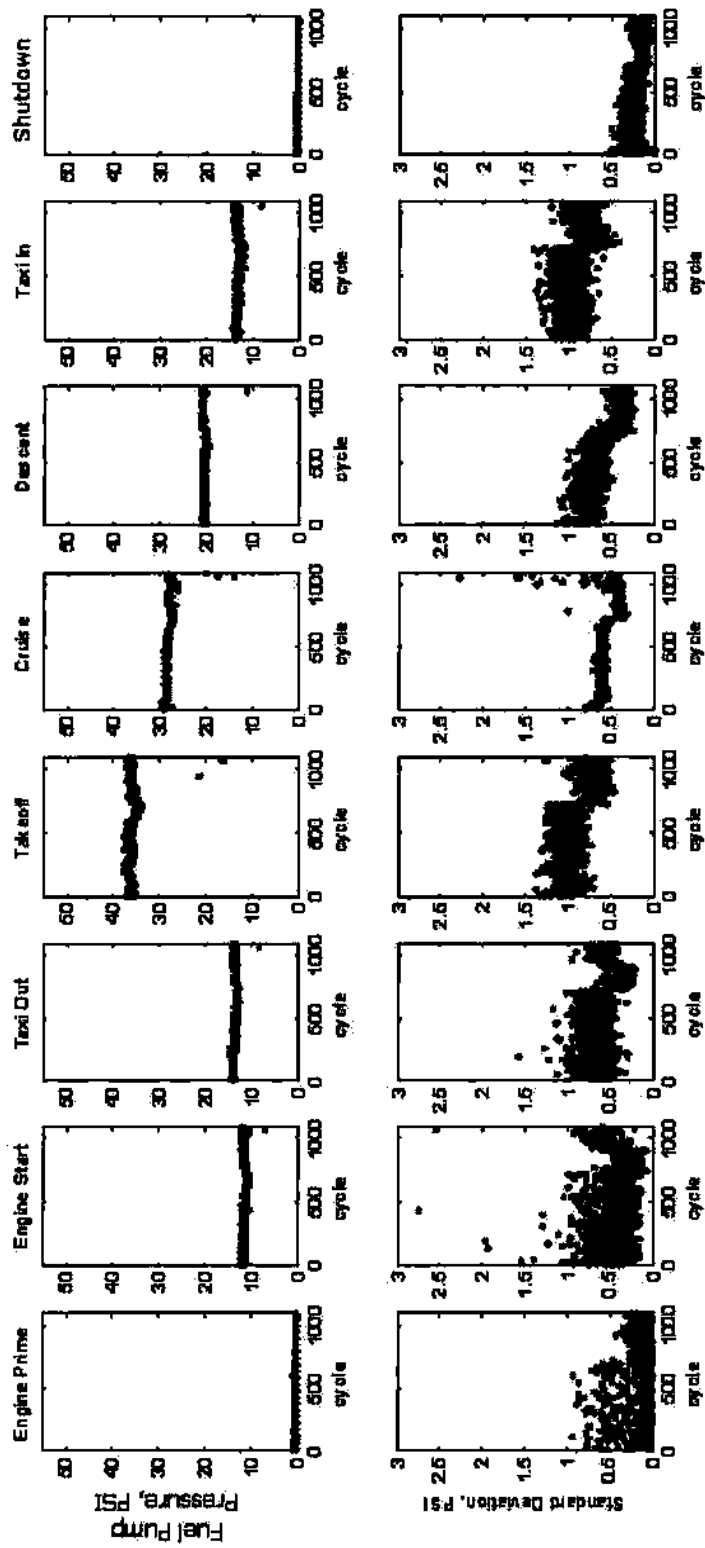


Figure 4.6. Fuel Pump Pressure Data, summarized per event.

By a subjective observation of Fig. 4.6, little evidence of system degradation was indicated by the data. A more objective analysis is included in Table 4.3 and Fig. 4.7. The table columns correspond to the appropriate event, and the rows list the calculated results from the data. The outline following the data gives a complete description of the meaning of each column.

Table 4.3 Summary Statistics for P_{pump}

	Engine Prime	Engine Start	Taxi Out	Takeoff	Cruise	Descent	Taxi In	Shutdown
N ^a	1073	1073	1073	1073	1072	1064	1066	1066
Mean (PSI) ^b	0.552	11.587	13.764	36.159	28.324	20.628	13.390	0.548
Std (PSI) ^c	0.1030	0.3418	0.3782	1.1822	0.8193	0.3953	0.4615	0.0828
Intercept (PSI) ^d	0.683	11.700	14.004	36.523	29.171	20.552	13.449	0.681
Slope (PSI/cycle) ^e	-244E-6	-210E-6	-446E-6	-678E-6	-2E-3	142E-6	-111E-6	-249E-6
Abs Change (PSI) ^f	-0.262	-0.225	-0.479	-0.727	-1.692	0.151	-0.118	-0.265
%Change ^g	-38.370	-1.927	-3.417	-1.991	-5.799	0.736	-0.881	-38.973

- a. The number of cycles evaluated in the data;
- b. The average fuel pressure during each event, over the lifetime of the test, given in PSI;
- c. The standard deviation (in PSI) of the mean values recorded over the lifetime of each event.
- d. The x-intercept of a linear regression line for each event (the green lines shown in Fig. 4.7). This corresponds to the fuel pressure at the onset of the test.
- e. The slope of a linear regression line, in PSI/cycle.
- f. The absolute change in fuel pressure (PSI) over the lifetime of the test
- g. The %change in fuel pressure over the test lifetime

First, the lower plots of Fig. 4.6, detailing the standard deviation of sample instances, indicate little change in system variability until system maintenance, which occurred at approximately cycle 720. At this point, a software revision was implemented which incorporated a more efficient digital filter. This resulted in the baseline shifts observed. For most events the sample noise was reduced. Beyond this, an increasing trend was observed toward the conclusion of the test. For example, the standard deviation of the "Taxi Out" event, shown within Fig. 4.6, showed a bias level shift at cycle 720, relating to the software revision. Then, beginning at approximately cycle 900, the standard deviation began to increase again. All events showed varying degrees of

similar trends. These observations were related to degradation of the motor. As the test neared completion, the motor was beginning to fail, resulting in inconsistent performance, as observed by the graphs of Fig. 4.6. This degradation will be further explored in Section 4.3.2.

Fig. 4.7 presents the data of Table 4.3 graphically, excluding the standard deviation which has been discussed. The data shown in Fig. 4.6 is superimposed by the regression lines shown in green, and a line with zero slope, centered at the test average, shown in black.

Statistical Evaluation

A statistical test was performed on each event, to determine if a trend existed in the data. The hypothesis tested was that the slope of the regression line for each event was equal to zero, at a 95% confidence level ($\alpha = 0.05$). Surprisingly, at a 95% confidence interval, the null hypothesis was rejected for each flight event, indicating that a trend was observed throughout each event in the test.

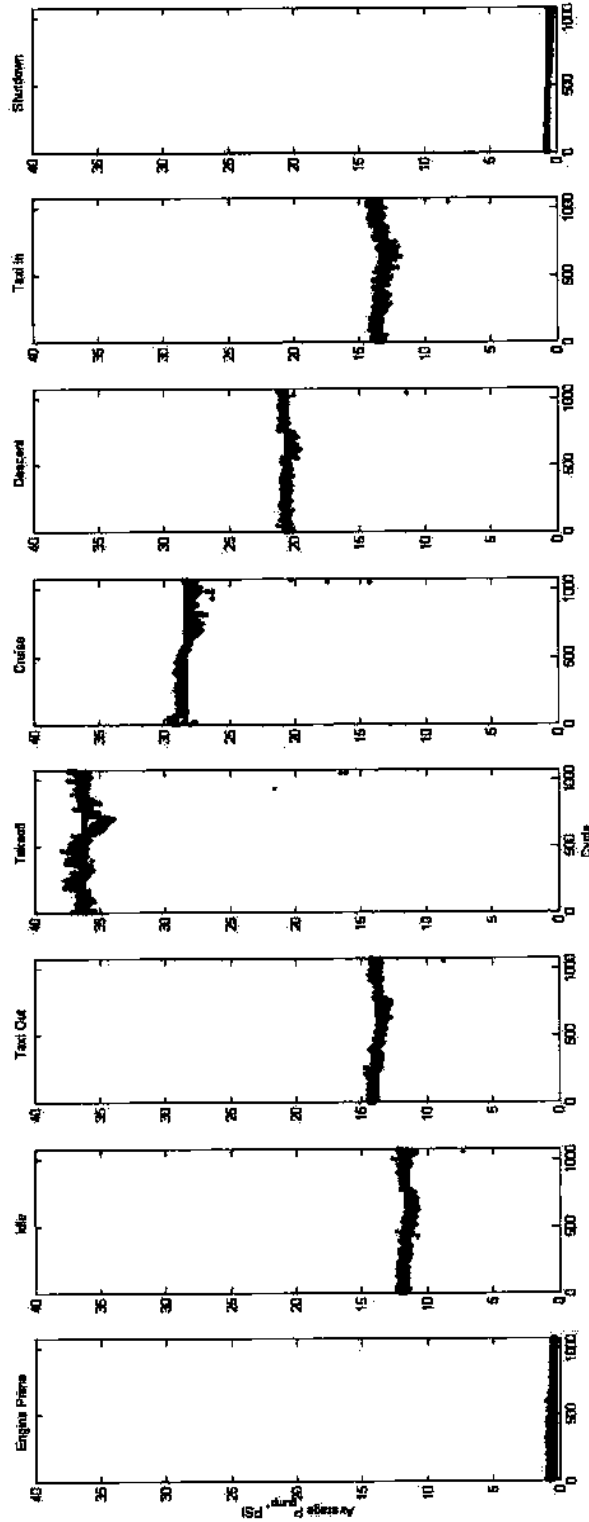


Figure 4.7. Summarized data for P_{pump} (red) with regression analysis (black) and the test average (green).

Practical Evaluation

The events “Engine Prime” and “Shutdown” had the largest change in readings, over 38%, corresponding to 0.25 PSI, a negligible amount, likely reflecting nothing more than expected measurement noise. Of the other events, the greatest change was during “Cruise” when the fuel pressure fell by 5.8%, -1.7 PSI over the lifetime of the test. The percent change was -1.93, -3.42, -1.99, -5.80, and 0.74 for events two (“Idle”) through seven (“Taxi In”).

Fuel Pressure Conclusions:

The data collected regarding P_{pump} indicated a worst-case decline of 5.7% during the lifetime of the test, corresponding to an absolute change of 1.7 PSI within the fuel line. At this point the cause of the decline in fuel pressure cannot be discussed further, as other system issues play a critical factor, as will be shown in the subsequent sections.

4.3.2. Motor current (I_{mot})

The second indication of the condition of the pump was the torque required to rotate it. This was indicated by I_{mot} , the motor current. Section 2.3.1 describes the relationship between motor current and applied torque, revealing a direct linear relationship. This section evaluates the data regarding the motor current.

Figure 4.8 presents an example cycle of motor current data, measured throughout the test, and lifetime averages as well as standard deviation are shown in Fig. 4.9. The

upper plots of Fig. 4.9 share a common y-axis range, from 0 to 3 A, with the x-axis being the lifetime of the test, delineated by the cycle number. The lower plots graph the measurement standard deviation, also in amperes.

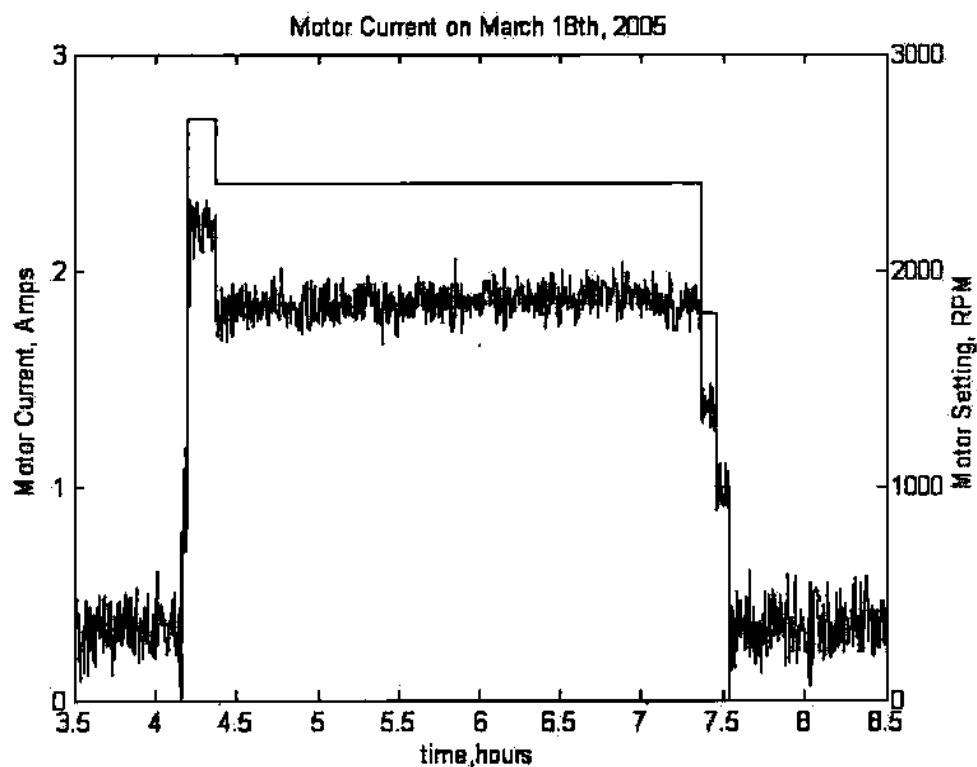


Figure 4.8. Example motor current data on March 18th 2005.

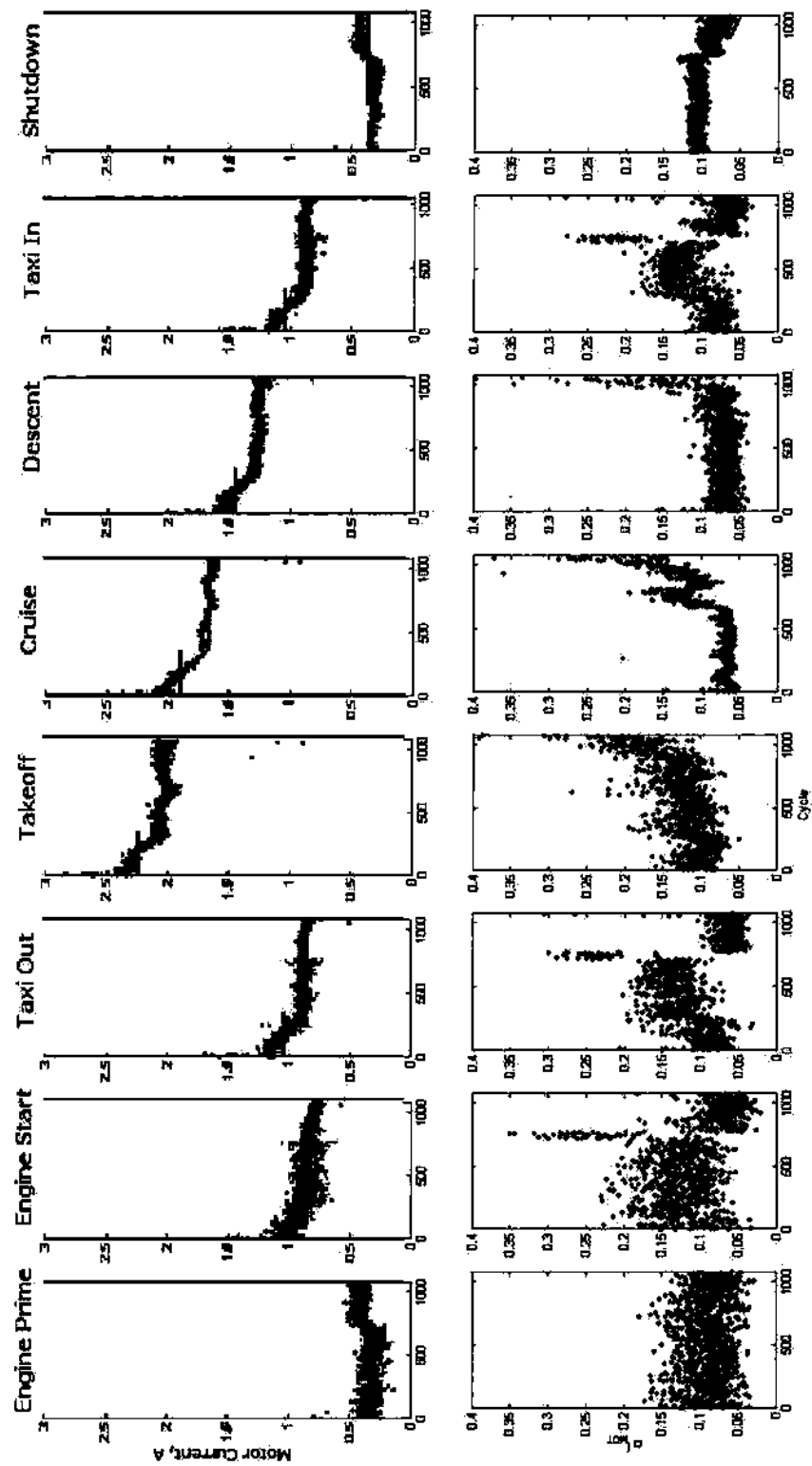


Figure 4.9. Average Motor Current (top) and Standard Deviation (bottom) per Event for the Lifetime of the Test.

The data were summarized throughout the test and are presented in Table 4.4. For reasons which will be discussed shortly, the data were parsed into two sections, the first 350 cycles, and the remainder of the test. The notes following the table give a detailed explanation of Table 4.4, especially as divided between the two partitions.

Table 4.4 Motor Current Statistics

	Engine Prime	Engine Start	Taxi Out	Takeoff	Cruise	Descent	Taxi In	Shutdown
N ^a	1073	1073	1073	1073	1072	1064	1066	1066
Mean (amperes) ^b	0.355	0.865	0.935	2.099	1.745	1.322	0.929	0.353
St. D. (amperes) ^c	0.071	0.101	0.115	0.138	0.137	0.117	0.115	0.060
Intercept {p1} (amperes) ^d	0.361	1.092	1.245	2.433	2.110	1.637	1.232	0.348
slope {p1} (amperes/cycle) ^e	-152E-6	-812E-6	-1E-3	-1E-3	-1E-3	-1E-3	-1E-3	-111E-6
Intercept {p2} (amperes) ^f	0.209	0.886	0.903	2.094	1.779	1.294	0.879	0.189
slope {p2} (amperes/cycle) ^g	219E-6	-88E-6	-34E-6	-89E-6	-152E-6	-48E-6	-14E-6	247E-6
Abs Change (amperes) ^h	0.211	-0.348	-0.376	-0.414	-0.459	-0.384	-0.360	0.216
%Change ⁱ	58.4	-31.9	-30.2	-17.0	-21.8	-23.5	-29.2	62.1

Notes:

- a. The number of cycles evaluated throughout the test lifetime.
- b. The average motor current for each event throughout the test, in Amperes.
- c. The standard deviation in the motor current between cycles 350 and the end of the test, as graphed in Fig. 4.9, in amperes.
- d. The intercept of the first regression line, between cycles 0 and 350. This corresponds to the motor current at the onset of the test, in amperes.
- e. The slope of the first regression line between cycles 0 and 350, in amperes/cycle.
- f. The intercept of the second regression line between cycles 350 and the end of the test. Units are amperes.
- g. The slope of the second regression line between cycles 350 and the end of the test, in amperes/cycle
- h. The absolute change between the motor current between the onset and conclusion of the test, in amperes.
- i. The percent change in motor current between the onset and the end of the test.

Regarding the upper graphs of Fig. 4.9, every event (except "Engine Prime" and "Shutdown", when the motor was still), during approximately the first 30 cycles, a

significantly larger initial motor current was encountered. For example, the motor current during the “Takeoff” event was between 2.5 and 2.8 Amps during the first few cycles, then fell sharply to 2.4 A. This is an indicator of an initial “break-in” period for both motor and pump, as any burrs, malformations, or other such physical frictions were worn away, yielding smooth system components requiring less torque to rotate.

During the next 350 cycles I_{mot} continued to decline during “Takeoff”, though less dramatically, reaching 2.1 A after the 350th cycle (approximately 1200 hours of flight time). During this period, between the 30th and 350th cycle, motor and pump continued to “break-in”, as the bearings loosened, the brushes within the motor smoothed the contacts, and the lubricant dispersed [15]. All together, the friction of the pump and the motor declined until it reached an operating point after 350 cycles. This is validated by the observation that the motor current had fallen by ~ 0.37 A, regardless of event. Recalling (3.2), the torque applied by the motor is directly proportional to the motor current. Also, the torque applied by the motor was used to pump the fuel, as well as overcome frictional losses within the motor and pump. Since the torque required to circulate the fuel was a variable dependent on RPM, and the 0.37 A decline in motor current was consistent throughout all events (though RPM was changing), therefore the reduction in motor current corresponded to a reduction in frictional losses, unrelated to fuel flow rate, validating the assertion of a “break-in” period.

After this period, between cycles 350 and the conclusion of the test, the motor current continued to decline, though not as dramatically as previously. During this period

the motor and pump continued to wear, and the torque required to overcome the internal losses continued to decline. As the motor wore throughout the remainder of the test, the motor speed may have declined also, as the contacts became worn, corroded and charred from sparking, resulting in intermittent contact and reduced armature voltage (more voltage lost in the contacts). Since the test was concluded by motor failure, the speed of the motor at the conclusion of the test could not be measured.

The standard deviation data (shown in the lower plots of Fig. 4.9) clearly shows that the motor current was a noisy measurement, with standard deviations a significant fraction of the means. Several discontinuities were observed throughout the test. "Engine Prime" remained "consistently noisy" at about 0.1 A, +/- 0.05 A. All other events showed a sudden increase in standard deviation occurring after system maintenance and lasting a few number of cycles (approximately cycles 720 through 750). During this period the software revision included an updated digital filter, which required several cycles to optimize. Once optimized, events 2, 3, 7 and 8 show a decline in measurement noise, indicating the digital filter decreased measurement noise during these events. The filter made little difference during "Takeoff" and "Cruise". The measurement noise during "Takeoff" showed an increase towards the end of the test. This can likely be attributed to the deterioration of the motor. Similar observations can be made during "Cruise" and "Descent". "Cruise" showed further anomalies, exhibited in two rapidly increasing sections, beginning prior to maintenance and again at maintenance. No explanation can be provided regarding this. However, the rapid

increase near the end of the test is likely due to the rapid deterioration of the drive motor. Finally, though both "Shutdown" and "Engine Prime" had no motor activity, "Shutdown" was significantly longer (2 hours versus 1 minute, 250 samples versus 11 samples), resulting in significantly more samples averaged during this event, and thereby reducing variation between cycles. Beyond this, during "Shutdown", the conclusion of the test showed a decline. The cause of this cannot be determined.

Statistical Evaluation of Average Motor Current

Both partitions of all events were tested for statistically significant slope. The hypothesis tested was that the slope was equal to 0, at a 95 % confidence level. The tests rejected the null hypothesis in every case, indicating the data revealed statistically significant trending for both partitions of all events.

Practical Evaluation of Average Motor Current

Two conclusions can be drawn from the data: 1) During the first 350 cycles I_{mot} fell approximately 0.37 Amperes, regardless of event, indicating a period of time when the motor and pump were "breaking in". 2) The trends show a continual *decline* in motor current throughout the test, indicating less torque was required to maintain fuel flow. This reveals the pump became more efficient throughout the lifetime, since the pump pressure decreased only slightly. The maximum decline was -31.9 %, observed during "Engine Start". Since this event required so little motor current to circulate the fuel, this percentage was exacerbated. The maximum decline in magnitude occurred during

“Cruise” with a value of 0.459 A, corresponding to -21.8 %. This better represents the changes occurring within the motor and fuel pump, since the system was operating with a significant fuel flow rate. This evaluation assumes the motor speed had remained consistent throughout the test, which will be discussed in Section 4.3.4.

4.3.3. Visual Inspection

The test was concluded because of failure of the motor. Upon disassembly, the commutation brushes showed signs of excessive heat and wear. The brushes had corroded to a fine black powder, which had circulated throughout the motor, causing wear throughout the internal assembly.

As for the pump itself, the final indicator of the effect of AGE fuel on the TCM fuel pump was the final inspection. No indication of corrosion or buildup was observed. Nor was there any sign of fuel leakage. A certified aircraft mechanic inspected the pump at the completion of the test and considered it to be in full working order.

4.3.4. Summary and Conclusions

The pump motor current had an initial drop in motor current of 0.37 A, regardless of event. During this period of time, fuel pressure remained consistent. Since this drop in applied torque was not dependent on motor speed, this indicated a “break in” period during which the friction of the bearings lessened as the lubricant dispersed [15].

Between the beginning and conclusion of the test, including the break-in period, the motor current showed a maximum decline during "Cruise", and resulted in a decline of -21.8 %. Also during the "Cruise" event, near the completion of the test the fuel pressure fell by -5.8%. As mentioned in Section 4.1, the test was concluded because of decomposition of the motor brushes. Throughout the test, the motor was operating at 25% of load (often less). At such loading, PMDC motors operate at less than 40% efficiency [16]. The lost power is dissipated as heat, which was observed in the brushes, as they appeared charred, pitted and had worn into a burnt black powder. Such degradation in the brushes also increases contact resistance between the motor drive and armature, reducing the armature voltage. Since the speed of a PMDC motor is dependent on the armature voltage [5], this corrosion would also result in a slowing motor as the brushes corrode. With a slowing motor, the fuel flow within the system would decrease, reducing the line pressure. With this reduced fuel flow, the torque required to rotate the fuel pump would also decrease, which was observed from the gathered data, indicating that near the end of the test, the applied torque and fuel pressure had decreased because of a slowing motor resultant from motor degradation.

Since the motor speed at the completion of the test could not be measured, no quantitative number can be provided regarding how much of these trends are attributable to this hypothesis. However, if it is assumed that the motor speed had remained constant, then the motor current showed that pumping the fuel became easier. If, on the other

hand, the motor speed had declined, then the trend observed in fuel pressure related to the condition of the motor and not fully to the condition of the pump.

Reference [3] found similar decomposition of the fuel pump motor, which they attributed to ethanol fuel having leaked into the motor. This was not the case in this test. Visual inspection found no sign of fuel leakage into the motor, and the coupling itself separated the motor from the pump, which would have prevented ethanol fuel from entering the motor if a leak did exist. The motor degradation was not attributable to ethanol exposure.

As mentioned, the visual inspection of the fuel pump revealed no evidence of fuel leakage during the test. Upon examination by a certified aircraft mechanic, the fuel pump was found to be in working order, no alarming indication of damage was observed.

As discussed in Section 2.2.2, the fuel pump is calibrated to operate at 120% of full load, with excess fuel returned to the fuel tank. The fuel pressure had fallen by only 6%, well within manufacturer tolerances, at the same time as the torque requirements had fallen by 21%, which is considered advantageous.

When all is considered, little evidence of alarming degradation of the fuel pump was observed throughout the test; in fact the fuel pump became more efficient as it operated using ethanol fuel.

4.4. Module 2: Fuel Servo

This section presents and evaluates the data recorded throughout the test relevant to the condition of the fuel servo. These data include the peak torque required to position the throttle and mixture lever arms, which was indicated by the peak current of the actuators during transition (labeled I_{thr} and $I_{mixture}$ throughout the text), and the pressure of the fuel leaving the servo for the flow divider, where fuel was returned to the fuel tank.

4.4.1. Throttle Actuation Peak Current

As an indication of the torque required to position the throttle lever arm from one setting to another, the current through the throttle's actuator was monitored throughout the test. An example movement is shown in Figure 4.10. Here, the current required to rotate the throttle lever arm from no throttle to full throttle is shown in blue, and the measurement of the peak current shown in black. This data was recorded using a Tektronix TDS-420 oscilloscope, prior to beginning the test and was used for initial calibrations. The current peaked after less than 30 ms, then steadily declined. Since the system was designed to sample at most every three seconds, the peak detection circuit, as discussed in Section 3.6.2, was implemented, and its resultant voltage is shown in black. The electronic circuit tracked the peak current and latched that value throughout each event, then, prior to a subsequent event, the peak was reset, allowing the circuit to latch the peak current of the subsequent event.

Also, prior to the actuator moving, at $t = 0.02$ seconds, the motor had a small current through it, in this case it was approximately 25mA. Even at moments in time when the actuators were not moving, a small holding current remained. In order for the actuation to occur, a certain current threshold was required. The exact threshold of current required for motion could not be measured because it varied with factors such as initial position and fuel flow rate; however, a threshold of 150 mA was a typical value. Therefore, if the current did not exceed 150mA, it was assumed the actuator was not moving.

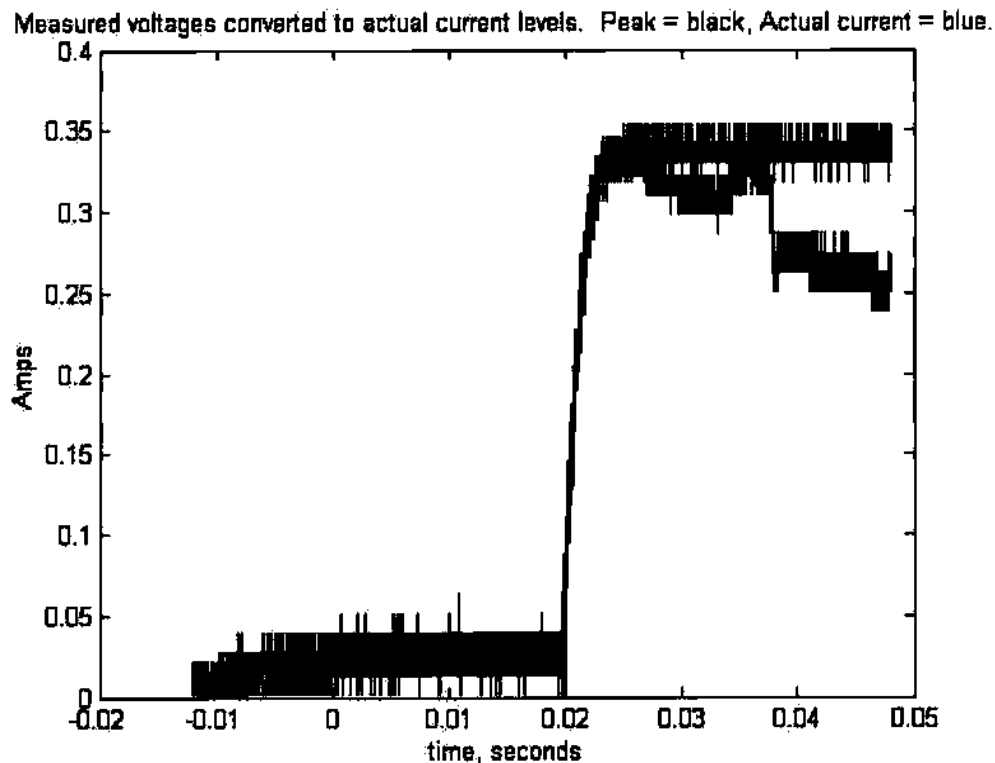


Figure 4.10. Example I_{thr} During an Event Transition.

An example cycle is shown in Figure 4.11. The peak actuation current is shown in green, and the throttle setting is shown in blue, with longer duration events labeled for reference. Observing the figure, the current required to move the lever arm from 10% throttle, during “Taxi”, to 100% throttle, during “Takeoff” was approximately 0.3 A. Then, to move the lever arm from 100% to 70% during “Cruise” was more, approximately 0.4 A. To move down to 50% during “Descent” required slightly more, perhaps 0.41 A. The same logic applies to each transition.

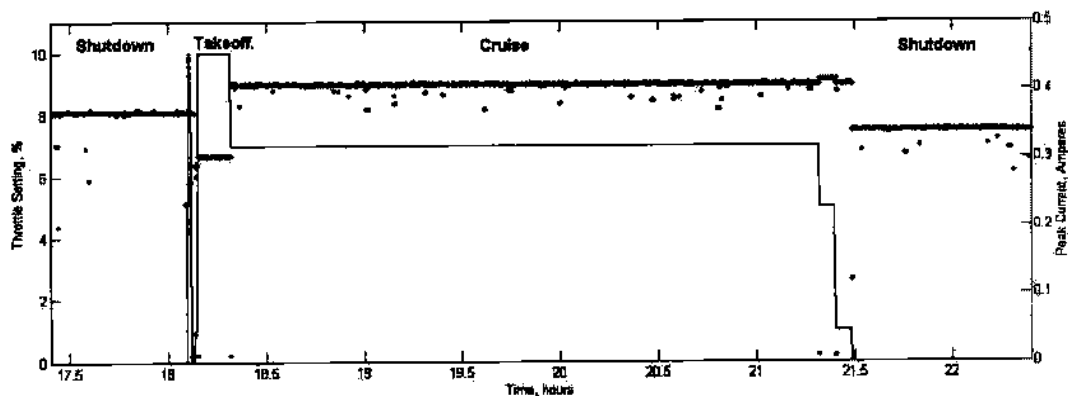


Figure 4.11. Example I_{thr} Data over a Single Cycle.

Figure 4.11 shows the system was subject to momentary fluctuations, observed easiest during “Cruise”. These most likely result from bit flips within the DAQ card’s ADC, or momentary fluctuations in measured voltages. Also, the current required from the first shutdown event was approximately 0.36 A, while the second shutdown required 0.34 A, a deviation of over 6% between a single cycle.

Figure 4.12 presents the data summarized as discussed in Section 4.2. Here, the peak current, measured in amperes, to position the throttle lever arm is shown in blue, versus the cycle number. Regression lines were superimposed in black, as well as the overall mean of the data for each event. Also, the data were parsed at cycle 720 for the first event, "Engine Prime" for reasons which will be discussed next.

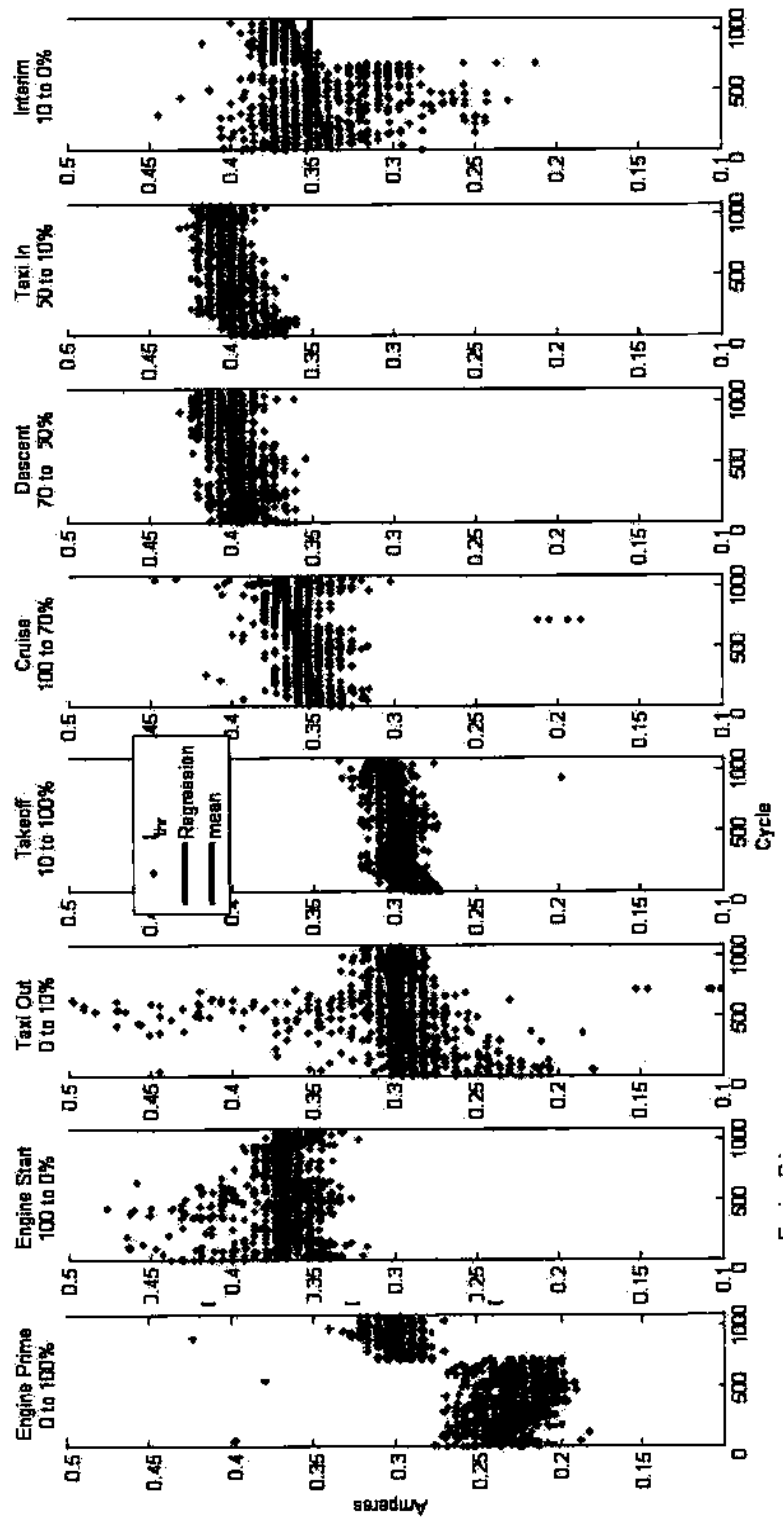


Figure 4.12. I_{br} throughout the Test, with Regression Analysis.

First noticed in these graphs is the significant amount of deviation within each event. This is likely due to the difficulty of peak detection. Any momentary spike in the input voltage, the Enable or the Up/Down pins of the digital potentiometer (see Section 3.6.2) was latched and held, in addition, false incrementing could have been cumulative within an event. Also, these data reveal several discontinuities in several events at cycle 720, when system maintenance was performed.

During “Engine Prime”, the peak current jumped approximately 0.05 A after system maintenance. Prior to cycle 720, the current had fallen 0.016 A, and after maintenance, the current increased by 0.012, both substantially less than the bias shift occurring during maintenance. It was mentioned in Section 4.1 that maintenance included adjusting the position of the lever arm when the setting was at zero throttle, to prevent the arm from reaching the physical limit. The data indicate the peak current required to move the lever arm from zero to 100% increased substantially because of maintenance, but only marginally because of deterioration within the actuators or fuel servo.

Also, during “Engine Start”, “Taxi Out” and “Interim”, the data indicated frequent outliers prior to maintenance, then after maintenance, this noise was reduced significantly. Maintenance involved tightening the mechanical couplings between the actuators and lever arms. As the test had progressed, the couplings loosened, allowing

increased slippage between the actuators and servo lever arms and increased inconsistency in peak current required to position the lever arm. After the couplings were retightened, the slippage was removed, resulting in more consistent data for the final 350 cycles of testing.

The summary statistics for the data are given in Table 4.5. The associated notes describe the data listed in the rows. The column associated with "Engine Prime" is split in two, in order to detail the effects of maintenance.

Table 4.5 Summary Statistics for I_{thr}

	Engine Prime	Engine Start	Taxi Out	Takeoff	Cruise	Descent	Taxi In	Shutdown
N^a	720	1073	1073	1073	1072	1064	1066	1066
Mean (Amperes) ^b	0.229	0.369	0.298	0.299	0.358	0.397	0.400	0.351
Std (Amperes) ^c	0.02	0.013	0.039	0.014	0.033	0.013	0.012	0.036
Intercept (Amperes) ^d	0.238	0.292	0.287	0.291	0.344	0.387	0.390	0.339
Slope (Amperes/cycle) ^e	-22E-6	34E-6	-6E-6	15E-6	25E-6	19E-6	18E-6	22E-6
Abs Change (Amperes) ^f	-0.016	0.012	0.023	0.017	0.027	0.020	0.020	0.023
%Change ^g	-6.987	4.013	7.882	5.689	7.815	5.169	5.019	6.857

Notes:

- a. The number of cycles evaluated throughout the test
- b. The overall average current required to position the lever arm during an event, in Amperes.
- c. The standard deviation of the mean of the data over the lifetime of the test, in amperes.
- d. The y-intercept of the regression line, corresponding to the current required to position the lever arm at the onset of the test. Units are Amperes.
- e. The slope the regression line indicated by the data. Units are Amperes per cycle.
- f. The absolute change in the current required to position the lever arm between test onset and conclusion. Units are amperes.
- g. The percent change in current between the onset of the test and the conclusion.

Statistical Evaluation

A statistical test was performed on the data to test the hypothesis that no degradation was observed over the lifetime of the test. The null hypothesis (H_0 : slope = 0) was tested at a 95% confidence level. The test rejected the null hypothesis for each event, indicating that a statistically significant trend was observed over the duration of the test.

Practical Evaluation

All events (except the first portion of “Engine Prime” and “Engine Start”) indicated a slight increasing trend, suggesting that over the test it became increasingly more difficult to adjust the lever arm. The worst-case change over the lifetime of the test was a 7.882% increase in the current required to position the lever arm, corresponding to an absolute change of 0.023 A, occurring during “Taxi Out” when the lever arm was moved from zero to 10%. The operational relevance of these data will be discussed in Section 4.4.5.

4.4.2. Mixture Actuation Peak Current

As with the throttle actuation system, as discussed in Section 2.3.2, the data regarding actuation of the mixture lever arm was collected through a peak detection circuit. An example cycle from Jan. 30th of 2005 is shown in Fig. 4.15. The figure is similar to the throttle actuator, the significant difference was that during several events the lever arm was not moved, resulting in a reset of the peak detector, with no corresponding motion to measure. During these events (2, 3, 4 and 7) the measured current was merely a holding current, and yielded no information regarding the condition of the fuel servo. Therefore, these events were excluded from analysis of the lever arm.

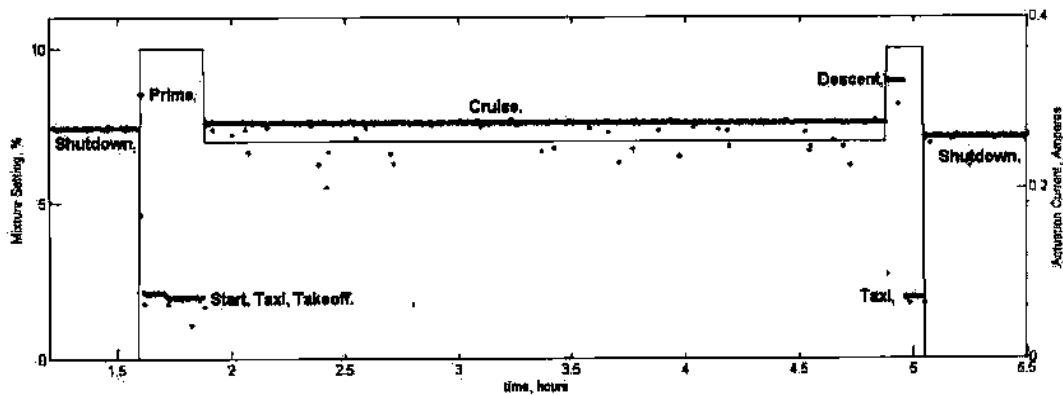


Figure 4.13. Mixture Current Measurements on Jan 30th 2005.

The mixture lever setting was not changed during each event. For example, in Fig. 4.13, the current required to rotate the lever arm from zero mixture (during the Shutdown event) to full rich (during “Engine Prime”) was 0.3 A. But then the mixture setting remained at full rich until the “Cruise” event, when it was scaled back to 70%. Therefore, the peak detector reset and latched nothing more than the holding current during the “Idle” “Taxi” and “Takeoff” events. The same occurred during the second “Taxi” event. These events were therefore ignored for evaluation, as they reveal no information relevant to the positioning of the servo’s lever arm.

Similar to the data regarding I_{thr} , the data for the mixture lever arm are shown in Figure 4.14, with the summary statistics included in Table 4.6.

Notes:

- a. The partition, "1" corresponds to the cycles between the onset and cycle 720, "2" corresponds to the cycles between cycle 721 and the conclusion of the test.
- b. The number of cycles evaluated in the partition
- c. The overall average of the peak-current required to position the mixture lever arm, in Amperes.
- d. The standard deviation of the means over all cycles, in amperes.
- e. The intercept of the regression line, corresponding to the amount of current required to position the lever arm at the onset of the test and at cycle 720.
- f. The slope of the regression line, in Amperes per cycle.
- g. The absolute change, in Amperes, between the required current at the onset of a partition and the conclusion of the same partition.
- h. The corresponding %change in required current for actuation.

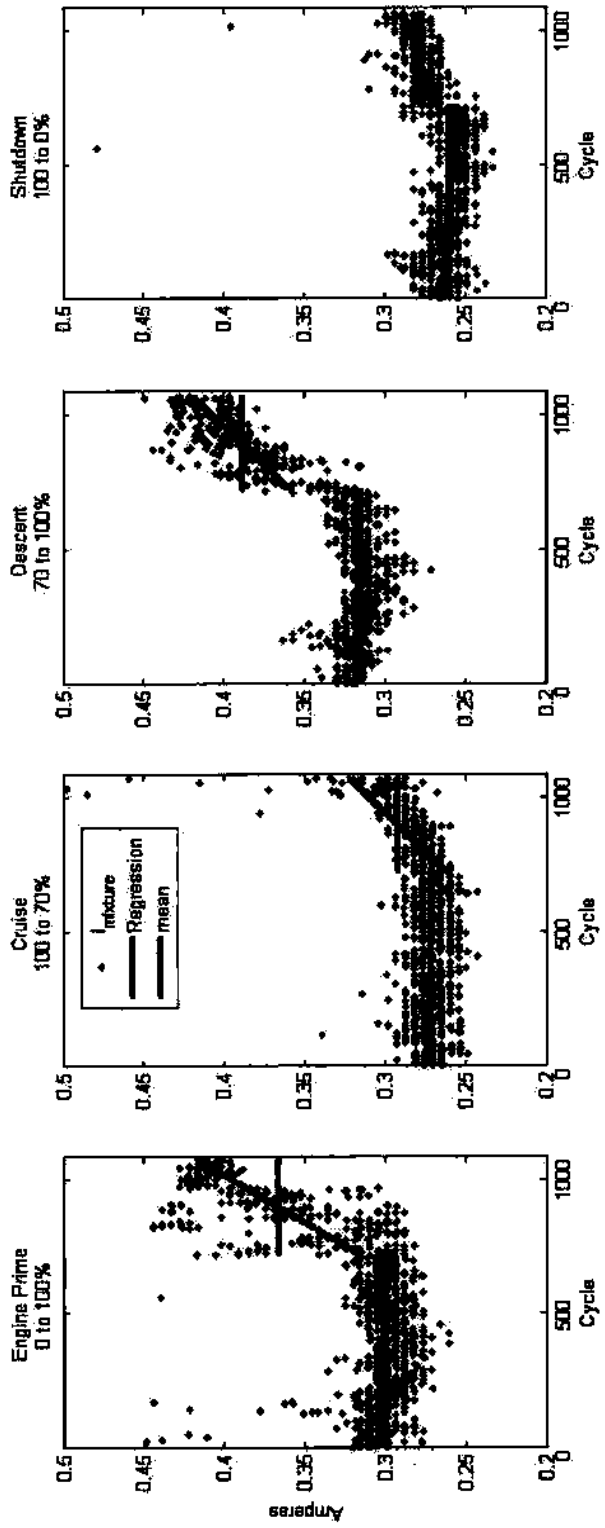


Figure 4.14. Summarized Mixture Actuation Current.

The first obvious observation is the discontinuity between events, occurring when system maintenance was performed. Though the most drastic disruption occurred during “Engine Prime” and “Descent”, all four events showed some evidence of alteration. Therefore the data were partitioned into “prior” and “post” maintenance periods.

The full explanation of the discontinuity in data cannot be explained by system maintenance. What is known is that the lever arm was found to be oscillating, and therefore the gain of the power amplifier was reduced (see Section 4.3.2). Such an action would reduce the precision of lever arm position, allowing more error between events, partially explaining the increased fluctuation in actuation torque required to position the lever arm. The practical evaluation section will discuss this in further detail.

Statistical Evaluation

The trends observed during the first portion of the test, prior to maintenance, were tested for statistical significance with a confidence level of 95%. At this level, the data indicated that during first portion of the test, a statistically significant trend in actuation current was observed for all events. Statistical tests for the second partition likewise indicated statistically significant trends.

Practical Evaluation

Prior to system maintenance the data indicated little practical change in torque. The largest change was a 3% decline in the current required to move the lever arm from 100 to 0% mixture, during “Shutdown”.

After maintenance was performed, “Engine Prime” and “Descent” showed a significant increase in torque, with changes of 27% and 15% respectively. Such an increase could be alarming. However, after the test was concluded the torque required to rotate the lever arm was measured directly, and was found to require approximately 2.5 kg-cm, which was 16 % less than the initial measurements performed on the lever arm. Admittedly, both the initial and final measurements of torque required to move the lever arm were rough measurements, this does indicate that factors beyond the condition of the lever arm were influencing the data. The full nature of these factors cannot be postulated at this time.

4.4.3. Throttle Fuel Pressure

The third indication of the performance of the fuel servo was the pressure of the fuel flowing out of the servo. This metric was labeled P_{thr} and corresponded to the fuel pressure leaving the servo for the fuel flow divider. Figure 4.15 shows an example cycle of operation, from January 30th of 2005, with the motor setting superimposed to yield insight into the timing structure. As with the other metrics discussed in preceding

sections, the data regarding the fuel pressure was parsed per event, shown in Fig. 4.16, and statistics were gathered and presented in Table 4.7.

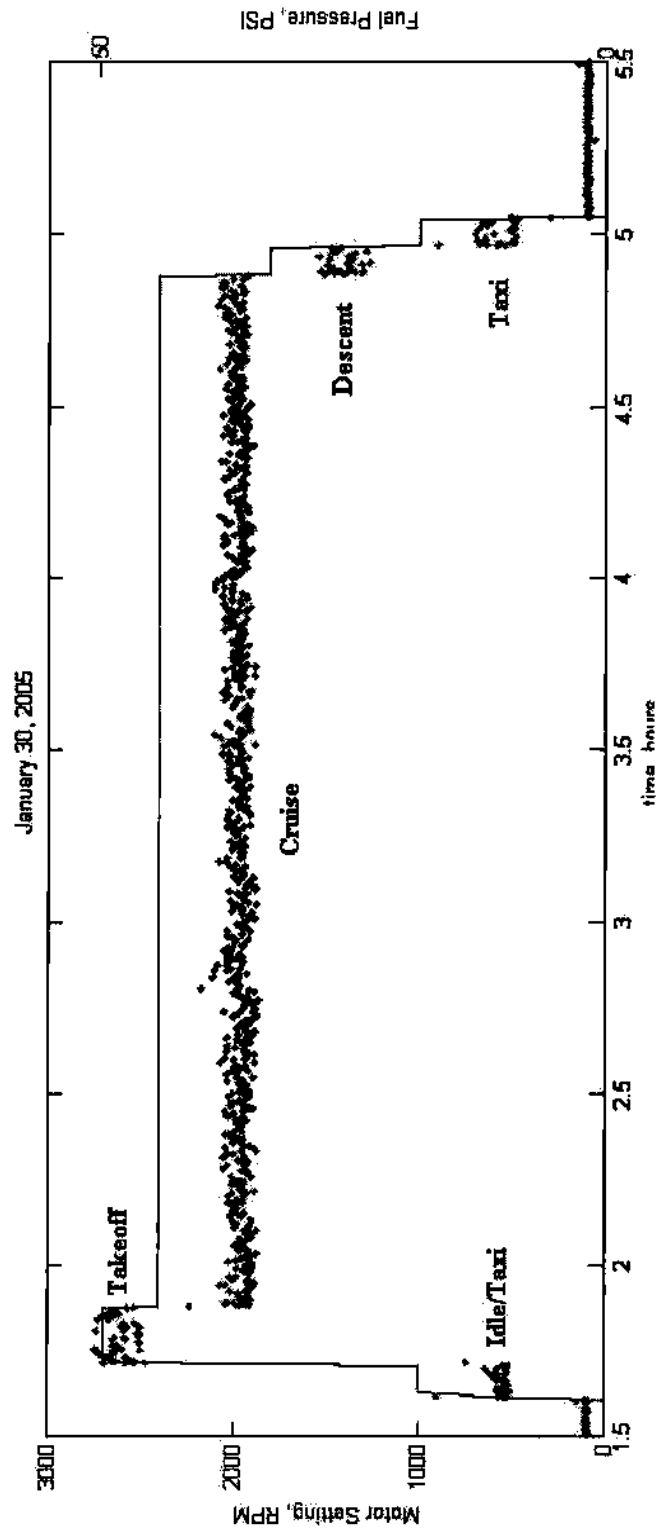


Figure 4.15. Fuel Pressure from the Fuel Servo to the Flow Divider, on January 30th, 2005.

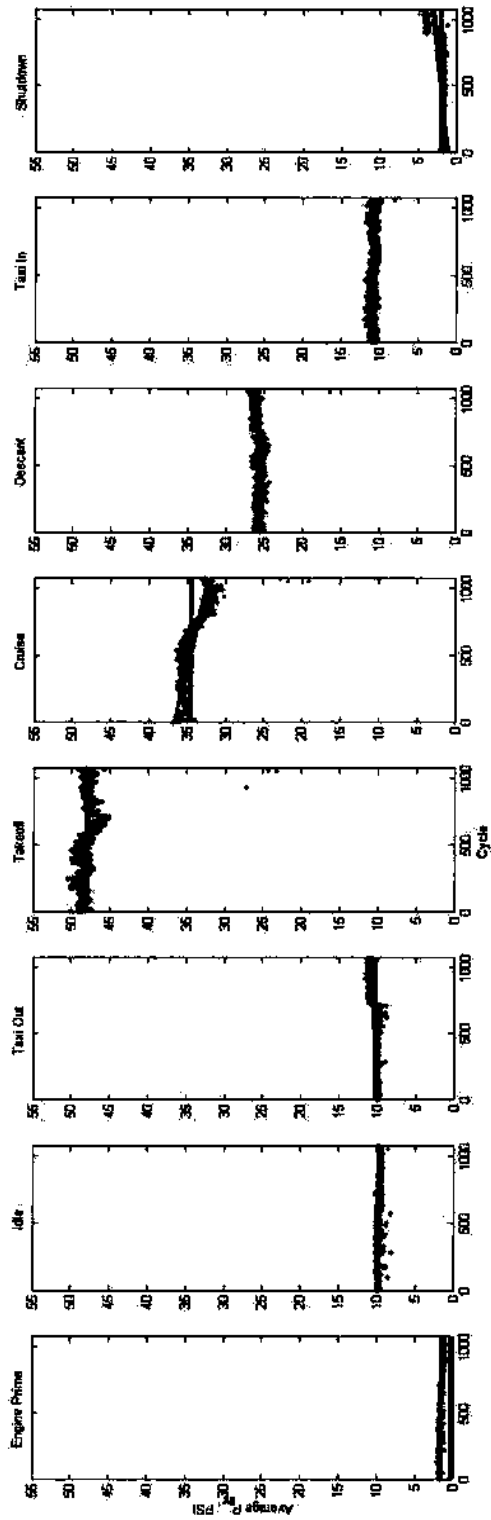


Figure 4.16 Fuel Pressure from the Servo to the Flow Divider.

Table 4.7 Summary Statistics for P_{thr}

	Engine Prime	Engine Start	Taxi Out	Takeoff	Cruise	Descent	Taxi In	Shutdown
N	1073	1073	1073	1073	1072	1064	1066	1066
Mean (PSI)	1.529	9.723	10.288	48.021	34.393	25.738	10.849	2.030
Std (PSI)	0.175	0.215	0.514	1.537	1.615	0.545	0.335	0.850
Intercept (PSI)	1.786	9.916	9.671	48.897	36.626	25.379	10.968	1.092
Slope (PSI/cycle)	-480E-6	-359E-6	1E-3	-2E-3	-4E-3	674E-6	-222E-6	2E-3
Abs Change (PSI)	-0.515	-0.385	1.232	-1.751	-4.462	0.718	-0.237	1.875
%Change	-28.829	-3.880	12.737	-3.580	-12.183	2.827	-2.162	171.715

Statistical Evaluation

A statistical test was performed on the data, testing the null hypothesis that the slope of the regression lines for all events was equal to 0. The test rejected the null hypothesis for all events. At a 95% confidence level, the data indicated statistically significant trends throughout the test.

Practical Evaluation

During "Taxi Out" a small baseline shift in the fuel pressure was observed, beginning at approximately cycle 720. The exact reason for this shift is unknown; however, since the data was consistent both prior and post-maintenance, it would appear to largely relate to adjustments made during maintenance, and not a change in the status of the fuel servo.

Another similar shift was observed during "Shutdown", though it did not begin with system maintenance, but at approximately cycle 850. As the test neared completion, the timing scheme was altered; the "Shutdown" period was reduced from two hours to 40 minutes. No other data was influenced by this. The shift observed here corresponded to the greater influence of the transient portion of the event transition. During the first several samples of data, the fuel pressure fell from approximately 11 PSI during "Taxi In" to approximately two PSI during "Shutdown". When the event was two hours long, over 250 samples were recorded, when reduced to 40 minutes, less than 100. Originally, the transient portion, which lasted approximately 12 samples, influenced the overall

average of the event only slightly. However, when the event length was shortened, this transient behavior influenced the average more substantially, resulting in the baseline shift observed.

Because the fuel pressure during “Engine Prime”, “Taxi out” and “Shutdown” was small (1.5, 10.2, and 2.03 PSI, respectively), the discontinuity in fuel pressure between the onset and conclusion of the test resulted in exaggerated percent changes - 28%, 12%, and 171% respectively, though the changes were only 0.5, 1.2 and 1.9 PSI, respectively. Because no fuel flows during “Engine Prime” and “Shutdown”, and the discontinuity was abrupt and consistent before and after maintenance for “Taxi Out”, it is unlikely that these indicate the servo was approaching failure.

The most relevant data recorded pertained to “Takeoff” and “Cruise”. During these events the fuel flow rate was the greatest and the data showed several discontinuities.

“Takeoff” showed an overall drop in fuel pressure of 3.6%, corresponding to 1.75 PSI. Locally within the lifetime of the test, prior to system maintenance, the data showed a period of declining fuel pressure. The cause of this cannot be explained at this time. However, after system maintenance, this decline in fuel pressure stopped, and the fuel pressure returned to near-original levels.

From the perspective of percent change, the most noticeable occurred during “Cruise”. During this event the fuel pressure at the outlet of the servo fell by over 12%, 4.4 PSI. Referring to Section 4.3, during the “Cruise” event the fuel pressure leaving the fuel pump and entering the servo fell by over 5%. It was obvious that as the fuel pressure entering the servo was reduced, the fuel pressure leaving the servo was likewise reduced. Therefore, the decline in fuel pressure observed here related to the condition of the fuel pump and motor, not solely to the condition of the fuel servo. At the onset of the test, when the servo was new, the ratio between the input fuel pressure (discussed in Section 4.3) to the outlet fuel pressure (being evaluated here) was approximately 1.22 during the “Cruise” event. Assuming a linear relationship between inlet and outlet fuel pressure, if the inlet fuel pressure fell by over 5 % (as shown in Section 4.3), the outlet fuel pressure would be expected to fall by over 7 %. Such an assumption leaves approximately 5 % reduction in fuel pressure arguably attributable to the condition of the servo. This corresponds to a drop of 1.8 PSI in fuel pressure possibly resulting from deterioration of the fuel servo.

The other events exhibited far smaller trends in the data, in the range of two to 3%. Such declines are not alarming; they do not indicate the system was approaching failure mode.

Throttle Fuel Pressure Conclusions:

The data collected regarding the fuel pressure exiting the servo to the flow divider showed a worst-case decline of -12% (4.4 PSI). This decline could not be fully attributed

to deterioration of the fuel servo, since during the same period the fuel pressure entering the fuel servo had declined by 5%, which would lead to at least a 7 % decline in the data evaluated here, leaving a true decline of 5 % attributable to the servo, corresponding to 1.8 PSL.

4.4.4 Visual Inspection

The final determinant of the state of the fuel servo was a visual inspection. The fuel servo was found to show no signs of leakage, the lever arms were found to be in working order. Inspection by a certified aircraft mechanic also considered the fuel servo to be in acceptable working order. No sign of significant or unusual deterioration was observed.

4.4.5. Fuel Servo Summary and Conclusions

Servo data indicated the peak current required to position the throttle lever arm increased over the test lifetime. This worst-case increase was observed during the "Cruise" event, when the lever arm was motioned from 100% to 70%. The trend, however, could not be fully attributed to changes within the fuel servo, since system maintenance introduced several discontinuities in the data. Since the visual inspection found the servo in working order, only marginal effects resulting from the use of ethanol fuel on the ability of the fuel servo to position the throttle lever arm could be concluded.

The current required to adjust the mixture lever arm increased by 27% over 5500 hours of testing. This was the worst-case change, observed in the "Engine Prime" data, when the lever arm was moved from zero to 100% mixture. This perhaps could cause alarm, except that the increase began at system maintenance after over 720 cycles. Prior to this, the lever showed little evidence of deterioration, indicating maintenance likely caused some disruption into the system. Further, when the torque required move this lever arm was measured by external means, it was found to require 16 % *less* torque to move the lever arm after the lifetime of the test. While, admittedly, the external measurements performed before and after the test were rough by nature, they do reveal that the data reflected issues external to the condition of the lever arm, and likely to be within the actuator itself.

Visual inspection found the fuel servo in working order. External torque testing proved that the data reflected issues unrelated to the condition of the fuel servo, no conclusive indication of significant component wear resulting from ethanol fuel could be confirmed.

As discussed in Section 2.2.3, the torque requirements to position the lever arms have no manufacturer specification, so long as they remain mobile, they can be considered acceptable. The increased torque demand observed here is considered trivial in light of the mechanical design of the pilot/servo interface. Within the cockpit the pilot positions a lever, requiring motion of his entire arm. The cockpit control is linked

through a stiff cable and housing to the servo, located near the engine, some 6 feet away. The amount of effort to move the cockpit lever arm is dominated by these components, the torque required at the servo itself is trivial in comparison.

After accounting for the decline in fuel pressure entering the servo, resulting from deterioration of the motor (see Section 4.3), the fuel pressure leaving the servo showed a worst-case decline of 5% during the "Cruise" event, corresponding to 1.8 PSI. Other events showed much smaller declines, in the 2 to 3% range. The data therefore indicated that the condition of the fuel servo caused the fuel pressure to decline by approximately 1.8 PSI over the lifetime of the test. Such a decline was not alarming, since visual inspection found the servo in working order, and the servo was still operating at 95 % efficiency after over 5500 hours of testing.

4.5 Auxiliary System Parts

This section presents the evaluation of the auxiliary system parts monitored during the test, including the fuel filter, fuel lines, fuel tank and flow divider. These components were evaluated through a visual inspection.

4.5.1. Fuel Filter

A visual inspection of the fuel filter was performed September 26th, 2005, after the completion of the test. First, the fuel filter was observed through the clear plastic housing, and no debris was found. The unit was then disassembled and cleaned, and

again, no significant particulates were observed. The filter itself was then reattached to a second similar rig-test and, as of this text writing, is performing perfectly.

4.5.2. Fuel Lines

A visual inspection of the fuel lines was performed on September 25th, 2005, at the completion of the test. No sign of corrosion or buildup was observed.

4.5.3. Fuel Tank

At the completion of the test, the fuel tank was drained and inspected for buildup or corrosion, and none was observed. Neither sealant degradation nor leaks along the seals were observed. Further, the fuel tank was refitted and, at this writing, is being used for a second rig test.

4.5.4. Flow Divider

The flow divider was inspected at the conclusion of the test. No unusual degradations were observed. Further, the flow divider has been integrated into a second rig test and is operating properly.

4.5.5 Summary and Conclusions

After performing visual inspections of the various auxiliary rig test components no unusual degradation was observed. Furthermore, several parts continue in operation in other testing assemblies.

4.6. Data Analysis Summary and Conclusions

Overall, results from the test showed some evidence of change throughout the 5500 hours of experimentation. However, significant deterioration of the tested components was not observed. From a worst-case standpoint, the motor current showed a decrease of 21.8%, during the "Cruise" event. This decline likely reflected both a "break-in" period at the very onset of the test, and then a slowing motor as the motor deteriorated, occurring near the completion of the test. The speed of the motor could not be verified, since the test concluded with motor failure. The conjecture is supported by the corresponding declines in measured fuel pressure entering and exiting the fuel servo of -5% and -12% respectively, both declines were worst-case and both occurred during the "Cruise" event, congruent with the worst-case change in motor current.

The current required to position the servo's throttle and mixture lever arms showed an increasing trend of 7% and 27% respectively. These were worst-case values, and occurred during "Taxi Out", when the throttle was increased from zero to 10%, and during "Cruise", when the mixture was reduced from 100 to 70%. These trends were found to be heavily influenced by external factors, unrelated to the condition of the fuel servo. However, assuming these trends *were* fully attributable to the condition of the fuel servo, should these trends continue they may eventually lead to an operator being unable to set the throttle and mixture properly. Yet, after 5500 hours of testing described in this paper, the unit was still found in acceptable working condition.

5. Project Conclusions

This work has involved the design, implementation and analysis of a rig test performed on a TCM manufactured aircraft fuel system subjected to an emulated lifetime of cycling ethanol-based fuel. The work began with system design and implementation, followed by analysis of the gathered data.

This section presents overall summary and conclusions of the work. It begins by discussing the system design, presenting strengths and weaknesses, and possible improvements for similar future tests. Then an evaluation of the performance of ethanol fuel is given.

5.1. System Design

Summary

This work began with construction of a closed fuel system to augment testing of the components using ethanol-derived fuel. This system included a fuel tank in which ethanol fuel was stored, fuel lines, filter, and flow divider through which the fuel pump circulated the fuel, and the fuel flow controller routed the fuel flow back to the tank, either through a fuel flow divider, emulating fuel consumed by the engine, or a return line.

To automate the speed of the fuel pump and the settings of the flow controller, as well as monitor the performance of the components subjected to ethanol-based fuel, an

electronic system was interfaced to the mechanical components, and controlled by a personal computer. A 0.5 HP PMDC motor powered the fuel pump at speeds emulating those expected during aircraft operation. Small PMDC motors with a simple position feedback and control scheme adjusted the mixture and throttle settings of the flow controller, again according to a scheme emulating the settings repeated throughout an aircraft's lifetime.

An electronic system was also implemented to monitor system performance by measuring certain metrics such as fuel pressure, torque required to circulate the fuel, torque required to adjust the flow controller's lever arms, and data external to the system, namely relative humidity, air and fuel temperature.

Conclusions

Upon completion of the test, the monitoring and control system performed acceptably. The physical system itself showed no weaknesses, fuel circulated consistently through the system with no outside interaction, and no leaks were observed.

Electronically, the system design had a few weaknesses. First, and foremost, the pump's motor became the limit to the test, as the brushes degraded over time.

Accurate motor sizing was challenging, as the data indicated. At the beginning of the test, when the motor and fuel pump were relatively new, the power required to

circulate the fluid was greater, because neither the motor nor the pump had been broken in. The motor was sized based on requirements at this period. Motor current data showed the motor itself was operating at a light load, approximately 25% of rated. At this loading, the efficiency of a motor is poor [16], resulting in more power dissipated as heat. The motor brushes, indeed, showed signs of this - appearing charred upon a visual inspection. Better motor sizing or a cooling system may have increased the length of the test. A second rig test, based on a Lycoming manufactured fuel system incorporates this proposition by using a vented motor, with a fan built on the end of the shaft.

The second weakness involved the position control scheme of the fuel servo's lever arms. The lever arms themselves were required to have a 90° range of motion, and the feedback potentiometers were chosen with the same range. This allowed no margin at either end of the lever arm motion. Beyond this, the feedback itself was nonlinear at the ends. These issues manifested in two ways. First, by having no margin, the throttle arm was reaching its mechanical limit, resulting in a high current through the motor as it tried to extend beyond the limit. Second, the nonlinearity of the potentiometers resulted in oscillation of the mixture's lever arm, possibly skewing the data, and causing unusual wear of the servo's slip rings. In future rig testing, choosing feedback potentiometers with a larger range of motion will prevent these issues.

5.2. Ethanol Fuel Performance

The rig test detailed in this work lasted for over nine months, during which the fuel system was subjected to an emulated 1070 flights, corresponding to 3712 hours of flight time, interspersed with brief periods of inactivity after each flight. For the fuel system considered here, two engine overhauls, the first after 1800 hours of flight time, and the second after 3600, should have been performed. The test, therefore, subjected the components to significantly more stress than intended by the manufacturer.

Auxiliary Components

Beginning with the auxiliary system components, such as the fuel lines, fuel tank, filter, and flow divider, the study indicated ethanol-based fuel did not result in unusual component degradation. Neither leaks, nor buildup or corrosion within the auxiliary system were observed. In fact, the fuel tank, filter and flow divider were immediately incorporated into a second rig test, and are performing without problem as of the writing of this text.

Fuel Pump

Visual inspection of the fuel pump at the completion of the test showed no indication of corrosion or buildup within the pump, nor were there any signs of leakage within the fuel pump.

The test data indicated a significant break-in period, for both the fuel pump and motor that powered it. During this time, beginning with a sharp initial period lasting 30 cycles, and continuing for approximately 350 cycles the torque declined significantly, while the fuel flow rate (as indicated by the fuel pressure) remained constant. Since the fuel flow rate during the break-in period did not change, the torque required to circulate the fuel also held constant; therefore, the reduction in applied torque related to the reduction in internal friction as the system reached steady-state. Such a break-in period is expected for any motor and bearing system [15] and does not correlate to a degradation resulting from ethanol-based fuel, especially since the bearings themselves were not exposed to ethanol fuel, and visual inspection revealed no fuel had bypassed the seals into the bearings.

After the pump and motor had broken-in, the torque applied to the pump continued to decline, finally reaching 21.8%, (worst-case) at the conclusion of the test. With this decline the fuel pressure within the fuel line declined (-5%). Conclusions were difficult to solidify, since the motor itself failed, causing the end of the test. The observed declines most likely indicated the speed of the motor was slowing as the brushes corroded near the completion of the test, and was not the result of a degradation in the fuel pump. Assuming a worst-case scenario, that the reduction observed did result entirely from changes within the fuel pump, the fuel pump was still operating at better than 95% original capacity, well within the manufacturer calibrated 20% tolerance, more than sufficient for aeronautical use, even beyond two scheduled overhauls.

Fuel Servo

A visual inspection of the fuel servo showed no indication of fuel leakage nor unusual corrosion or buildup. The servo's output fuel pressure data indicated that the fuel pressure at the exit of the servo declined by 5%, after accounting for the decline in fuel pressure at the inlet of the servo, which was attributed to the degradation of the motor. Assuming that the decline resulted from ethanol-based fuel, the fuel servo was still delivering 95% of the initial fuel amount to the flow divider, even though a time period equivalent to two scheduled overhauls had been allowed to elapse.

The data also indicated the torque required to position the throttle lever arm had increased approximately 5%, while the torque required to adjust the mixture lever arm increased by 27%. Assuming this was entirely attributable to ethanol fuel, these changes were still considered small. External testing indicated the lever arms remained sufficiently mobile for aircraft operation, even after two scheduled overhauls had elapsed, and data from the fuel pressure output indicated the fuel flow remained consistent, from the beginning of the test to the end.

Overall, the test indicated some change in performance of the fuel pump and fuel servo throughout the lifetime of the parts. The change was not alarming in any fashion. Even after the test had ran beyond a time period equivalent to two scheduled overhauls, the parts were still adequate for safe aircraft operation. As a replacement fuel, this test

indicated ethanol caused no significant degradation to fuel system components, and no unexpected issues within the fuel system can be anticipated as a result of its use.

References

- [1] "Aviation Grade Ethanol Materials Compatibility Evaluation," Final Report, Energy & Environmental Research Center, University of North Dakota, December-2004, pp. 1-37.
- [2] "Grade 82 UL Aviation Gasoline Specification Background Information," ASTM Committee D02, Subcommittee J on Aviation Fuels Research Report R:D02-1427, June 1999, pp.7:1-12
- [3] "Evaluation of Ethanol Based Aviation Spark Ignition Engine Fuel," Cessna Engineering Report, July 2002, pp 30-47, 67-70
- [4] *Portable E Series Multifunction DAQ*, Austin, TX: National Instruments, Inc. web site: www.ni.com, downloaded May 14th, 2003.
- [5] *Handbook of Electric Motors*. Edited by R. Engelmann and W. Middendorf. New York, NY: Marcel Dekker, Inc., 1995, pp. 83-84
- [6] *Model P255 Stainless Steel Pressure Transducer*, Moorpark, CA: Kavlico Corporation. Web site: www.kavlico.com, downloaded February 28th, 2005
- [7] M.H. Rashid, *Microelectronic Circuits, Analysis and Design*. Boston, MA: PWS Publishing Company, 1999, pp. 330-331
- [8] A. S. Sedra and K. C. Smith, *Microelectronic Circuits*, New York, NY: Oxford Press, 5th ed., 2004, pp.89, 94-102
- [9] *DC Motors Speed Controls Servo Systems*. Hopkins, MN: Electro-Craft Corporation, 5th ed., 1980, pp.2-7

- [10] *Current Transducer LA 25-NP*, Milwaukee, WI: LEM Holding USA, Inc. web site: www.lem.com, downloaded May 26th, 2006.
- [11] *Medium Power Op Amp, 0041 Series*, Liverpool, NY: MS Kennedy Corp. web site: www.mskennedy.com, downloaded March 11th, 2005.
- [12] R. Mancini, *Op Amps for Everyone, Design Reference*. Dallas, Texas: Texas Instruments Inc., 2002, p.3-3
- [13] *Increment/Decrement Digital Potentiometer, AD5220*, Norwood, MA: Analog Devices. Web site: www.analog.com, downloaded August 17th, 2004
- [14] *TLV3701 TLV3702 TLV3704 Family of Nanopower Push-Pull Output Comparators*, Austin, TX: Texas Instruments, Inc. web site: www.ti.com, downloaded August 17th, 2004
- [15] M. Shaw and F. Macks, *Analysis and Lubrication of bearings*. York, PA: McGraw Hill, 1949, pp.426-430
- [16] A. Pansini, *Basics of Electric Motors, Including Polyphase Induction and Synchronous Motors*. Englewood Cliffs, NJ: Prentice Hall, 1989, p.28

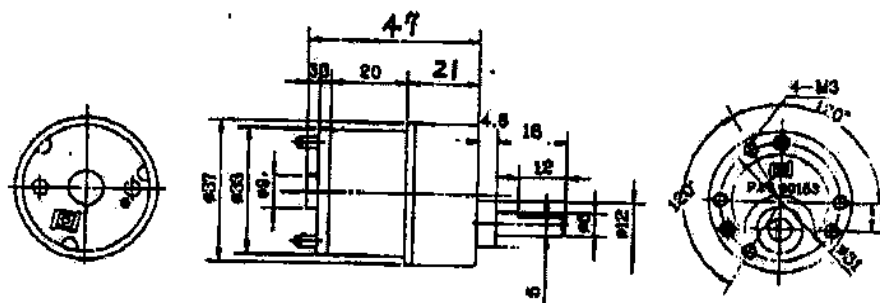
APPENDIX A: Servo Actuators Manufacturer Specifications

DATE: AUG. 29, 98
 NO. : 889808290.1
 PAGE: 1/2

CUSTOMER NAME :
 TYPE: HM-GH35GM8 TYPE
 MODEL NO. : HM-GH12-1641T
 CUSTOMER PART NO.:

Jameco Part Number 155838

I. OUTER DIMENSIONS :



II. GEAR RATIO : 270:1

TYPE	A	B	C	D	E	F	G	H	I	J	K	L	M	N	O	P	Q	R
RATIO	6	10	18	30	50	60	75	90	100	150	180	270	500	810	900	1000	1500	10000
DIM "L" MM	19.5	18.5	18.5	18.5	18.5	18.5	18.5	18.5	18.5	24	24	21	24	24	24	24	26	26
EFF %	81	81	73	73	66	66	66	66	66	58	58	58	59	53	53	53	48	48
ALLOWABLE TORQUE kg-cm	0.7	0.7	1.0	1.3	2.3	3	4	4	5	6	6	6	6	6	6	6	6	6

Figure A.1. Actuator Motor Specifications.

SPECIFICATION SHEET

DATE: AUG.29.98
NO. : SS98082902
PAGE: 2/2

CUSTOMER NAME :
TYPE: HN-GH35GMB TYPE
MODEL NO. : HN-GH12-1641T
CUSTOMER PART NO.:

III. SPECIFICATIONS :

1. RATED VOLTAGE : DC 12
2. DC VOLTAGE OPERATING RANGE : DC 3 - 12V
3. TORQUE(LOAD) AT MAXIMUM EFFICIENCY : 3.0 Kg-cm
4. STALL TORQUE : 10 Kg-cm
5. NO LOAD SPEED: 20 RPM \pm 10%
6. SPEED AT MAXIMUM EFFICIENCY(UNDER LOAD AT 3.0 Kg-cm): 15 RPM \pm 10%
7. NO LOAD CURRENT : 65 mA
8. CURRENT AT MAXIMUM EFFICIENCY(UNDER LOAD AT 3.0 Kg-cm) : 250 mA
9. SHAFT END PLAY : 0.8 M/M
10. STARTED TORQUE : 10 Kg-cm
11. INSULATION RESISTANCE : 10 M OHM
12. DIELECTRIC STRENGTH : 300V DC
13. GEAR RATIO: 270:1

Figure A.2. Actuator Motor Specifications (continued).

Appendix B: Position Transducer Manufacturer Specification Data

Honeywell Sensing and Control



640CS103A06NAAY

TH100 Rotary Position Transducer, 180 degrees Mechanical Travel, 10,000 Ohms Resistance value

Features

- Long rotational life
- Economical package
- Sealed construction
- High rotational torque

Typical Applications

- Marine controls
- Off-road vehicles

Description

The TH100 Series puts Honeywell's proven variable-resistor technology to work in angle-management applications such as control-lever sensing and equipment position feedback. High performance and low cost make it attractive for a wide range of applications. Special electrical and mechanical configurations, including dual tracks, D-shape rotor holes, etc. are available on special order.

Supply Voltage	350 Vdc max.
Measurement Type	Rotary
Housing Size	39,47 mm [1.55 in] x 45,72 mm [1.8 in]
Total Mechanical Travel	180°
Electrical Travel	170°
Linearity	± 5 %
Shaft Material	Plastic
Shaft Diameter	6,35 mm [0.25 in] thru hole with 2,67 mm [.105 in] wide x 2,29 mm [.09 in] diameter slot
Type of Element	Conductive plastic
Housing Style	Plastic
Termination	Three 20 AWG, 152,4 mm [6.0 in] wire leads
Operating Temperature Range	-40 °C to 120 °C [-40 °F to 248 °F]
Vibration	15 g at 50 Hz to 1000 Hz
Shock	50 g half sine
Operating Life	one million full cycles

Total Resistance	10,000 Ohms
Resistance Tolerance	± 15 %
Dielectric Strength	500 V rms
Sealing	Withstands hose-directed water spray and immersion at limited depth
UNSPSC Code	41111937
UNSPSC Commodity	41111937 Rotary position sensors
Availability	Global
Comments	0.5 W max. Power Rating
Series Name	TH100 Series

Appendix C: Humidity Sensor Manufacturer Specification Data



EWS-RH

Relative Humidity/Temperature Transmitter

Additional EWS Series Models Available

Model	Description
EWS-TC-(*)	Wall mount thermocouple sensor (* = insert type J, K, T, E)
EWS-RTD	Wall mount RTD sensor (100 Pt., .00385)
EWS-TX	Wall mount solid state temperature transmitter
EWS-BP-A	Wall mount barometric pressure transmitter

Theory of Operation

A 4-20 mA loop is a series loop in which a transmitter will vary the current flow depending on the input to the transmitter. In the EWS-RH the amount of current allowed to flow in the loop will vary depending on the relative humidity or temperature being measured by the sensor. Some advantages of a current output over a voltage output is that the signal measured is less susceptible to electrical noise interference and the loop can support more than one measuring instrument as long as the maximum loop resistance is not exceeded.

A typical application utilizing a current loop will normally consist of a power supply, the transmitter and a meter, recorder or controller to measure the current flow. The loop resistance is the sum of the measuring instruments and wire used. The maximum allowable loop resistance for the EWS-RH to function properly is found by using the following formula:

$$R_{\max} = (\text{power supply voltage} - 8 \text{ volts}) / .02 \text{ amps}$$

For applications that require a voltage output signal the EWS-RH has a built-in 250 Ohm shunt resistor that will convert the transmitters output to a 1-5 Vdc signal when wired correctly. See "Transmitter Wiring Examples" in this manual.

Recommended Accessories

Power Supply, OMEGA® Part No.: PSU-93

Shielded 4-conductor cable, OMEGA® Part No.: TX4-100

Conduit Box Mounting Kit, OMEGA® Part No.: EWS-MB

EWS-RH
Relative Humidity/Temperature Transmitter

NOTE

Note: These units are not designed, nor recommended for medical, Explosive Environment or outdoor applications.

Mounting

OMEGA's EWS Series of sensors and transmitters are designed for wall mounting in locations that are free from dirt, grease, food particles and condensing moisture such as manufacturing clean rooms, computer rooms and laboratory type environments. Plastic wall anchors and mounting screws are included for mounting to standard wallboard. A conduit box mounting bracket/wall plate adapter kit is also available as an option that will allow the transmitter to be mounted to a standard electrical conduit box.

Order OMEGA® Model No.: EWS-MB.

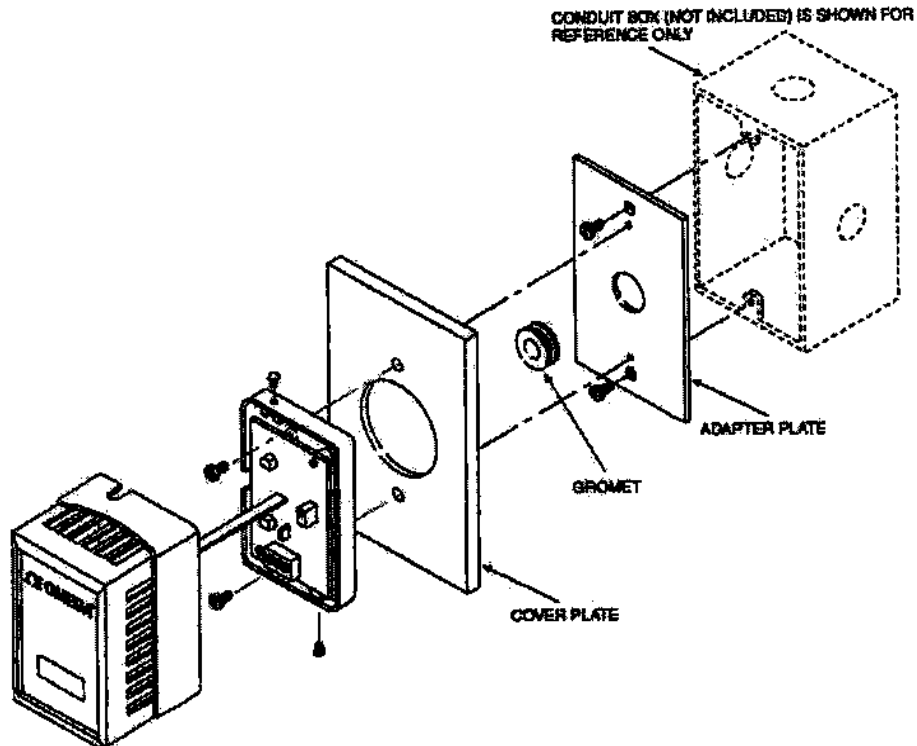
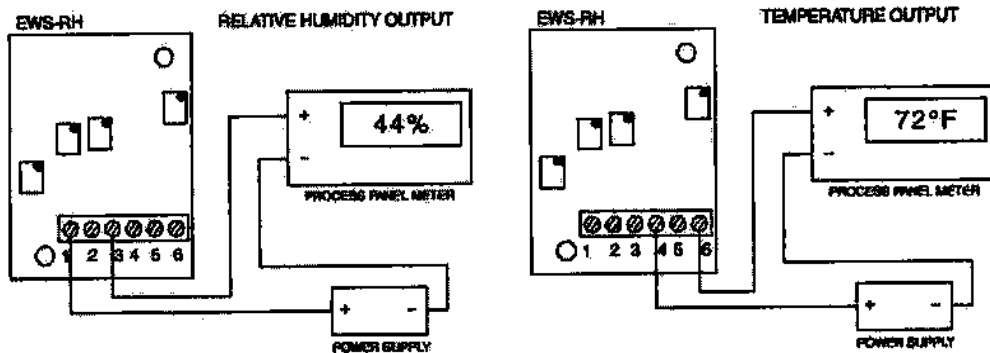
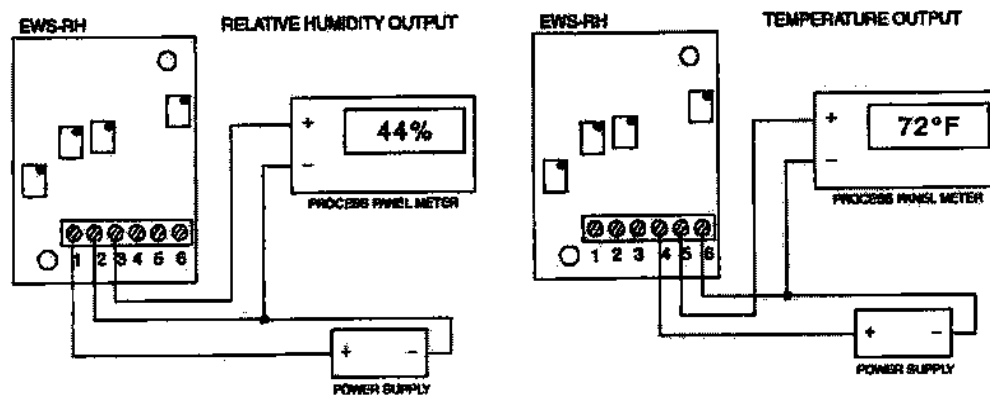


Figure 1: Mounting Diagram

EWS-RH
Relative Humidity/Temperature Transmitter



**Figure 2: Transmitter Wiring Examples
 For Current Output (4-20 mA)**



**Figure 3: Transmitter Wiring Examples
 For Voltage Output (1-5 Vdc)**

FWS-RH 

Relative Humidity/Temperature Transmitter

RH/Temperature Calculations

To calculate % Relative Humidity by measuring current output in milliamperes.

$$\left(\frac{\text{Current output} - 4}{.16} \right) = \% \text{ RH}$$

To calculate Temperature by measuring current output in milliamperes:

$$\left(\frac{\text{Current output} - 4}{16} \times 135 \right) + 5 = \text{Temp } (^{\circ}\text{F})$$

RH Measured Vs Output Reading

% Relative Humidity	Output	
	Current(mA)	Voltage(Vdc)
5	4.8	1.2
10	5.6	1.4
15	6.4	1.6
20	7.2	1.8
25	8	2
30	8.8	2.2
35	9.6	2.4
40	10.4	2.6
45	11.2	2.8
50	12	3
55	12.8	3.2
60	13.6	3.4
65	14.4	3.6
70	15.2	3.8
75	16	4
80	16.8	4.2
85	17.6	4.4
90	18.4	4.6
95	19.2	4.8

Temperature Measured Vs Output Reading

Temperature °C (°F)	Output	
	Current(mA)	Voltage(Vdc)
-15 (5)	4	1
-10 (14)	5.07	1.27
0 (32)	7.20	1.80
10 (50)	9.33	2.33
20 (72)	11.94	2.99
30 (86)	13.60	3.40
40 (104)	15.73	3.93
50 (122)	17.87	4.47
60 (140)	20	5

EWS-RH **Relative Humidity/Temperature Transmitter**

Calibration

Your transmitter has been factory calibrated to meet or exceed the specifications outlined in this manual. To maintain original specifications it is generally recommended that your transmitter be recalibrated on an annual basis depending on operating conditions.

Relative Humidity Calibration Procedure

Recommended equipment:

Humidity Generator/Calibrator Kit, OMEGA® Model No.: RHCL-KIT
Handheld Digital Multimeter, OMEGA® Model No.: HHM29

NOTE

Note: Do not make adjustments to potentiometer "P3", this is a factory setting and is not field adjustable. If "P3" is disturbed the transmitter will need to be returned to the factory for service.

1. Remove enclosure cover
2. Connect transmitter as shown in figure below.
3. Apply power to transmitter and allow to warm up for 15 min.
4. Place sensor in a 20% RH environment and allow to stabilize for 20 min.
5. Adjust potentiometer "P1" for a output reading of 7.2 mA
6. Place sensor in a 80% RH environment and allow to stabilize for 20 min.
7. Adjust potentiometer "P2" for an output reading of 16.8 mA
8. Repeat steps 4, 5, 6, 7 as necessary until proper readings are maintained.
9. Calibration complete.

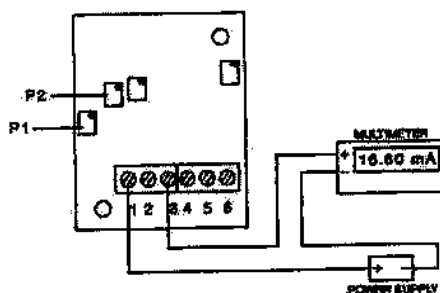


Figure 4: Relative Humidity Calibration Procedure



Temperature Calibration Procedure

Recommended equipment:

Series 860 Thermistor Meter OMEGA® Model No. 865F or 865C
 Series 400 Thermistor Probe, OMEGA® Model No.: ON-406-PP
 Handheld Digital Multimeter, OMEGA® Model No.: HHM29

1. Remove enclosure cover.
2. Connect transmitter as shown in figure below.
3. Apply power to transmitter and allow to warm up for 10 min.
4. Place unit on workbench with temperature reference probe next to unit.
5. Allow output from transmitter and reference probe to stabilize.
6. Observe the reading on the handheld thermometer coming from the reference probe.
7. Without touching the unit with your hand, adjust potentiometer "P4" for a current output of the transmitter that matches the temperature measured by the reference probe. Note: if you hold the unit with your hand, the unit will sense heat from your hand and cause a bad calibration.

Use this formula:

$$\left(\frac{\text{Ambient} - 5}{135} \times 16 \right) + 4$$

Example:

If your reference probe measures 70°F (21.11°C) you need to adjust the transmitter's current output to be 11.70 mA.

8. Calibration complete.

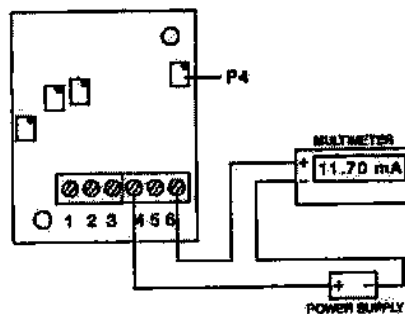


Figure 5: Temperature Calibration Procedure

**EWS-RH****Relative Humidity/Temperature Transmitter****Relative Humidity Specifications**

Range:	5-95% (non-condensing)
Accuracy @ 25°C:	From 5-20%, ± 4% RH From 20-80%, ± 3% RH From 80-95%, ± 4% RH
Repeatability:	± 1% RH
Temp. Compensation Range:	5 to 140°F (-15 to 60°C)
Output:	4-20 mA or 1-5 Vdc (scaled for 0 to 100% RH)
Power:	8-24 Vdc @ 20mA
Max Loop Resistance:	Ohms = (V supply - 8V) / .02 A
RH Time Constant:	100 sec., from 20-90%, 60 sec from 90-20%
Sensor Type:	Thin Film Polymer Capacitor

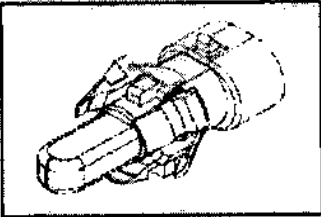
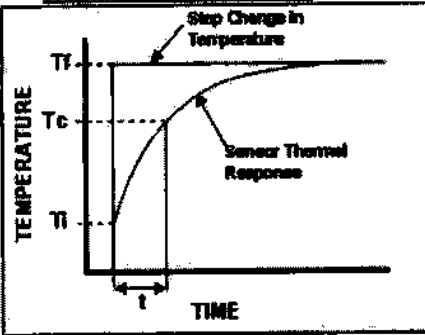
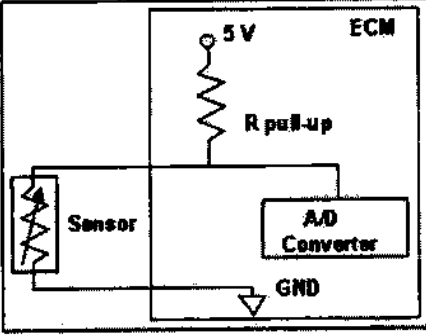
Temperature Specifications

Range:	5 to 140°F (-15 to 60°C)
Accuracy @ 25°C	
In Still Air:	± 1.2°F (0.7°C) @ 25°C ± 2.5°F (1.4°C) across full range
In Moving Air:	± 2.5°F (1.4°C) @ 25°C ± 3°F (1.7°C) across full range
Note:	Not recommended for fast moving air applications.
Repeatability:	± 0.5°F (0.3°C)
Output :	4-20 mA or 1-5 Vdc (scaled across range)
Temp. Time Constant:	(for 63.2% response) 9 sec. in moving air (1 M/sec.), 30 sec. in still air
Power:	8-24 Vdc @ 20 mA
Max Loop Resistance:	Ohms = (V supply - 8V) / .02 A
Sensor Type:	Solid State

General Specifications

Enclosure Material:	Acrylonitrile Butadiene
Dimensions:	79 x 54 x 45mm (3.12 L x 2.12 W x 1.76" H)
Weight:	54 g(.12 lb)

Appendix D: Air Temperature Sensor Manufacturer Specification Data

DELPHI Automotive Systems	TEMPERATURE SENSOR PRODUCT DATA
OUTSIDE AIR TEMPERATURE SENSOR PART NUMBER 15416387	
FEATURES: <ul style="list-style-type: none"> - Design for Manufacturability - Cost Effective - Robust Design - Few Components - Few Assembly Processes - Thermistor Technology - 100% Calibration Certified 	
THERMAL & ELECTRICAL PROPERTIES Typical Voltage Supply: 5V DC Operating Temperature: -40 C to 80 C Resistive Range (Ohms): See Table Dissipation Constant*: N/A Thermal Time Constant**: 45 seconds Accuracy: See Table	MECHANICAL PROPERTIES Sensor Body Material: Nylon 6/12 33% GF Mating Connector TPA: N/A Mating Connector & Seal: 12046753 Overall Weight: 4.7g Color: Black
THERMAL TIME CONSTANT	CIRCUIT SCHEMATIC
	
<p>* The ratio, at a specified ambient temperature, of the change in the power dissipation of the sensor to the resultant temperature change of the thermistor. Test medium: dry air stream flowing at 5000 mm/sec.</p> <p>** The time required for the sensor to achieve 63.2% of its steady state value when subjected to a step change in ambient temperature [$T_c = (T_2 - T_1) * 63.2% + T_1$]. Test medium: dry air stream flowing at 5000 mm/sec.</p>	
Part Revision Level: B02 Data Sheet Revision Date: 01/16/2001	

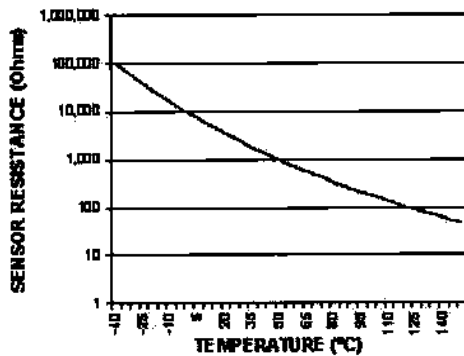
DELPHI

Automotive Systems

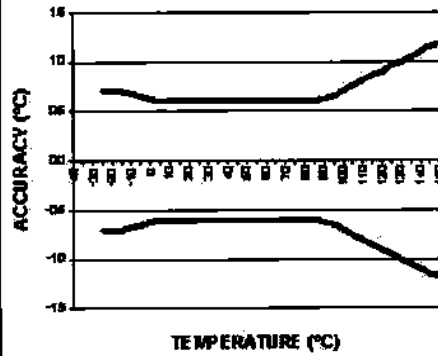
**TEMPERATURE SENSOR
PRODUCT DATA**

PART NUMBER 15416387

**UNLOADED RESISTANCE vs TEMPERATURE
CHARACTERISTIC CHART**



TEMPERATURE ACCURACY CHART



Note: Temperature Sensor Calibration Resistance Guaranteed by 100% Automated Calibration Certification.

Temp (°C)	Res (Ohms)	Res (±%)	Ref Acc (±°C)	Temp (°C)	Res (Ohms)	Res (±%)	Ref Acc (±°C)	Temp (°C)	Res (Ohms)	Res (±%)	Ref Acc (±°C)
-40	100665	4.87	0.70	25	2795	2.50	0.80	90	242	2.10	0.70
-35	72437	4.64	0.70	30	2240	2.45	0.80	95	207	2.21	0.70
-30	52584	4.43	0.70	35	1808	2.40	0.80	100	178	2.31	0.80
-25	38583	4.21	0.70	40	1465	2.36	0.80	105	154	2.42	0.80
-20	28682	4.00	0.70	45	1185	2.31	0.80	110	133	2.52	0.90
-15	21371	3.80	0.70	50	980	2.27	0.80	115	118	2.61	0.90
-10	16120	3.60	0.60	55	809	2.23	0.80	120	101	2.68	1.00
-6	12261	3.40	0.60	60	671	2.18	0.80	125	88	2.75	1.00
0	8399	3.21	0.60	65	559	2.15	0.80	130	78	2.80	1.10
5	7263	3.08	0.60	70	469	2.11	0.80	135	68	2.84	1.10
10	5858	2.92	0.60	75	395	2.07	0.80	140	60	2.87	1.20
15	4441	2.78	0.60	80	334	2.04	0.80	145	53	2.88	1.20
20	3511	2.64	0.80	85	283	2.00	0.80	150	48	2.90	1.20

Important: The values above are for the unloaded thermistor, as shipped from Delphi Packard Electric, and does not reflect the effects of application system errors and aging.

Notes: Please contact Delphi Packard Engineering for the resistance vs temperature curve for your temperature sensor application. Due to self-heating effects of the thermistor, the resistance is dependent upon the application.

Since thermistors are "continuous function devices", resistance vs temperature data is available for numbers beyond those specified above.

For more information contact:

Delphi Packard Electric Systems
Sensor Business Segment M/S 93B
North River Road
Warren, OH 44483

Phone: (330) 373-3589

Fax: (330) 373-3442

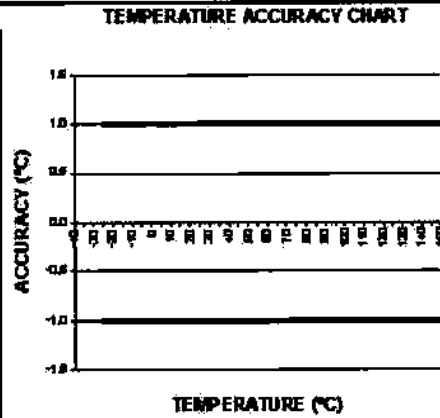
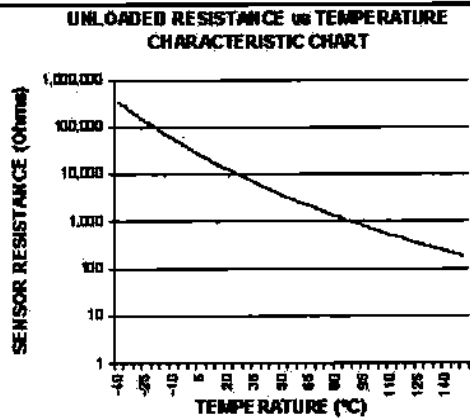
Appendix E: Fuel Temperature Sensor Manufacturer Specification Data

DELPHI Automotive Systems	TEMPERATURE SENSOR PRODUCT DATA
COOLANT TEMPERATURE SENSOR PART NUMBER 15461715	
FEATURES: <ul style="list-style-type: none"> - Design for Manufacturability - Cost Effective - Robust Design - Few Components - Few Assembly Processes - Thermistor Technology - 100% Calibration Certified 	
THERMAL & ELECTRICAL PROPERTIES Typical Voltage Supply: 5V DC Operating Temperature: -40 C to 135 C Resistive Range (Ohms): See Table Dissipation Constant*: 12 mW/C Thermal Time Constant**: < 15 seconds Accuracy: See Table	MECHANICAL PROPERTIES Sensor Body Material: 316 SS Connector: PBT 30% GF O-Ring: Fluorocarbon Hex Size: 5/8" Thread Size: M10 x 1.5 Mating Connector & Seal: 1-987644-7 AMP Installation Torque: 10-14 N-m Overall Weight: 15.30 grams
THERMAL TIME CONSTANT 	CIRCUIT SCHEMATIC
<p>* The ratio, at a specified ambient temperature, of the change in the power dissipation of the sensor to the resultant temperature change of the thermistor. Test medium: silicone oil</p> <p>** The time required for the sensor to achieve 63.2% of its steady state value when subjected to a step change in ambient temperature [$T_c = (T_1 - T_2) * 63.2% + T_1$]. Test medium: silicone oil.</p>	
Part Revision Level: 601 Data Sheet Revision Date: 2/18/2003	

DELPHI
Automotive Systems

**TEMPERATURE SENSOR
PRODUCT DATA**

PART NUMBER 15461715



Note: Temperature Sensor Calibration Resistance Guaranteed by 100% Automated Calibration Certification.

Temp (°C)	Res (Ohms)	Res (±%)	Ref Acc (±°C)	Temp (°C)	Res (Ohms)	Res (±%)	Ref Acc (±°C)	Temp (°C)	Res (Ohms)	Res (±%)	Ref Acc (±°C)
-40	332776	6.63	1.00	25	10000	4.38	1.00	90	916.4	3.08	1.00
-35	240264	6.40	1.00	30	8080	4.25	1.00	95	786.8	3.01	1.00
-30	175427	6.18	1.00	35	6536	4.13	1.00	100	678.1	2.94	1.00
-25	128449	5.98	1.00	40	5331	4.02	1.00	105	586.5	2.87	1.00
-20	86481	5.78	1.00	45	4373	3.91	1.00	110	509.1	2.80	1.00
-15	72592	5.60	1.00	50	3608	3.81	1.00	115	443.3	2.73	1.00
-10	55108	5.43	1.00	55	2889	3.70	1.00	120	387.3	2.67	1.00
-5	42193	5.26	1.00	60	2490	3.60	1.00	125	339.5	2.61	1.00
0	32566	5.10	1.00	65	2085	3.51	1.00	130	298.4	2.55	1.00
5	25338	4.94	1.00	70	1754	3.42	1.00	135	263.1	2.48	1.00
10	19869	4.79	1.00	75	1482	3.33	1.00	140	232.6	2.44	1.00
15	15895	4.65	1.00	80	1257	3.24	1.00	145	206.1	2.39	1.00
20	12488	4.51	1.00	85	1071	3.16	1.00	150	183.2	2.33	1.00

Important: The values above are for the unloaded thermistor, as shipped from Delphi Packard Electric, and does not reflect the effects of application system errors and aging.

Notes: Please contact Delphi Packard Engineering for the resistance vs temperature curve for your temperature sensor application. Due to self-heating effects of the thermistor, the resistance is dependant upon the application.

Since thermistors are "continuous function devices", resistance vs temperature data is available for numbers beyond those specified above.

For more information contact:

Delphi Packard Electric Systems
Sensor Business Segment MAS 93B
North River Road
Warren, OH 44483

Phone: (330) 373-3688

Fax: (330) 373-4147